Energy recoil determination due to charge exchange collisions and SIMION transmission simulations of the CHEOPS setup

June 22, 2021

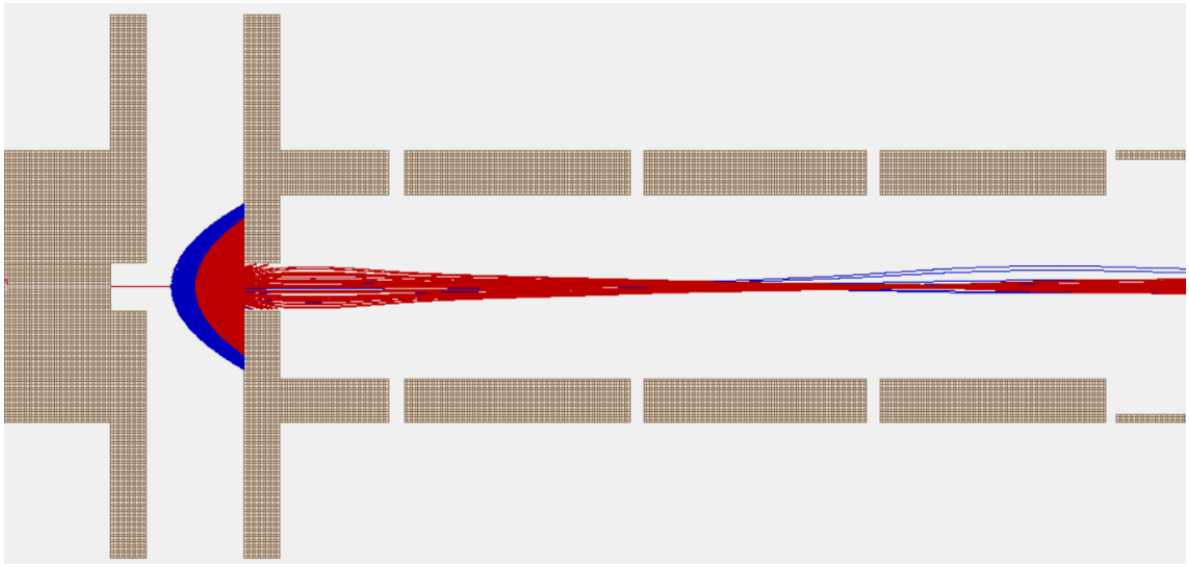

Author:
Wouter van Tellingen

Supervisors:
prof. dr. Ir. R.A. Hoekstra
dr. T.A. Schlathölter
PhD student Subam Rai

Abstract

This report focuses on 2 main topics regarding the charge exchange collision described by the classical over barrier model of energetic Sn and He ions colliding with H_2 molecules. The first topic consists of calculating the momentum and energy recoil of H_2 molecule due to the charge exchange reaction. In the second part the software SIMION is used to build a model of the CHEOPS setup found in the lab of the QISD group facilitated by the University of Groningen and ASML. The model consists of an extraction region and a time of flight spectrometer. H^+ and H_2^+ ions are created in the extraction region with an initial velocity v_0 in a random direction. These ions correspond to the reaction products of target particles that have interacted with a projectile ion. Within the extraction region of the model an approximately uniform electric field is simulated due to the plates of the extraction region being electrically charged. This field guides the positively charged ions towards the side of the extraction region where a diaphragm is located. Behind the diaphragm lies the extraction tube which consists of a number of electrostatic lenses focusing the ion beam towards the MCP at the end of the extraction tube. The SIMION model is used to simulate the effect of the position of the ion beam in a extraction region on the H_2^+ or H^+ ion transmission through the diaphragm, as well as the transmission of simultaneously emitted proton pairs due to the decay of the H_2 molecule as a result of the its ionisation. The energy recoil the H_2 molecule experiences calculated in the first topic of the report is simulated in the SIMION model as well. The results of the SIMION simulations are compared to actual lab measurements. With the calculations done on the energy recoil, it is found that the energy recoil decreases exponentially when the projectile energy is increased and the higher the charge of the projectile ion, the more recoil energy is transferred to the target particle. In the case an offset of the ion source in the x or y direction with the CHEOPS setup SIMION model, it is found that only an offset of the source in the x direction can cause a slight difference between the results of two separate lab experiments. For a shift in the x direction the b/f transmission ratio decreases rapidly when the source is brought closer to the diagram. For a shift in the y direction, the b/f transmission ratio for transmission is relatively constant in a region where the y shift is smaller than 2 mm. regarding the transmission of simultaneously emitted proton pairs it is found that if the source is shifted less than 1 mm in the y or z direction there is no effect seen on the ion pair transmission. After a shift of 1.5 mm in the y or z direction, the ion pair transmission declines increasingly fast. Zero ions are transmitted when the shift of the point source in the y or z direction is larger than 2.333 mm. This is less than the radius of the diaphragm of 2.5 mm. When simulating the energy recoil a peak broadening is seen in the time of flight spectrum. However, this effect is not noticeable in experiments done in the lab.

Acknowledgement

This Thesis could not have been written without others who taught me the necessary knowledge and helped me along the way. First of all I want to give my deepest appreciation to my first supervisor, prof. dr. Ir. R.A. Hoekstra, who guided me along the journey of my thesis. He motivated me to continue my work and facilitated me with everything that was needed to progress. I am especially thankful for the fact that he helped me to find a planning solution for me being unable to work for a couple months due to sudden health problems. Thanks to the possibility of a flexible planning and a slight change in subject focus, I could resume my work and eventually finish this thesis. I also want to thank my supervisor Subam Rai who was always there to answer my direct questions and taught me all the necessary skills to operate the experimental setup in the lab. In addition I would like to thank Klaas Bijlsma for answering some of my questions as well. Although he was not my direct supervisor, he did answer my questions if I had one. I would like to thank my fellow student Lukas Raap with whom I worked closely to collect data for this thesis. I also want to thank my fellow student Bas Schoonbeek for giving me tips and advise on writing my thesis report. Lastly i want to thank my parents for supporting me while doing my thesis and facilitating me with a good study environment.

Contents

Abstract i

Acknowledgement iii

1 Introduction 1

2 Aims and objectives 2

3 Theory 3
- 3.1 Classical Overbarrier Model (COBM) . . . 3
  - 3.1.1 Model . . . 3
  - 3.1.2 One electron capture . . . 5
  - 3.1.3 Two electron capture . . . 6
  - 3.1.4 Momentum and energy recoil . . . 7
- 3.2 Experiment . . . 9
  - 3.2.1 Ion beam facility ZERNIKELEIF . . . 9
  - 3.2.2 Chopper sweeper system . . . 10
  - 3.2.3 CHEOPS . . . 11
  - 3.2.4 MCP . . . 13
- 3.3 Physics related to CHEOPS . . . 14
  - 3.3.1 Molecular hydrogen levels . . . 14
  - 3.3.2 Transmission . . . 15
  - 3.3.3 Time difference Δt . . . 15
  - 3.3.4 Transmission ratio . . . 17
  - 3.3.5 t_0 correction . . . 20
- 3.4 SIMION model . . . 22
  - 3.4.1 SIMION software . . . 22
  - 3.4.2 CHEOPS setup SIMION model . . . 22
- 3.5 Peak broadening processes . . . 24

4 Results 26
- 4.1 One electron capture . . . 26
  - 4.1.1 Recoil momentum distributions . . . 26
  - 4.1.2 Angular distribution . . . 28
  - 4.1.3 Recoil energy distributions . . . 29
  - 4.1.4 Recoil as a function of projectile energy . . . 31
- 4.2 Two electron capture . . . 33
  - 4.2.1 Recoil momentum distributions . . . 33
  - 4.2.2 Angular distribution . . . 35
  - 4.2.3 Recoil energy distributions . . . 36
  - 4.2.4 Recoil as a function of projectile energy . . . 38
- 4.3 SIMION simulations with energetic protons . . . 40
  - 4.3.1 Time-of-flight (ToF) histograms . . . 40
  - 4.3.2 Time difference Δt . . . 42
  - 4.3.3 Transmission ratio . . . 43
  - 4.3.4 Shift x position . . . 45
  - 4.3.5 Shift y position . . . 50
  - 4.3.6 Ion pair transmission . . . 56
- 4.4 Molecular ions . . . 58
  - 4.4.1 Full histogram . . . 58

4.4.2 Recoil energy effect on time of flight spectrum of H_2^+ ions . . . 60

5 Discussion **64**
5.1 Momentum and energy recoil . . . 64
5.1.1 One electron capture . . . 64
5.1.2 Two electron capture . . . 65
5.2 SIMION simulations . . . 66
5.2.1 Time of flight spectra SIMION model . . . 66
5.2.2 Time difference Δt . . . 66
5.2.3 Transmission . . . 67
5.2.4 Shift x position . . . 68
5.2.5 Shift y position . . . 69
5.2.6 Ion pair transmission . . . 69
5.2.7 Recoil energy effect on time of flight spectrum Molecular Hydrogen . . . 69

6 Conclusion **71**

7 Outlook **73**

Bibliography **74**

Appendix **76**
7.1 One electron capture . . . 76
7.1.1 Transverse momentum . . . 76
7.1.2 Angular distribution . . . 78
7.1.3 Recoil energy . . . 79
7.2 Two electron capture . . . 81
7.2.1 Transverse momentum . . . 81
7.2.2 Angular distribution . . . 83
7.2.3 Recoil energy . . . 84

1 Introduction

The number of devices an average person owns that requires a fast amount of computing power becomes larger every year. With the rise of artificial intelligence and an increased integration of electronics in society it is expected that this trend will continue. To supply the demand of this all increasing need for computing power, better higher density computer chips need to be developed and produced. The number of transistors on a computer chip is an indication of the computing power that can be achieved with that chip. The smaller the transistors the less energy they consume and the more will fit on a single chip. The focus of the industry behind developing computer chips is thus to increase the number of transistors and to reduce the size of these transistors. Moore's law states that the number of transistors per silicon chip doubles about every 2 years due to continuous innovation in this field. [1] [2] [3] [4]

To produce computer chips, a process called photo-lithography is used. With this process extremely precise and small geometric shapes can be created on a silicon substrate called a wafer. The basic principle behind photo-lithography is to apply a thin layer of a substance called photo-resist on a silicon wafer and using an intense beam of photons to edge out channels in this photo-resist layer. The wafer is then treated with a chemical to remove a thin layer of silicon in the places where the photo-resist has been edged out. The parts of the wafer where the photo-resist layer is still present is shielded from the chemical and hence the silicon will not be removed in those areas. This way thin channels will be made in the silicon wafer. This process can be repeated multiple times to create a number of layers of channels in the silicon wafer. By edging out the channels in the right way, a complex array of billions of transistors can be created that are packed closely together. [4] [5] [6] [7]

The size of the channels that can be produced depends on the wavelength of the light used to edge them out. The smaller the wavelength of light, the smaller the channels that can be made. To achieve the goal of producing ever more and smaller transistors on a single computer chip, the wavelength of light used to edge out the channels in the wafer has to follow this trend of becoming smaller as well. ASML is the world's leader in producing photo-lithography machines. Their latest generation of photo-lithography machines uses extreme ultraviolet light to edge out the channels on the wafer. This extreme ultraviolet light is referred to as EUV for short. This light has a wavelength of 13.5 nm. [4] [8] [9]

Creating an intense beam of EUV light is very challenging. The most feasible way to achieve this as of today is to use plasma emission from highly charged ions [4]. ASML uses Sn droplets that are exposed to an infrared laser. This laser will transfer an enormous amount of energy to the Sn droplet creating a Sn plasma. This Sn plasma emits the 13.5 nm EUV light. The light that originated from this Sn plasma is emitted in all directions. To focus most of it into a single narrow beam that can be used to edge out channels in the wafer, a hemispherical mirror is placed close to the location where the plasma is created that focuses the EUV light onto the wafer. This mirror needs to be able to focus the EUV light very accurately and hence needs to be polished to extreme precision. This makes the mirror a very expensive and delicate part of the machine.

The energetic Sn ions that are created to produce the EUV light can be harmful to the photo-lithography machine and in particular to the very expensive and delicate hemispherical mirror. To prevent these Sn ions from doing too much damage they need to be contained to prevent them from reaching the mirror. One way to contain the ions is to create a high pressure H_2 gas atmosphere in the chamber where the Sn plasma is produced. This way the Sn ions will be stopped by the H_2 gas before they can reach the hemispherical mirror. The scientific theory behind the stopping of energetic ions in gas is not complete. [4] [10]

ASML is interested in the scientific theory behind the stopping of energetic ions in a gas. To obtain a better understanding about the processes that occur in the stopping of energetic ions in a gas, ASML collaborates with the Quantum Interactions and Structural Dynamics (QISD) group facilitated by the University of Groningen. This group does research on energetic ion stopping in gas to build a scientific theory to describe it. This thesis is a contribution to that research.

2 Aims and objectives

ASML is interested in the science behind the stopping of energetic positively charged ions in a gas to be able to optimize their advanced photo-lithography machines with which state of the art computer chips can be fabricated. The gas particle of interest is molecular hydrogen also referred to as H_2. This is the gas particle that is currently used by ASML in their lithography machines to stop energetic Sn ions from hitting the delicate parts of the machine. This to prevent it from damage and extend the lifetime of the machine.

To build on the theory behind ion-gas particle interactions, this Thesis dives deeper into the analytical descriptions of these interactions. The charge exchange collision described by the classical over barrier model of energetic Sn and He ions colliding with H_2 molecules is researched. Calculations are done to determine the momentum and energy recoil of H_2 molecules due to these charge exchange reactions with these energetic ions. The main goal of this analytical research is to determine to what extend kinetic energy referred to as recoil energy is transferred from an incoming energetic positively charged ion to a H_2 molecule with which this ion undergoes a charge exchange collision. This knowledge can be used to optimize the ion stopping process of an energetic ion in a H_2 molecule gas.

In addition, research is done on the experimental measurement setup found in the lab of the QISD group facilitated by the University of Groningen and ASML. This setup's purpose is to research energetic ion stopping in a gas. The setup creates a beam of energetic positively charged ions which is guided to a measurement device referred to as the CHEOPS setup. The CHEOPS setup consists of two main components, namely the extraction region and the time of flight spectrometer. These two components are separated by a plate with a diaphragm in it. Within the extraction region of the CHEOPS setup, ions from the energetic positively charged ion beam interact with gas particles. In this Thesis a SIMION model is build that resembles this CHEOPS setup found in the lab. With this SIMION model accurate simulations can be done of particles moving through the CHEOPS setup. The main goal of the SIMION simulations is to determine the effect of an offset of the energetic ion beam coming into the extraction region of CHEOPS setup.

When energetic positively charged ions undergo a charge exchange collision with a H_2 molecule, a proton or H^+ ion pair can be created. This ion pair is emitted with a 180 degrees difference with respect to each other and with an initial velocity v_0. Another goal to achieve by the use of SIMION simulations is to determine the ion pair transmission ratio through the diaphragm in the extraction region of the CHEOPS setup.

Lastly, the recoil energy that is analytically calculated for a particular charge exchange collision is used in SIMION simulations. This energy is given to an ionized H_2^+ ion. This is a possible reaction product of a charge exchange collision between an energetic positively charged ion and a H_2 molecule. The main goal of these SIMION simulations is to determine the effect of the recoil energies on the time of flight spectrum of ions created by a charge exchange collision moving through the CHEOPS setup.

The knowledge obtained with the research done with the aid of the SIMION model can be used in future experiments to improve the CHEOPS setup and get a better understanding about the experimental results obtained by measurements done with this setup.

3 Theory

3.1 Classical Overbarrier Model (COBM)

3.1.1 Model

The Classical Overbarrier Model or COBM for short describes the charge exchange collision between an ion and an atom or molecule. Lets consider an ion with a certain kinetic energy encountering a stationary atom in its path. When the charged ion approaches the atom sufficiently close, the charge exchange reaction can occur. The incoming ion is referred to as the projectile, while the stationary atom is referred to as the target. The COBM describes these charge exchange reactions as follows

$$A^{q+} + B \rightarrow A^{(q-r)+} + B^{r+} \tag{1}$$

Here A is an arbitrary projectile ion, B is an arbitrary target atom or molecule, q is the charge of the incoming ion and r is the number of electrons captured by the projectile ion. Depending on the charge of the projectile ion and the nature of the target particle, one or more electrons can be captured. Note that it is also possible for no electron to be captured at all in such a collision process. In this report the main focus lies on one- and two electron capture of Sn ions interacting with a H_2 molecules, as well as He ions interacting with a H_2 molecule. [11] [12]

For charge exchange to occur between the two particles, electrons have to be transferred from the target to the projectile. First consider an one electron capture process, here only one electron is transferred from the target to the projectile. The electron to be captured can be described as trapped in the potential well of the target particle. When there is no ion approaching sufficiently close to the target, the electron is kept in this potential well with no way to escape classically. However when a projectile ion approaches the target sufficiently close, the potential well of the target containing the electron will start to overlap with the potential well of the projectile ion. This is visualised in figure 1.

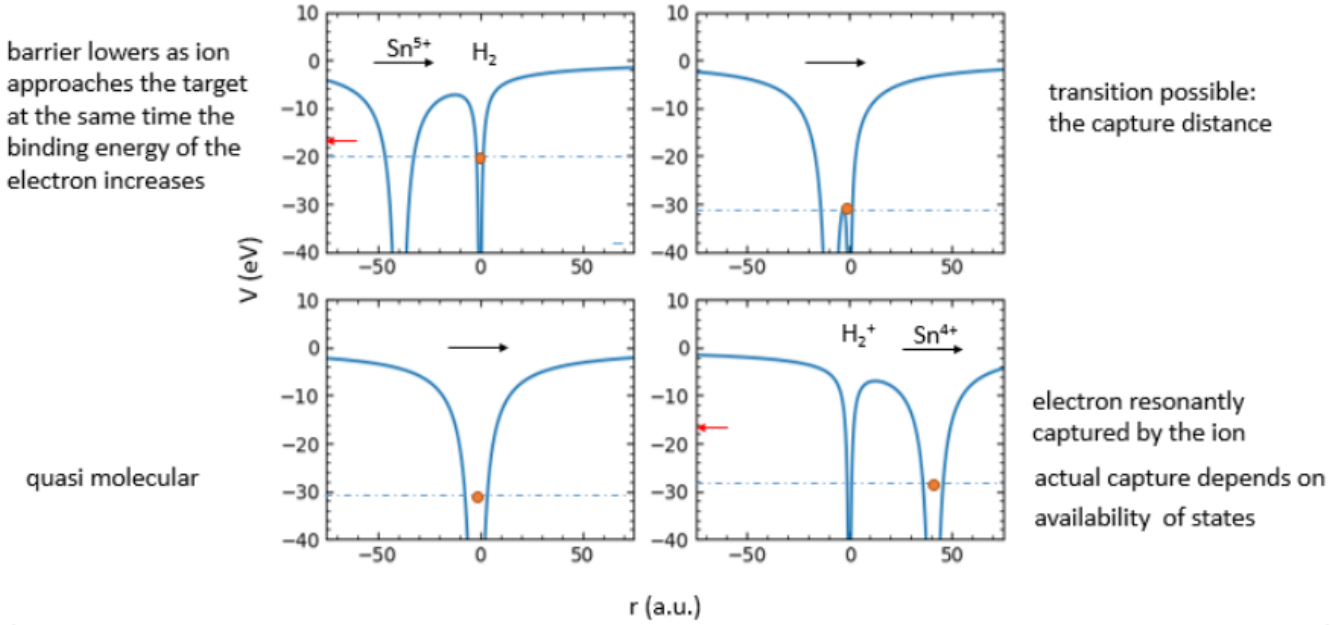

Figure 1: One-electron capture potential landscape shown for 4 different stages in the charge exchange collision between Sn^{5+} and H_2 according to the COBM. The potential energy V is plotted on the y-axis in eV and the location r is plotted on the x-axis in atomic units.

The potential barrier between the two potential wells will lower as the distance between the two particles decreases. When both particles get sufficiently close to each other the barrier will get so low that the electron located in the potential well of the target can pass over the barrier. At this moment the electron can be seen as shared between the two particles. This electron sharing resembles the electron sharing in a molecular bond, hence this phenomena can be referred to as a quasi molecular state. At a certain point in time, the projectile and the target reach their distance of closest approach. From that point on the distance between the two particles will increase again. This means that the two potential wells will start to separate and the potential barrier re-emerges. The height of this barrier will increase as the distance between the two particles increases. When the barrier height surpasses the binding energy of the electron that is shared between the two particles, the electron will end up in one of the two potential wells. Either in the one of the target or the one of the projectile. Depending in which potential well the electron will end up, the electron will be either captured by the projectile or recaptured by the target. In this report the interest lies in electron capture, hence it will focus on the process where the electron ends up in the potential well of the projectile ion. The electron is transferred from the target to the projectile and charge exchange occurs. [11] [12]

To predict at which distances between the target and the projectile electron transfer can occur, the capture radius R needs to be introduced. The capture radius is the distance between the particles at which an electron is no longer only in the potential well of the target, but is shared between the target and the projectile in a joint potential well. I.e electron transfer can occur when the distances r between the projectile and the target is smaller than the capture radius r<R. The target particle might have multiple electrons that can be captured. All of these electrons will have their own capture radius R, depending on their binding. In the case of H_2 molecules there are only 2 electrons that can be captured. Due to the fact that the actual electron capture changes the potential landscape of the interaction, the capture radius for the incoming projectile is slightly different from the capture radius of the outgoing projectile. They will be referred at as R_i^{in} and R_i^{out} respectively. Here i corresponds to the electron number, starting with i=1 for the electron that has the lowest binding energy with the target and counting up from there. R_i^{in} can be determined as follows

$$R_i^{in} = \frac{i + 2\sqrt{iq}}{-E_{b,i}} \tag{2}$$

Here $E_{b,i}$ is the binding energy of the i'th electron. The capture radius of the outgoing projectile R_i^{out} can be related to the capture radius of the incoming projectile R_i^{in} as follows

$$R_i^{out} = R_i^{in}\left(\frac{\sqrt{q - c_i} + \sqrt{i + c_i}}{\sqrt{q} + \sqrt{i}}\right)^2 \tag{3}$$

Here c_i is the number of electrons that has already been captured when the i'th electron is being captured or recaptured. An electron is considered captured or recaptured when r>R_i^{out}. Be aware that the most strongly bound electron has the smallest outgoing capture radius R_i^{out}. This electron is the first electron to be either captured or recaptured, but it has the highest electron number i. For example, in the case of two electron capture, the first electron that can be considered captured is electron i=2. In this case c_2 is 0 since no electrons have been captured or recaptured at this time. The second and last electron to be captured is electron i=1. In this case c_1 will be 1. For single electron capture $R_i^{in} = R_i^{out}$, since in this case i=1 and c_1 = 0. [11]

3.1.2 One electron capture

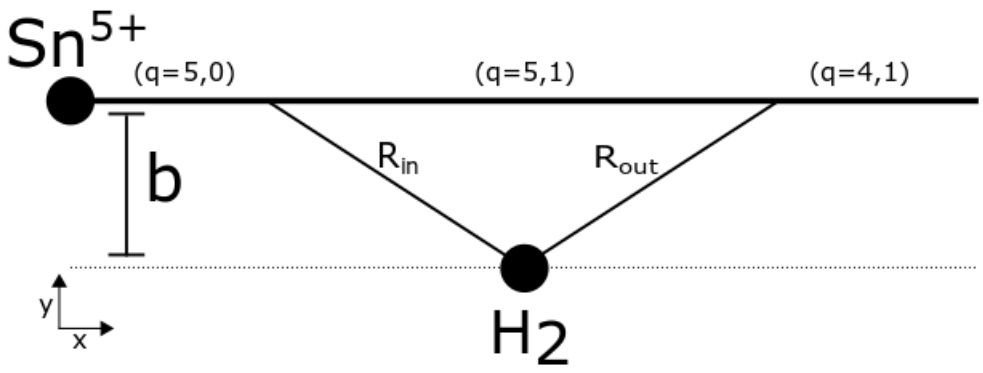

Figure 2: One-electron capture interaction according to the COBM. The figure shows the interaction between the projectile ion Sn^{5+} and the target molecule H_2 for each stage of the interaction process in a Cartesian coordinate system. The Sn^{5+} projectile ion moves from left to right over the straight line encountering 3 regions. Above each region the charges of the projectile and the target that are experienced by the other particle is stated.

In figure 2 an one electron capture charge exchange collision is visualized. The projectile is a Sn^{5+} and the target is a H_2 molecule. The variable b is called the impact parameter which is the perpendicular distance between the path of the projectile and the line parallel to the projectiles direction of motion that intersects the target. The Sn^{5+} projectile ion moves from left to right over the straight line encountering 3 regions. The region on the left where the electron potential wells of both Sn^{5+} and H_2 are still separate from each other. The electron to be captured is still in the potential well of the target molecule H_2. The region in the middle where the distance between the projectile ion Sn^{5+} and target molecule H_2 is smaller than R_{in}. Here the electron to be captured is no longer localized in the potential well of H_2, but now moves in a joint potential well of Sn^{5+} and H_2. Lastly, the region on the right where the distance between the projectile and target is larger than R_{out}. The originally outer most electron of H_2 is no longer in a shared potential well between the two particles and the electron now moves in the potential well of the projectile ion which has now become Sn^{4+}. The electron can now be considered captured.

3.1.3 Two electron capture

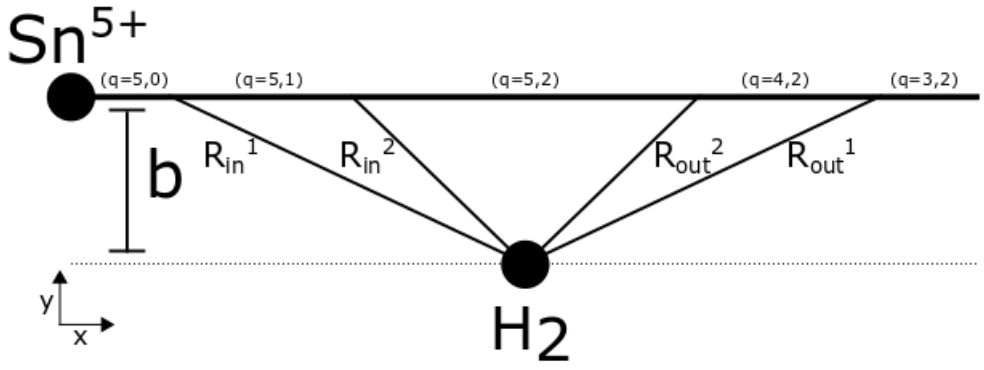

Figure 3: Two-electron capture interaction according to the COBM. The figure shows the interaction between the projectile ion Sn^{5+} and the target molecule H_2 for each stage of the interaction process in a Cartesian coordinate system. The Sn^{5+} projectile ion moves from left to right over the straight line encountering 5 regions. Above each region the charges of the projectile and the target that are experienced by the other particle is stated.

In figure 3 a two electron capture charge exchange collision is visualized. Once again the projectile is a Sn^{5+} ion and the target is a H_2 molecule. The Sn^{5+} projectile ion moves from left to right over the straight line encountering 5 regions. The region on the left where the electron potential wells of both Sn^{5+} and H_2 are still separate from each other. The electron to be captured is still in the potential well of the target molecule H_2. The region on the right of the first region, where the distance between the projectile ion Sn^{5+} and target molecule H_2 is smaller than R_{in}^1. Here the outer most electron of H_2 is no longer localized in the potential well of H_2, but now moves in a joint potential well of Sn^{5+} and H_2. The region in the middle where the distance between the projectile ion Sn^{5+} and target molecule H_2 is smaller than R_{in}^1 as well as R_{in}^2. Here both of the electrons of H_2 are no longer localized in the potential well of H_2. They both move in a joint potential well of Sn^{5+} and H_2. The region to the right of the middle where the distance between the projectile ion Sn^{5+} and target molecule H_2 is larger than R_{out}^1 but smaller than R_{out}^2. The originally inner most electron of H_2 is no longer in a shared potential well between the two particles and the electron now moves in the potential well of the projectile ion which has now become Sn^{4+}. Lastly, the region on the right where the distance between the Sn projectile ion and H_2 target molecule is larger than R_{out}^1 as well as R_{out}^2. The originally outer most electron of H_2 is now also no longer in a shared potential well between the two particles and the electron now moves in the potential well of the projectile ion which has now become Sn^{3+}. Both electrons can now be considered to be captured.

3.1.4 Momentum and energy recoil

When the projectile and the target share one or more electrons during the capture process, a Coulomb force will act on both of the particles. This is due to the fact that the shared electron does no longer contribute to screening of the nuclear charge of the target as can be seen in figure 2 and figure 3. Hence from the perspective of the projectile, the target is now positively charged. The coulomb force in atomic units is given by

$$F = \frac{q_1 q_2}{R^2} \tag{4}$$

In the case of the charge exchange collision the force parallel to the direction of motion is assumed to cancel out. Only the coulomb force in the transverse direction is taken into account. The Coulomb force in transverse direction is given by

$$F_y = \frac{q_1 q_2 b}{(x^2 + b^2)^{\frac{3}{2}}} = \frac{\partial p}{\partial t} \tag{5}$$

Here x is the position of the projectile along its trajectory and b the impact parameter (see figure 2 and 3). This Coulomb force transfers momentum from the projectile to the target in the transverse direction. To determine the momentum transferred, the Coulomb force needs to be integrated over time.

$$p_{trans} = \int F_y \, dt = \frac{1}{v_p} \int F_y \, dx \tag{6}$$

Here v_p is the projectile velocity. If this integral is solved for all the regions with different charge distributions along the ion's trajectory (section 3.1.2 and section 3.1.3), the following relation for the transverse momentum is obtained

$$p_{trans} = \frac{1}{v_p b} \left(\left[\sum_i q \sqrt{1 - \left(\frac{b}{R_i^{in}} \right)^2} + t_i \sqrt{1 - \left(\frac{b}{R_i^{out}} \right)^2} \right] + (q - r) r \right) \tag{7}$$

Here t_i is given by

$$t_i = (q - c_i)(i + c_i) - (q - c_{i-1})(i - 1 + c_{i-1}) \tag{8}$$

c_i is again the number of electrons that has already been captured when the i'th electron is being captured or recaptured. c_{i-1} is the number of electrons that is captured when electron i-1 is captured or recaptured. Note again that electron i-1 is captured or recaptured after electron i, since the most strongly bound electron with the highest number i will be the first one to be captured or recaptured. In the case of one electron capture the sum will disappear and t_1 will equal 1 since $c_1 = 0$ and $c_{1-1} = c_0 = 1$. The relation for the transverse momentum then simplifies to

$$p_{trans} = \frac{1}{v_p b} \left[(q + 1) \sqrt{1 - \left(\frac{b}{R_1} \right)^2} + (q - 1) \right] \tag{9}$$

With equation 8 and equation 9 the transverse momentum transfer to the target can be determined as a function of the impact parameter b. The impact parameter in a particular charge exchange collision can take a range of values. The likelihood of a certain impact parameter b to occur in the particle interaction and hence also the likelihood of a certain transverse momentum transfer to occur depends on the geometrical cross section $d\sigma = 2\pi b db$. To obtain a transverse momentum distribution of target particles interacting with projectiles possessing a certain charge q and a certain velocity v_p, this cross section has to be taken into account. The probability and hence the expected intensity of a certain transverse momentum transfer can be determined by the relation

$$\frac{d\sigma}{dp_{trans}} = \frac{d\sigma}{db} \left| \frac{db}{dp_{trans}} \right| = 2\pi b \left| \frac{db}{dp_{trans}} \right| \tag{10}$$

The transverse momentum that is transferred to the target can also be expressed in terms of kinetic energy. To go from momentum to kinetic energy the following relation can be used

$$E = \frac{{p_{trans}}^2}{2m_t} \tag{11}$$

Here m_t is the mass of the target. Be aware that due to the fact that this is a quadratic relation, the bin size changes going from transverse momentum to kinetic energy. If one wants to plot the kinetic energy distribution, the intensity distribution needs to be adjusted for this change in bin size by multiplying it with the factor m/p_{trans}. When the projectile transfers momentum to the target it will itself obtain momentum in the opposite direction. This will change the traveling direction of the projectile compared to the original direction of motion. The angle with which it changes depends on the transverse momentum according to the relation $p_{trans} = m_p v_p \theta$, where m_p is the mass of the projectile.

3.2 Experiment

3.2.1 Ion beam facility ZERNIKELEIF

An overview of the experimental measurement setup found in the lab of the QISD group is shown in figure 4. This setup's purpose is to research energetic ion stopping in a gas.

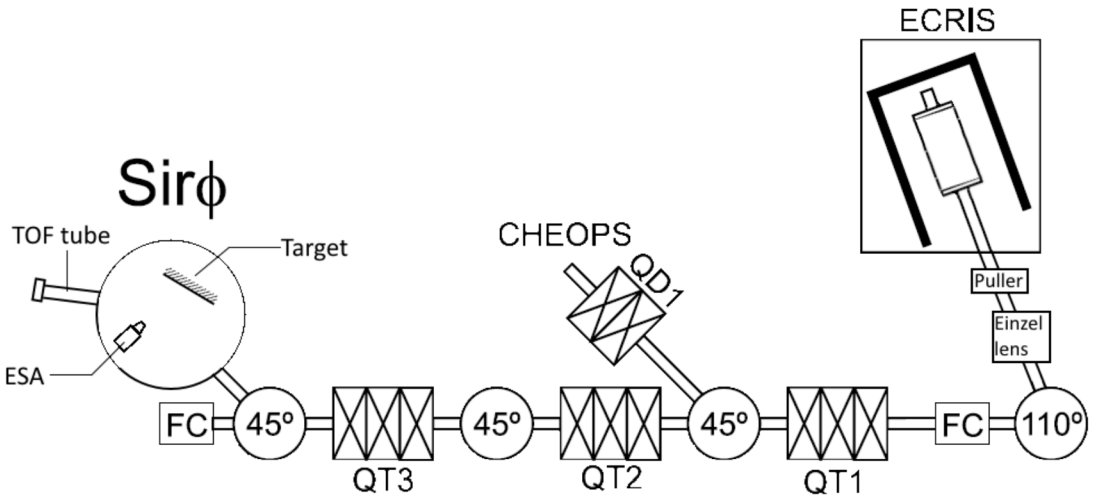

Figure 4: An overview of the experimental measurement setup found in the lab of the QISD group facilitated by the University of Groningen and ASML. [13]

The experimental setup consists of a number of modules. One of the models is an ion source called the ECRIS. ECRIS stands for Electron Cyclotron Resonance Ion Source. With this module various types of ions can be produced for a range of different charge states. The kinetic energy of the ions can be selected. The produced ions will exit the ECRIS in the form of an ion beam that will be guided through a vacuum pipe referred to as the beamline. The ECRIS can not produce one single type of ion by itself. There will always be various ion charge states produced at the same time and depending on the source material used, various isotopes of ions are produced as well. These different isotopes will all have different masses.

Behind the ECRIS lies the 110° degree bending magnet. This magnet will bend the ion beam produced by the ECRIS. The degree with which an ion is bend depends on its velocity, charge state and mass. This means that the 110° degree bending magnet can be used to select for one particular ion type from the various ion types that are produced by the ECRIS. Only an ion with a particular charge and mass will be bend to such a degree that it will continue to move through beamline. The other ion types with other mass and charge combinations will be disposed of by letting them collide with the wall of the beamline.

Behind the 110° degree bending magnet lies a magnetic lens referred to as the Triplet. This Triplet consists of three quadrupole magnets. The purpose of the Triplet is to counteract the ion beams natural desire to diverge. This behavior is due to the fact that particles with the same charge repel each other.

After the Triplet the ion beam encounters a 45° degree bending magnet. This bending magnet bends the ion beam either towards the CHEOPS setup or the Sirϕ setup. In this thesis only the CHEOPS setup will be discussed. CHEOPS stands for Charge Exchange Observed by Particle Spectroscopy. Between the CHEOPS setup and the bending magnet lies another magnetic lens referred to as the Doublet. The Doublet only consists of two quadrupole magnets and can again be used to focus the beam.

In front of the CHEOPS setup lies a chopper sweeper system. This system cuts the incoming ion beam into short beam pulses. After being chopped the beam pulses enter the CHEOPS setup. With the CHEOPS setup measurements regarding the stopping of energetic ions in a gas can be executed. [14] [15]

3.2.2 Chopper sweeper system

The Chopper Sweeper system chops a continues beam into small beam pulses. This is desirable for measurements done with the CHEOPS setup since the MCP can not endure a high intensity irradiation of ions for an extended period of time and foremost the pulses are a natural start for time of flight (ToF) type of experiments. The Chopper Sweeper system works by letting the projectile ion beam pass in between two plates. These plates are electrically charged. One plate is charged with a positive potential while the other is charged with a negative potential. The charge state of the plates alternate in time creating an electric field that alternates in time as well. The alternating electric field will bend the beam up and down in the region between the two plates. At the end of this region lies a diaphragm. The beam is sweeped over this diaphragm many times due to the alternating bending of the beam. The beam can only be transmitted through the diaphragm when it is swept over it. This will only be the case for a short amount of time shortly after the moment the two charged plates change polarity. Due to this sweeping over the diaphragm, only short beam pulses are transmitted through it and the beam is considered chopped behind the diaphragm. A 2D representation of the Chopper Sweeper system is given in figure 5

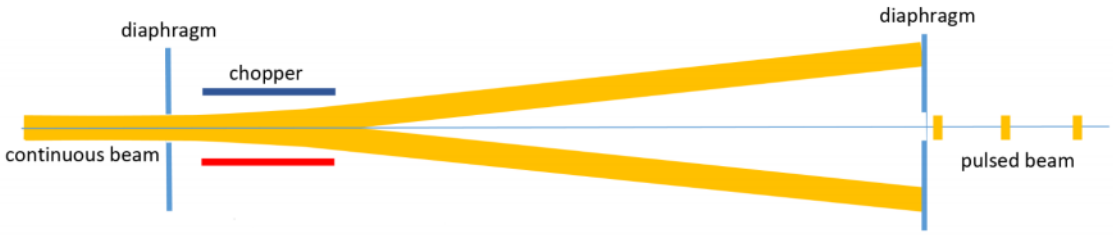

Figure 5: 2D representation of the working principal of the Chopper Sweeper system found in the lab of the QISD group facilitated by the University of Groningen and ASML. [16]

3.2.3 CHEOPS

The projectile ion beam produced in the ECRIS as described in section 3.2.1 is guided towards the CHEOPS setup, which is dedicated to study ion-gas target interactions. CHEOPS stands for Charge Exchange Observed by Particle Spectroscopy. A 2D representation of the CHEOPS setup found in the lab of the QISD group is depicted in figure 6.

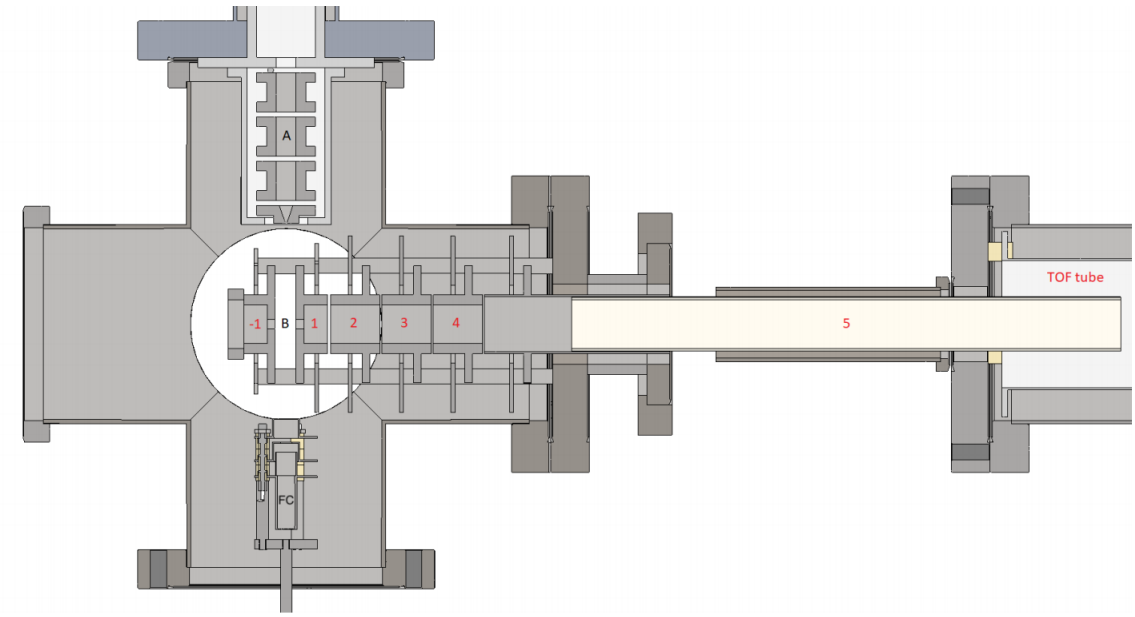

Figure 6: 2D representation of the CHEOPS setup in the horizontal plane. The projectile ion beam enters the setup from the 'top' through the electrostatic lens system A. Section B is the extraction region. Here the projectile ions may undergo a charge exchange collision with gas target particles. This will ionize the gas target particles. The ionized particles in the extraction region are subject to an approximately uniform electric field. This electric field guides the ions to the extraction plate in which a diaphragm is located, right of B. Behind the diaphragm lies the entrance of the time of flight spectrometer which consists of a number of electrostatic lenses focusing the extracted ions towards an ion counter at the end of the time of flight drift tube. [17]

In front of the CHEOPS setup lies a chopper sweeper system described in section 5. This system cuts the incoming projectile ion beam into short beam pulses. In the CHEOPS setup the projectile ion pulses cross the extraction region from the top marked by the letter B as seen in the figure. In this extraction region a gas is present. This gas consists of many individual target particles with which the projectile ions in the beam pulses can undergo a charge exchange collision. If a projectile ion in the beam pulse undergoes a charge exchange collision with a target particle in the extraction region, the target particle is ionized into a positively charged ion as described in section 3.1.

In figure 7 a schematic 3D representation of the extraction region in the CHEOPS setup is depicted with the aim of illustration of the x,y,z coordinate system used throughout this thesis.

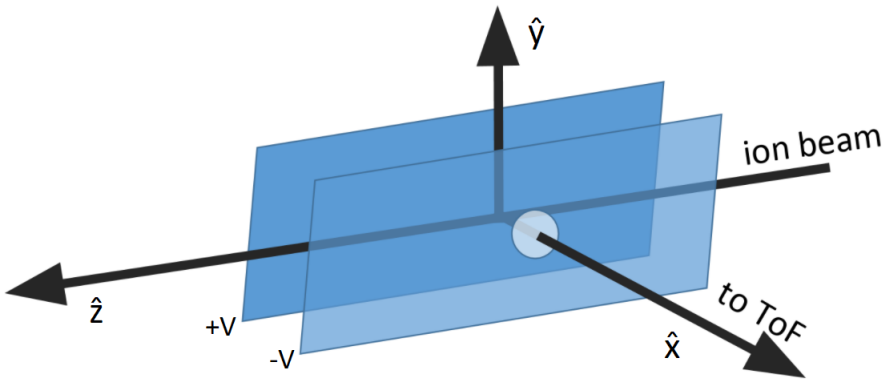

Figure 7: 3D representation of the extraction region in the CHEOPS setup. An ion beam pulse comes in from the z direction. Ionized target particles created by a charge exchange collision between the projectile ions and the target gas particles are extracted in the x direction. The extraction plates posses opposite voltages with respect to each other such that the potential in the centre is 0 V.

The ion beam pulses come in from the z direction and pass through the collision region. The two plates (or electrodes) are positioned on either side of the beam to generate a (near) homogeneous field to extract target ions from the collision region. The plate that does not contain the diaphragm seen at the left side of the extraction region in figure 6 and seen in the back in figure 7 is operated on a charge of +20 V. The plate containing the diaphragm seen at the right side of the extraction region in figure 6 and seen in front in figure 7 is on a voltage of -20 V. The charges on the plates creates an approximately uniform electric field which guides positively charged ions in positive x direction towards the plate with the diaphragm that serves as entrance to the time of flight spectrometer. The ionized particles created in front of the diaphragm can be transmitted through this diaphragm. The projectile ions themselves feel the same electric field. However, due to their high velocity their presence in the extraction region is brief. Hence the effect of the electric field on these ions is minimal. Behind the diaphragm lies the time of flight spectrometer. This consists of a number of electrostatic lenses which focus the ionized particles created by the charge exchange collisions that are transmitted through the diaphragm towards the end where the ions will be counted and their arrival time registered. [15] [17] [18]

3.2.4 MCP

At the end of the time of flight spectrometer of the CHEOPS setup explained in section 3.2.3 the ions need to be registered. The intensity of the ions coming in is very low hence a very sensitive ion detector is needed to count the ions accurately. The type of detector used in the CHEOPS setup is a MicroChannel Plate also referred to as MCP. A MicroChannel Plate is a thin disc in which many microchannels are present that will allow ions to enter. The diameter of such a microchannel is in the range 10-100 μm. These microchannels lie nearly parallel to the direction of motion of the ions, but have a slight angle with it such that an ion that enters one of these microchannels will inevitably hit the wall of the microchannel. A MicroChannel Plate is usually fabricated from a lead glass that is treated in such a way that upon a collision with a particle, electrons are released. These electrons in their turn will travel further through the microchannel and will in all likelihood collide with the wall of the channel at a later time. This collision will again release electrons. The process will repeat several times, increasing the number of electrons in the tube and hence increasing the signal strength. Between the front- and the backside of the MCP there is a potential difference applied. This will guide the produced electrons to the back of the MicroChannel Plate. The MicroChannel Plate's main purpose is to amplify the signal such that it is more easily detectable. Behind the MicroChannel Plate the pulse of electrons is registered by dedicated electronics. Note that it is not possible to know what kind of particle triggered the detection. [19] [20]

In figure 8a a MicroChannel Plate is visualized. In figure 8b the microchannel is enlarged and the electron multiplication process is shown.

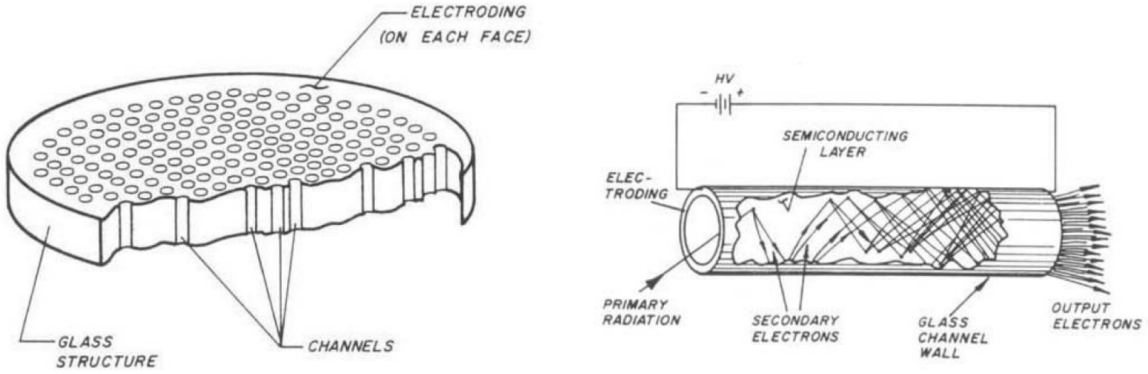

(a) MicroChannel Plate

(b) Microchannel multiplication.

Figure 8: Figure 8a shows a MicroChannel Plate containing many microchannels. The diameter of a microchannel is in the range 10-100 μm. The microchannels lie nearly parallel to the direction of motion of the ions, but have a slight angle with it such that an ion that enters one of these microchannels will inevitably hit the wall of the microchannel. In each microchannel an electron multiplication process can occur seen in figure 8b. [19]

3.3 Physics related to CHEOPS

3.3.1 Molecular hydrogen levels

ASML is mainly interested in energetic positively charged ions reacting with H_2 molecules. Lets consider a gas chamber full of H_2 molecules and let a beam of positively charged energetic ions pass through it. On an individual level some of these incoming energetic projectile ions interact with the H_2 molecules described by the COBM (section 3.1). This interaction causes a charge exchange collision, which ionizes the H_2 molecules. H_2 molecules can be ionized into several energy levels. Not all of these energy levels are stable and the ionized H_2 molecule can decay into its atomic H sub particles. In figure 9 the energy levels of neutral and ionized H_2 are shown.

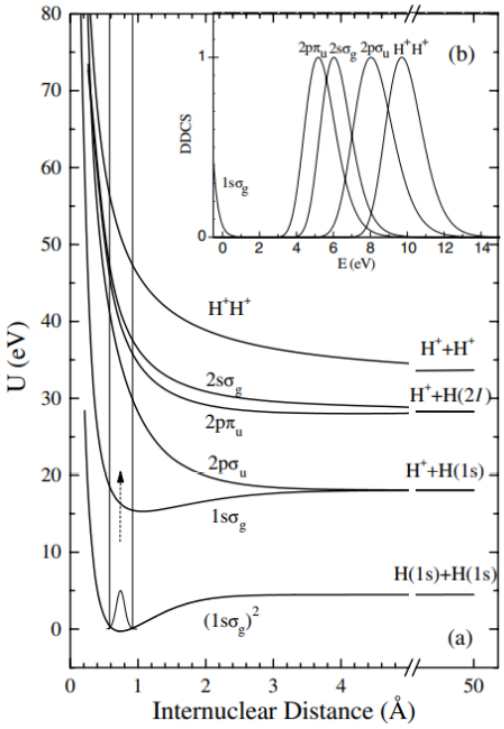

Figure 9: Potential energy levels for H_2 molecules and its ionized levels. The potential energy U is plotted on the y-axis in eV and the internuclear Distance is plotted on the x-axis in Ångström. On the right of each energy level it is stated what ionized level the level corresponds to. The potential curves that do not exhibit a well structure will decay into atomic H or H^+ particles. The energy released during the decay process will be transferred in the form of kinetic energy to the H or H^+ particles. In the upper right corner of the graph, normal distributions of half of the decay energy of each energy level is given, corresponding to the energy each of the two decay fragments receives. [21]

H_2 molecules that are ionized by the projectile ion will be excited to one of the ionized levels following the Franck-Condon principle. This principle states that during the electronic transition, the inter nuclear distance remains the same. Either one or two electrons can be captured by the projectile ion. When two electron capture occurs there is only 1 possible energy level to which the H_2 molecule can be excited. This is the highest energy level seen in figure 9. This level is repulsive and will decay immediately into two H^+ ions. Both of these H^+ ions will each have a kinetic energy of about 9.7 eV due to the energy released by the decay process. When only one electron is captured by the projectile ion there are multiple levels to which the H_2 molecule can be excited. The lowest energy level that it can be excited to is $1s\sigma_g$. This energy level is stable and the H_2 molecule can keep itself together in the form of H_2^+. Due to quantum uncertainty it is still possible for this H_2^+ ion to decay into a H^+ ion and a H atom. These two decay products will posses almost no kinetic energy. The other three energy levels the H_2 molecule can be excited to after one

electron capture are repulsive and will decay immediately into a H^+ ion and a H atom. In the upper right corner of figure 9, normal distributions of half of the decay energies of each of these energy levels is given, corresponding to the energy a single fragment receives. [16] [17] [21]

3.3.2 Transmission

After two electron capture an ionized H_2 molecule decays into two H^+ ions referred to as an ion pair. Each ion of this ion pair possesses a kinetic energy of about 9.7 eV, giving them an initial velocity v_0 in a random direction. The initial velocity v_0 can be calculated from the kinetic energy with the following equation

$$v_0 = \sqrt{\frac{2U_i}{m}} \tag{12}$$

Here U_i is the initial kinetic energy of the ion and m is the mass of the ion. The whole system is bound to conserve momentum, hence the ions in an ion pair are always emitted with a 180° difference with respect to each other. The H^+ ions are created in the centre of an extraction region where an extraction field is present. The ions will be accelerated towards the diaphragm in the side of the extraction region. A 2D representation of the trajectories of H ions in a extraction region is visualized in figure 10. [18]

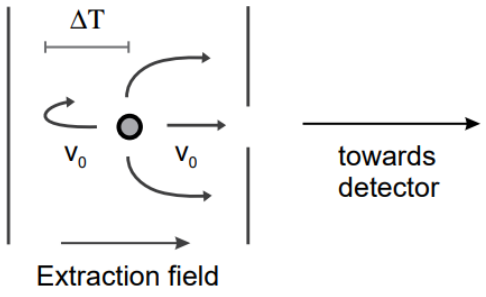

Figure 10: 2D representation of the extraction region in a TOF extraction setup. Positive ions are created in the centre between the extraction electrodes with an initial velocity v_0 in a random direction. The source of the ions is indicated by the grey dot. The electrode on the left side is positively charged and the one on the right is negatively charged. The approximately uniform electric field that this creates guides the positive ions towards the right. [18]

3.3.3 Time difference Δt

Due to the nature of the setup, only ion pairs that are emitted roughly in line with the diaphragm will be transmitted, represented by the horizontal arrows coming out of the point source in figure 10. Ion pairs that are not emitted in line with the diaphragm are represented by the vertical arrows coming out of the point source in figure 10. Instead of passing through the diaphragm, these ion pairs will hit the side plates and will not be transmitted. When an ion is emitted with a velocity component towards the side of the electrode with the diaphragm (towards the right as seen in figure 10), it is referred to as a forward emitted ion. The electric field will accelerate the forward emitted ion towards the diaphragm side. The forward emitted ions emitted in line with the diaphragm are transmitted through it. When an ion is emitted with a velocity component away from the diaphragm (towards the left as seen in figure 10), it is referred to as a backward emitted ion. The electric field in the extraction region will turn the backward emitted ion around. A backward emitted ion that is emitted in line with the diaphragm is transmitted through the diaphragm at a later time than its corresponding forward emitted ion. The difference in travel time to reach the diaphragm between the forward- and the backward emitted ion is represented by the term Δt. The value of Δt can be obtained by solving the following equation

$$\Delta t = \frac{\sqrt{8\mu U_{ker}}}{qE} \tag{13}$$

Here U_{ker} is the kinetic energy released in the decay process, E is the strength of the electric field the ions are in, q is the charge of each ion (which for H^+ ions is equal to 1) and the term μ is given by

$$\mu = \frac{m_1 m_2}{m_1 + m_2} \tag{14}$$

Where m_1 and m_2 correspond to the masses of the two ions. Note that equation 13 assumes an ion pair perfectly emitted in line with the diaphragm. In real world measurements and in SIMION simulations, ions that have a slight deviation from a perfectly in line emitted ion pair will also be transmitted through the diaphragm. This will give these ions a slightly lower average travel time difference Δt than the value calculated with equation 13. [18]

3.3.4 Transmission ratio

As previously mentioned, not all of the ions created between the electrodes will be transmitted through the diaphragm. Most of the ions will in fact hit the walls. Hence, it is useful to determine a transmission ratio that describes the number of ions that are transmitted through the diaphragm compared to the total number of ions that are created. There are two main factors governing the position of the ions over time. The initial velocity v_0 and the Coulomb force acting on the ions due to the electric field in the extraction region. Lets first consider an ion that is created with a velocity v_0 in a random direction without it being acted on by an electric field. All the possible positions this ion can be located at after a certain time t can be described by the boundary of a sphere that grows over time with a radius of $r = v_0 * t$. If one now applies a uniform electric field on this ion, it will feel a Coulomb force. This force will accelerate the ion with an acceleration of

$$a = \frac{qE}{m} \tag{15}$$

Here E is the strength of the uniform electric field, m the mass of the ion and q the charge of the ion. Considering both the starting velocity v_0 and the electric field acting on the ion, all the possible positions the ion can be located at at a certain time t can be described by a sphere that is accelerating with an acceleration of $a = \frac{qE}{m}$ and that grows over time with a radius of $r = v_0 * t$. In figure 11 a 2D representation of all the possible positions of an ion created in the extraction region accelerated towards the diaphragm is shown for different times t.

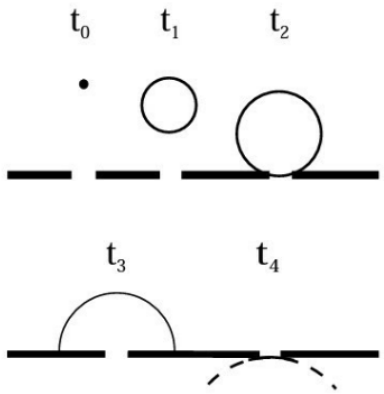

Figure 11: 2D representation of the possible positions of an ion originating from a point in the extraction region. The ion is created at t_0 with an initial velocity v_0 in a random direction. The ion is accelerated in uniform magnetic field towards the diaphragm. In each of the time steps, the boundary of sphere drawn as a circle corresponds to all possible positions the ion can be located at at that time step. The sphere is accelerating with an acceleration of $a = \frac{qE}{m}$ towards the diaphragm and that grows over time with a radius of $r = v_0 t$. [18]

Considering a point source from which ions are emitted, the transmission ratio of forward- and backward emitted ions can be determined as a function of the radius of the diaphragm r_d, the distance between the source and the end of the diaphragm D, the ion acceleration a and the starting velocity v_0. Note that the acceleration a can be calculated with equation 15. In figure 12 a schematic 2D representation of the times at which forward- and backward emitted ions are transmitted is shown.

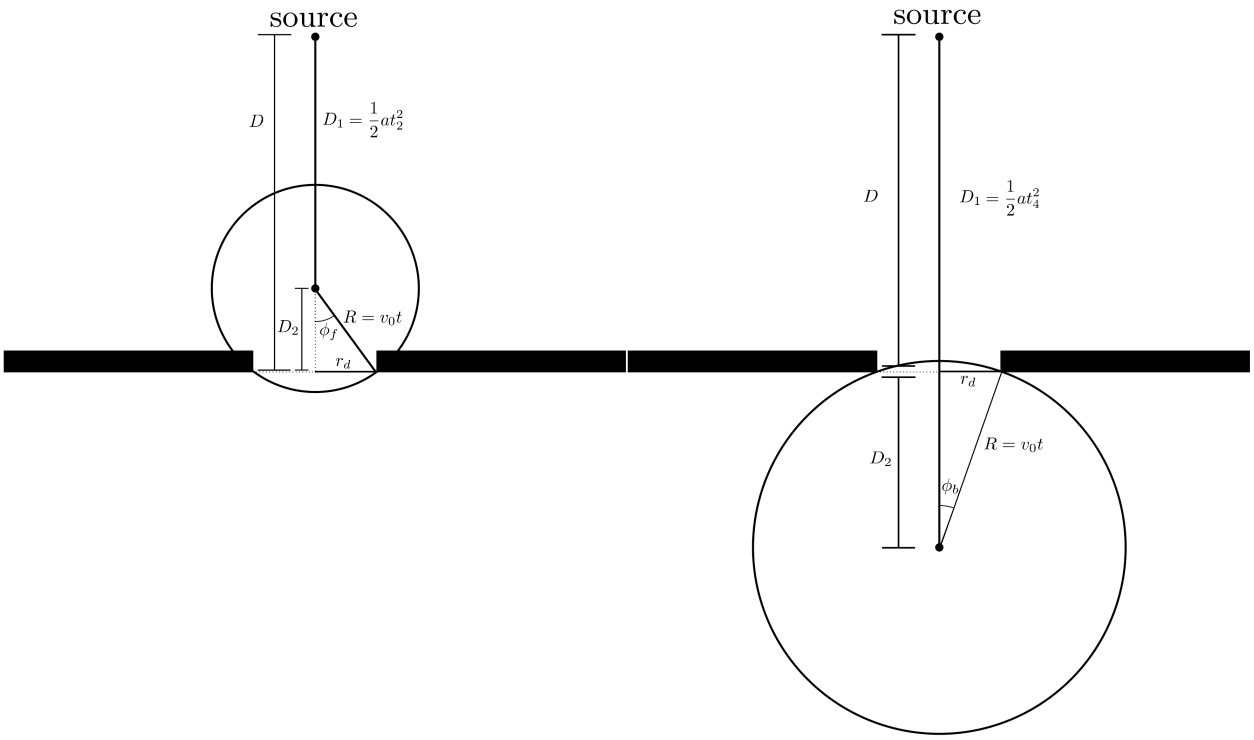

(a) Situation at t_2 **(b)** Situation at t_4

Figure 12: 2D representation of the possible positions of an ion created in the point source on the top of both figures with an initial velocity v_0 in a random direction. The ion is accelerated in uniform electrostatic field towards the diaphragm. The part of the circle that passes through the diaphragm correspond to the transmitted ions. Figure 12a shows the situation at t_2 seen in figure 11, The part of the circle passing through the diaphragm at this time represent the forward emitted ions. Figure 12b shows the situation at t_4 also seen in figure 11, here the part of the circle passing through the diaphragm at this time represent the backward emitted ions. In 3D the circle will become a sphere instead.

Figure 12a shows the situation at t_2 from figure 11, this is the time at which forward emitted ions are transmitted. Figure 12b shows the situation at t_4 from figure 11, this is the time at which backward emitted ion are transmitted. D_1 represents the distance traveled due to the constant acceleration of the ion in the electric field E and it is given by $D_1 = \frac{1}{2}at^2$. R is the radius of the sphere at time t which is equal to the the distance traveled due to the initial velocity v_0. It is given by $R = v_0t$. D_2 is the vertical component of R and is given by $D_2 = cos(\phi)R$. ϕ_f and ϕ_b are the acceptance angles for the forward- and the backward emitted ions respectively. r_d is the radius of the diaphragm.

In the case of forward emitted ions, the distance from the point source to the end of the diaphragm can be expressed in terms of the initial velocity of the particle v_0, the time t_2 and the acceleration of the ion a as follows

$$D = D_1 + D_2 = \frac{1}{2}at_2^2 + cos(\phi_f)v_0t_2 \tag{16}$$

The same can be done for backward emitted ions at time t_4 seen in figure 12b as follows

$$D = D_1 - D_2 = \frac{1}{2}at_4^2 - cos(\phi_b)v_0t_4 \tag{17}$$

The acceptance angles ϕ_f and ϕ_b can in their turn be expressed in terms of the radius of the diaphragm r_d, the initial velocity v_0 and the time t_2 or t_4 in the following way

$$\phi_f = arcsin\left(\frac{r_d}{v_0 t_2}\right) \tag{18}$$

$$\phi_b = arcsin\left(\frac{r_d}{v_0 t_4}\right) \tag{19}$$

By substituting ϕ_f and ϕ_b into equation 16 and equation 17, it is possible to solve for t_2 and t_4. Substituting t_2 and t_4 back into equation 18 and equation 19, ϕ_f and ϕ_b can be determined.

Knowing the acceptance angles ϕ_f and ϕ_b, it is possible to determine the transmission ratios for the forward- and backward emitted ions. This is done by taking the area of a spherical cap with either the acceptance angle ϕ_f or ϕ_b and radius R and dividing that by the area of half a sphere with radius R. The are of the spherical cap corresponds to the fraction of the sphere that contains either the forward- or backward emitted ions that are transmitted through the diaphragm and the area of half the sphere corresponds to all the forward- or backward emitted ions that were emitted in total. Dividing the two will hence give the transmission ratio. The area of a spherical cap on a sphere with radius R and angle ϕ is given by

$$A = 2\pi R^2(1 - cos(\phi)) \tag{20}$$

The area of half a sphere with radius R is given by

$$V = 2\pi R^2 \tag{21}$$

Dividing equation 20 by equation 21 gives the following equation for the transmission ratio κ

$$\kappa = (1 - cos(\phi)) \tag{22}$$

The acceptance angles ϕ_f and ϕ_b can be substituted in equation 22 to determine the transmission ratios for the forward- and backward emitted ions respectively. These transmission ratios can also be expressed as a transmission percentage by multiplying the ratio times 100. [18]

3.3.5 t_0 correction

The time of flight values that follow from a lab experiment with the CHEOPS setup are counted as the time difference between the moment the projectile beam is chopped and the moment the H^+ or H_2^+ particle is counted at the MCP. It is much more accurate to represent the time of flight as the time difference between the moment that the H_2 molecule is ionized after a charge exchange collision and the moment an H^+ or H_2^+ particle is counted at the MCP. To obtain the true time of flight values, the time between the chopping of the beam and the ionisation of the H_2 molecule has to be subtracted from the total time of flight values. In figure 13 an example time of flight spectrum is given. In this figure the time between the chopping of the beam and the ionisation of the H_2 molecule is indicated as t_0. The time between the moment of a possible creation of a H^+ ion and the moment this H^+ ion reaches the MCP is indicated as t_1^*. The time between the moment of a possible creation of a H_2^+ ion and the moment this H_2^+ ion reaches the MCP is indicated as t_2^*. [17]

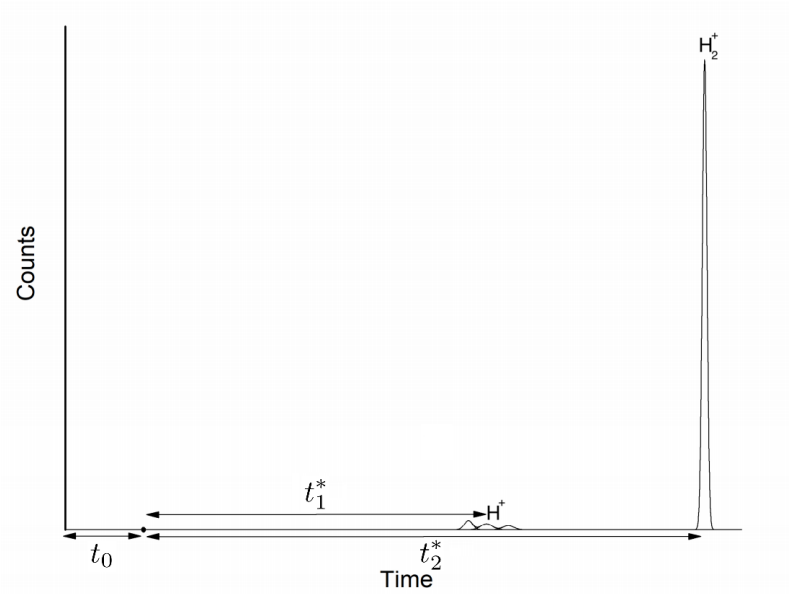

Figure 13: Example time of flight spectrum of a general lab experiment. The time between the moment of a possible creation of a H^+ ion and the moment this H^+ ion reaches the MCP is indicated as t_1^*. The time between the moment of a possible creation of a H_2^+ ion and the moment this H_2^+ ion reaches the MCP is indicated as t_2^*. [17]

The time between the chopping of the beam and the moment the created H^+ ion reaches the MCP is indicated as t_1. The time between the chopping of the beam and the moment the created H_2^+ ion reaches the MCP is indicated as t_2. The values of t_1 and t_2 can be related to the values of t_1^* and t_2^* with the following relations

$$t_1 = t_1^* + t_0 \tag{23}$$

$$t_2 = t_2^* + t_0 \tag{24}$$

The ratio of t_1^* and t_2^* can be represented as

$$\frac{t_2^*}{t_1^*} = \sqrt{\frac{m_2}{m_1}} = \sqrt{2} \tag{25}$$

with equation 23, 24 and 25, the value of t_0 can be determined by

$$t_0 = \frac{\sqrt{2}t_1 - t_2}{\sqrt{2} - 1} \tag{26}$$

[17]

3.4 SIMION model

3.4.1 SIMION software

SIMION is an easy to run software package that can simulate charged particles moving through either electric or magnetic fields. A 3D model of electrodes, magnets and walls can be build in SIMION that resembles a setup in the real world. Particles can be simulated moving in this model and their behavior can be studied. For this report SIMION is used to simulate H^+ and H_2^+ particles in the CHEOPS setup discussed in section 3.2.3.

3.4.2 CHEOPS setup SIMION model

A 3D model of the CHEOPS setup was made in SIMION. A 2D representation of this model is shown in figure 14. The model consists of extraction electrodes, acceleration lenses and the drift tube towards the detector (only the first part of the tube is shown in figure 14). In the actual CHEOPS setup, ion beam pulses are send through the extraction region. The extraction region itself is filled with gas. The ion beam consists of many projectile ions of the same type. The gas consists of many individual target particles. On an individual level some of these incoming energetic projectile ions undergo a charge exchange collision with the gas target particles. This charge exchange collision can ionize the gas particles. For the present experiment H_2 is the gas of choice. When these H_2 particles are ionized completely they will fragment into H^+ ions with a kinetic energy of about 9.7 eV (section 3.3.1). In the SIMION model the trajectory of such 9.7 eV H^+ ions is traced. The kinetic energy gives the ions a velocity v_0 in a random direction. Within the extraction region an approximately uniform electric field is simulated. This is done by electrically charging the left electrode with a charge of +20 V and the right electrode with a charge of -20 V. The electric field that is produced between the electrodes guides positively charged H^+ ions towards the right electrode in which a diaphragm is located. Behind the diaphragm lies the time of flight spectrometer. This consists of a number of electrostatic lenses focus the H^+ ions that are transmitted through the diaphragm towards the MCP at the end of the time of flight spectrometer. With the SIMION model it is possible to simulate the flight paths of many individual ions in the CHEOPS setup.

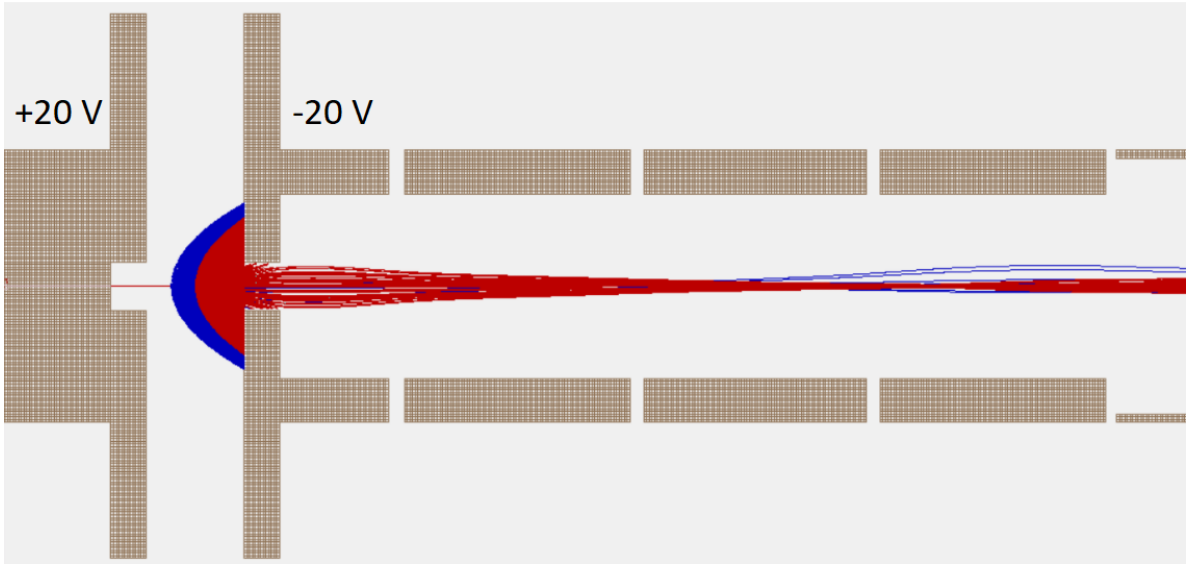

Figure 14: 2D representation of the CHEOPS setup model made in SIMION. Each brown square represents an area of 0.1 mm by 0.1 mm. On the left side of the figure the extraction region can be seen. Here ions are created with a kinetic energy giving them a velocity v_0 in a random direction. In the extraction region ions are subject to an approximately uniform electric field. This electric field guides the ions to the side of the extraction region where a diaphragm is located. Behind the diaphragm lies the time of flight spectrometer which consists of a number of electrostatic lenses focusing the ion beam toward the MCP at the end of the time of flight spectrometer.

3.5 Peak broadening processes

In a perfect world delta peaks would be seen in the time of flight spectra of the CHEOPS setup. The delta peaks would correspond to all the different types of reaction products produced after charge exchange collisions between the projectile ions and H_2 molecules. It will be delta peaks because all reaction products of the same type are expected to obtain exactly the same amount of kinetic energy and hence arrive at exactly the same time at the MCP. This perfect world assumes that there are no processes that can cause the peaks to broaden. In the real world there are however non perfect conditions that may lead to peak broadening in the time of flight spectra. Some of these non perfect conditions are discussed and elaborated in this section. This to explain some of the discrepancies that are seen between lab measurements and the SIMION simulations.

One thing that leads to peak broadening is the fact that not all reaction products produced after a charge exchange collisions between the projectile ions and H_2 molecules are created exactly in the centre of the extraction region in a lab experiment. In a lab experiment a projectile ion beam pulse passes through the extraction region of the CHEOPS setup. The projectile ions in this beam pulse can undergo charge exchange collisions with H_2 molecules over the entire length of their path through the extraction region. This means that ions created by these charge exchange collisions can be produced in a region that has a cylindrical shape with a length equal to the extraction region itself and a radius equal to the radius of the beam pulse. This peak broadening process can be accounted for in SIMION simulations by using a cylindrical source of ions as well. The ions emitted from this source will correspond to the ions created by the charge exchange collisions with H_2 molecules. For an accurate representation of a lab experiment, this cylindrical source needs to have the same diameter as the diameter of the beam. The length of the cylindrical source needs to be longer than the diameter of the diaphragm on the side of the extraction region. This length does not have to be taken equal to the length of the extraction region itself, since only the ions that can reasonably be transmitted through the diaphragm and reach the MCP are of interest. Ions that are produced relatively far away from the diaphragm can still have a path that allows them to be transmitted through the diaphragm, however these ions will be transmitted with such an angle out of the diaphragm that they will never be able to reach the MCP.

Another peak broadening process occurs due to the fact that reaction products produced after charge exchange collisions between the projectile ions and H_2 molecules can obtain a certain kinetic energy from the decay process of the ionized H_2 molecule. This energy gives these ions a velocity v_0 in a random direction. Due to the random nature of the emission direction, the x component of the velocity as seen in figure 7 is different in every case. This in combination with the fact that these reaction products can be produced at different locations in a cylindrical region in the extraction region allows reaction products with different velocity components in the x direction to be transmitted and counted at the MCP. Furthermore the energy that a certain type of reaction product obtains due to the decay of the ionized H_2 molecule is not absolute. As is explained in section 3.3.1, the energy released by the decay process of ionized H_2 molecules is distributed in a Gaussian. Not only the component in the x direction might differ in every case, also the total amount of kinetic energy obtained by the reaction products is different in every case. This will lead to even more peak broadening.

In section 3.1.4 it is discussed that when a H_2 molecule is ionized by undergoing a charge exchange collisions with a projectile ion, it will obtain a certain recoil energy. This recoil energy depends on how close the projectile and the ion approach each other given by the impact parameter b. This additional kinetic energy can give the ionized H_2 molecules a velocity in a random direction that is transverse to the direction of motion of the projectile ion. This also leads to a spread of the peaks seen in the time of flight spectra.

Till now it was assumed that the H_2 molecule gas particles are completely stationary. This is of course not the case. The gas particles move around in the extraction region depending on the temperature. Since the temperature in the lab setup is significantly above 0° K, the H_2 gas particles already posses a kinetic energy before the charge exchange collision has occurred. This background energy will also broaden the peaks in the time of flight spectra.

Lastly, there are some peak broadening processes that depend on the experimental setup itself. The first thing of the experimental setup that affects the peak widths is the bunch length of the ion beam pulse that

is created by the chopper sweeper system discussed in section 5. The bunch length is the time between the moments the first ion and last ion pass the diaphragm of the chopper sweeper system [16]. Reaction products produced by a charge exchange collision can be created anywhere within this beam pulse.

lets consider a beam pulse passing through the extraction region of the CHEOPS setup of a certain bunch length τ_c A reaction product can be created at a coordinate in the extraction region where the beam pulse passes. This can happen during the whole time the beam pulse takes to pass by. This means that reaction products can be created at a certain coordinate in the extraction region where the beam pulse passes at different times. The starting time of a reaction product that moves through the CHEOPS setup is thus not the same every time and the peak widths in the time of flight spectra broaden as a result. Another peak broadening process occurs due to the time uncertainty in the detector and its electronics [16]. The detector might be inconsistent in the time to process the counts which may also lead to peak broadening.

In the SIMION simulations some of these non perfect conditions can be accounted for by for example using a cylindrical shaped source instead of particles that are emitted perfectly in line with the diaphragm. However, there are much more processes that lead to peak broadening that can not be accounted for in SIMION simulations but that are present in lab measurements. These processes will inevitably lead to differences in the peak widths between time of flight data obtained with a lab experiment and time of flight data obtained with a SIMION simulation.

4 Results

In this chapter the results for 1 and 10 keV Sn^{5+} colliding on H_2 molecules are discussed as showcases to illustrate the basic results. Additional results for 0.1 keV Sn^{5+} as well as for 1 and 5 keV/amu He^{2+} are available in the appendix.

4.1 One electron capture

4.1.1 Recoil momentum distributions

With the Classical Overbarrier Model or COBM for short, The transverse momentum and recoil energy are calculated for the charge exchange collisions between projectiles and targets. This is done with the equations discussed in section 3.1. To make the process of solving the equations for countless input parameters feasible, programming language has to be used to run a script to solve the calculations. For the results in this report the programming language Python is used. The projectile- and target particles studied in this report are tin (Sn) or helium (He) ions as the projectile particles and molecular hydrogen (H_2) as the target particles. The Sn projectile in question is of the isotope ^{120}Sn. The report mostly discusses the results with Sn ions as the projectile. The results with He ions will be added in the appendix.

First lets look at one electron capture during a charge exchange collision described by the COBM. The transverse momentum transferred to a H_2 molecule is calculated as a function of the impact parameter b with equation 9. Recall that the transverse momentum transfer is induced by the repulsive Coulomb force perpendicular to the direction of motion of the projectile due to the charges involved according to the Classical Overbarrier Model as stated in section 3.1.4. The transverse momentum transfer is calculated for 3 different energies of $^{120}Sn^{5+}$ projectiles undergoing a charge exchange collision with H_2 molecule targets. The projectile energies studied are 0.1 keV, 1 keV and 10 keV. Figure 15 shows the graphs for the transverse momentum as a function of the impact parameter b in the case of one electron capture. Only the plots for the projectile energies of 1 keV and 10 keV are shown. The graph for 0.1 keV $^{120}Sn^{5+}$ and the graphs for the case of He projectile ions are found in the appendix.

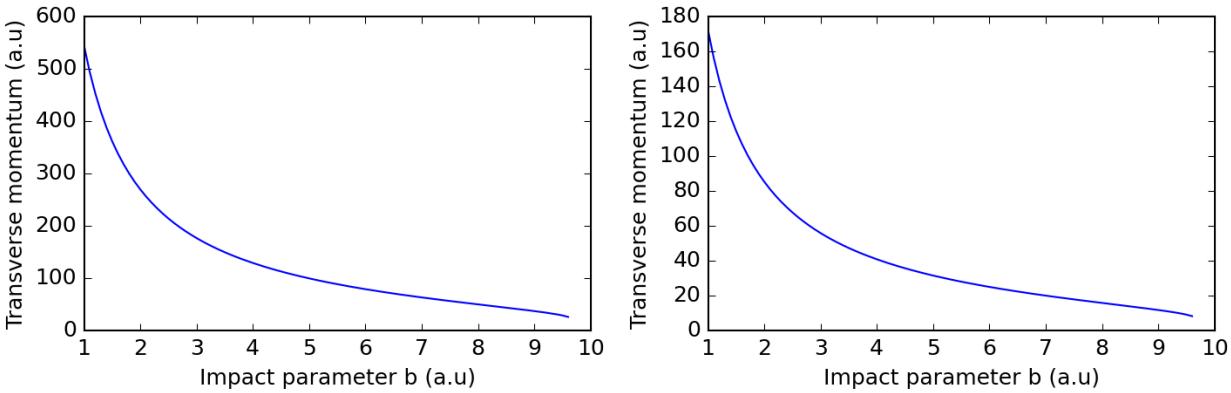

(a) $^{120}Sn^{5+} + H_2$ 1keV **(b)** $^{120}Sn^{5+} + H_2$ 10keV

Figure 15: Transverse momentum as a function of the impact parameter b for one electron capture.

It can be seen that the transverse momentum transferred to the H_2 molecule decreases exponentially as the impact parameter b increases. In the case of a higher energy projectile of 10 keV, it can be seen that the overall transverse momentum transfer is lower than that for the lower energy projectile of 1 keV.

To get a better insight in which of the transverse momenta transferred to the target in figure 15 is most likely to be seen in the charge exchange collision, the transverse momentum distribution is determined. The intensity of the possible transverse momenta for a certain impact parameter b relates to the reaction cross section σ as stated in section 3.1.4. The transverse momentum distribution is obtained by plotting the transverse momenta determined with equation 9 and plotting it against its corresponding intensity determined with equation 10. The intensity is normalized to give the maximum intensity a value of 1. The transverse momentum distributions in the case of one electron capture with 1 keV and 10 keV $^{120}Sn^{5+}$ projectiles colliding on H_2 molecules are given in figure 16. The graph for 0.1 keV $^{120}Sn^{5+}$ and the graphs for the case of He projectiles are found in the appendix.

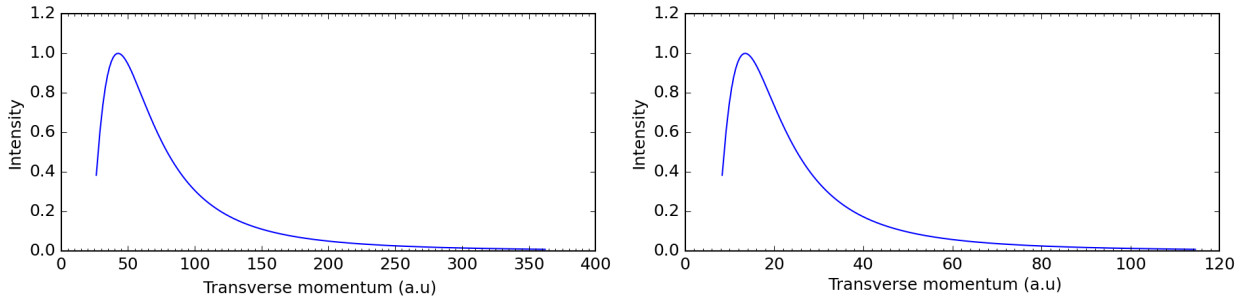

(a) $^{120}Sn^{5+}$ on H_2 1keV

(b) $^{120}Sn^{5+}$ on H_2 10keV

Figure 16: Transverse momentum distribution for one electron capture.

It can be seen that there is a clear peak in intensity for a particular transverse momentum. This peak corresponds to the most likely transverse momentum transferred to the target after a charge exchange collision. In the case of a 1 keV $^{120}Sn^{5+}$ projectiles, this peak lies at about 40 atomic units of momentum. In the higher energy case of a 10 keV $^{120}Sn^{5+}$ projectiles, it can be seen that this peak lies at a lower value of about 12 atomic units of momentum.

4.1.2 Angular distribution

Due to the Coulomb force acting on both the projectile and the target during the interaction, the flight path of the projectile ion will be altered. The angle between the original flight path and the new flight path can be calculated as discussed in section 3.1.4. In figure 17 the angular distribution is shown in the case of one electron capture, calculated for a 1 keV- and a 10 keV $^{120}Sn^{5+}$ projectiles. The graph for 0.1 keV $^{120}Sn^{5+}$ and the graphs for the case of He projectiles are found in the appendix.

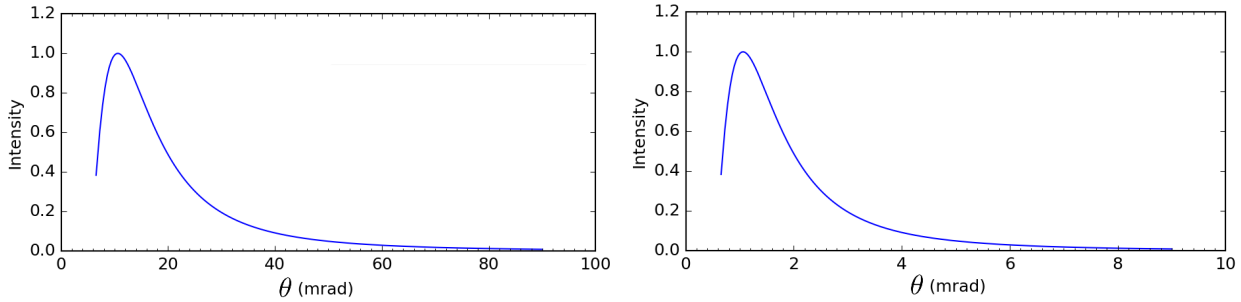

(a) $^{120}Sn^{5+}$ on H_2 1keV

(b) $^{120}Sn^{5+}$ on H_2 10keV

Figure 17: Angular distribution of the projectile ions for one electron capture in mrad.

It can be seen that there is a clear peak in intensity for a particular angle just as is seen for the momentum distributions. This peak corresponds to the most likely angle between the projectiles original flight path and their new flight path after a charge exchange collision. In the case of a 1 keV $^{120}Sn^{5+}$ projectile, this peak lies at about 10 mrad. In the higher energy case of a 10 keV $^{120}Sn^{5+}$ projectile, it can be seen that this peak lies at a lower value of about 1 mrad.

4.1.3 Recoil energy distributions

The transverse momentum that is transferred to the target particle can also be expressed in terms of kinetic energy as discussed in section 3.1.4. This kinetic energy is referred to as the recoil energy. To get an insight in how much recoil energy is transferred to a target, the recoil energy transferred to targets is calculated with equation 12. Figure 18 shows the graphs for the recoil energy as a function of the impact parameter b in the case of one electron capture. Only the plots for the projectile energies of 1 keV- and 10 keV $^{120}Sn^{5+}$ projectiles undergoing a charge exchange collision with H_2 molecule targets are shown. The graph for 0.1 keV $^{120}Sn^{5+}$ and the graphs for the case of a He projectiles are found in the appendix.

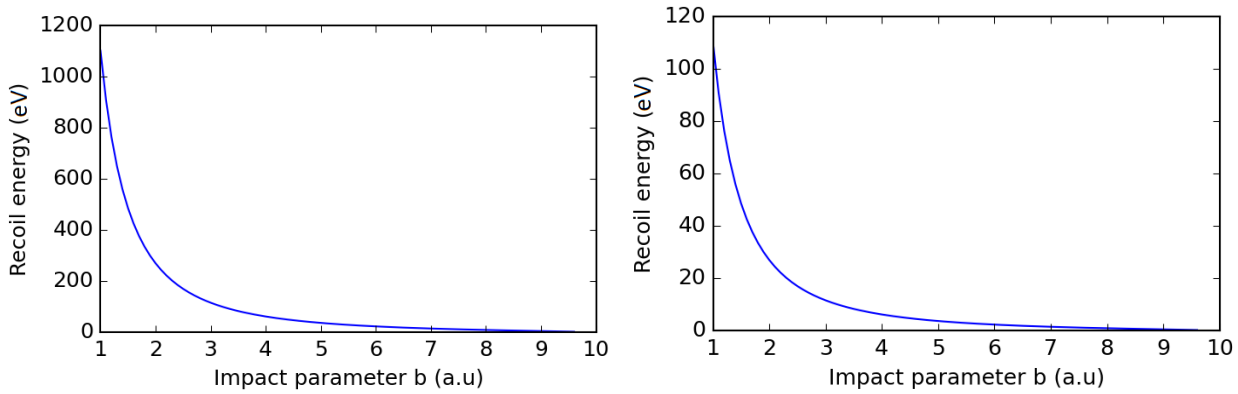

(a) $^{120}Sn^{5+}$ + H_2 1keV **(b)** $^{120}Sn^{5+}$ + H_2 10keV

Figure 18: Recoil energy as a function of the impact parameter b for one electron capture.

It can be seen that the recoil energy transferred to the H_2 molecule target decreases exponentially as the impact parameter b increases. This is also seen for the transverse momentum in figure 15. In the case of a higher energy projectile of 10 keV, it can be seen that the recoil energy is overall lower than that for the lower energy projectile of 1 keV.

Similarly as for the transverse momenta transferred to the target particles, a recoil energy distribution is plotted to get an idea of which recoil energy is likely to be seen in a charge exchange collision. The recoil energy distribution is obtained by plotting the intensity as a function of the recoil energy derived from the transverse momentum transfer with equation 12. This intensity is derived from the intensity of the transverse momentum transfer obtained with equation 10, but has to be adjusted for the bin size change (section 3.1.4). The intensity is normalized to give the maximum intensity a value of 1. The recoil energy distributions of 1 keV- and 10 keV $^{120}Sn^{5+}$ projectiles undergoing a charge exchange collision with H_2 molecules are shown in figure 19. The graph for 0.1 keV $^{120}Sn^{5+}$ and the graphs for the case of a He projectiles are found in the appendix.

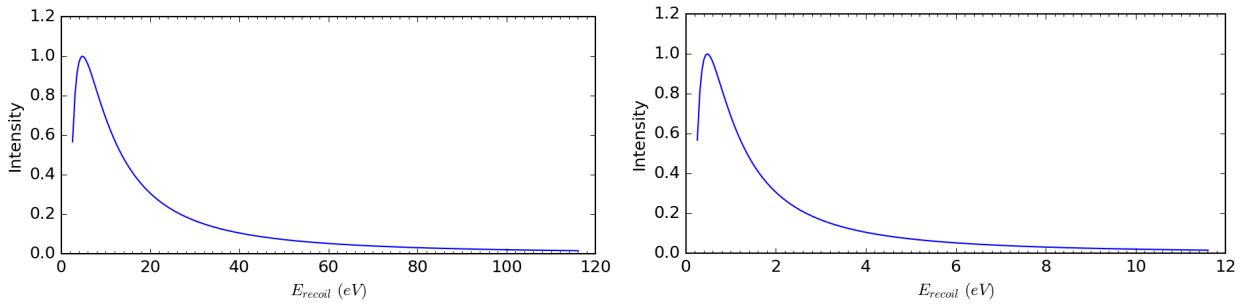

(a) $^{120}Sn^{5+}$ on H_2 1keV

(b) $^{120}Sn^{5+}$ on H_2 10keV

Figure 19: Recoil energy distribution for one electron capture.

It can be seen that there is a clear peak in intensity for a particular recoil energy. This peak corresponds to the most likely recoil energy the target obtains after a charge exchange collision. In the case of a 1 keV $^{120}Sn^{5+}$ projectile this peak lies at about 4 eV. In the higher energy case of a 10 keV $^{120}Sn^{5+}$ projectile, it can be seen that this peak lies at a lower value of about 0.4 eV.

4.1.4 Recoil as a function of projectile energy

To get an insight in the relation between the projectile energy and the recoil energy transferred to the target particle, the recoil energy of the peak intensity seen in in figure 19 is studied as a function of the projectile energy. This is done for several different different charge states of a Sn projectile of the isotope ^{120}Sn undergoing a charge exchange collision with a H_2 molecule. This is plotted in a log-log plot shown in figure 20

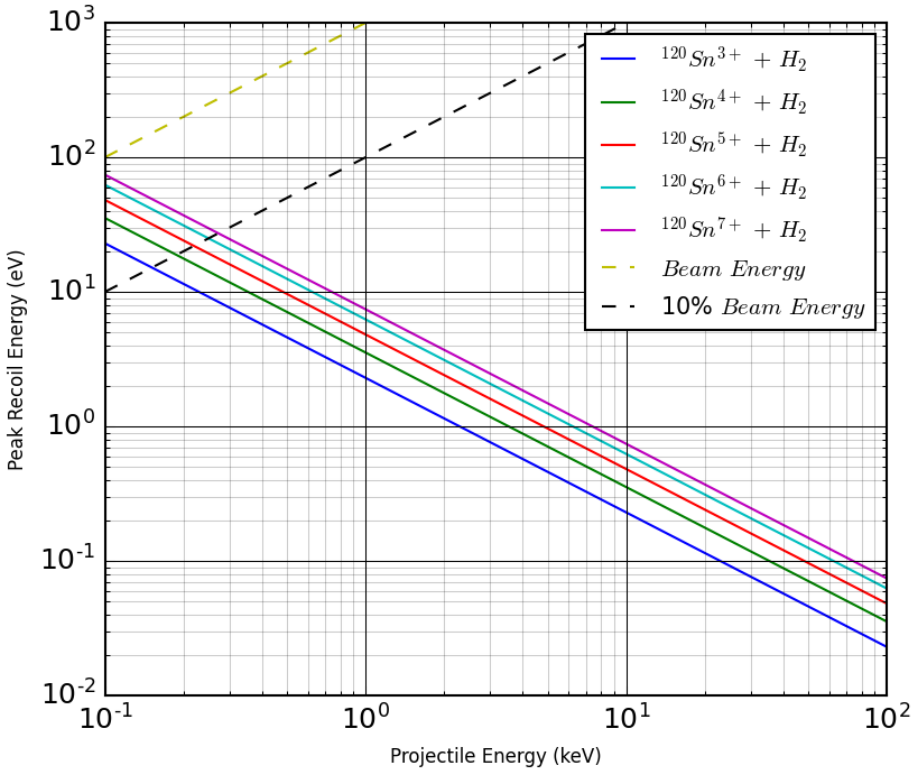

Figure 20: log-log plot of the peak position in the recoil energy distribution in eV as a function of the projectile energy in keV for one electron capture. The projectile ion is ^{120}Sn for several different charge states. The target particle is H_2.

It can be seen that the maximum in the recoil energy distribution decreases exponentially with the Sn projectile energy. The peak position gets lower when the positive charge of the Sn projectile is lower. In the upper left corner of the figure 2 additional dotted lines are plotted. The green dotted line corresponds to the projectile energy, the black dotted line corresponds to 10% of the projectile. If the recoil energy would get above the green dotted line, more energy would be transferred to the target than the projectile possesses to begin with. This is of course not feasible. The COBM assumes that the deviation from the flight path of the projectile ions due to the Coulomb force as well as the deviation of the target particle from its stationary position due to this same Coulomb force can be neglected in the time span of the charge exchange collision (see figure 2 and figure 3). However for really low energies, and hence low velocities, this assumption does not hold. The recoil energies calculated for very low projectile energies will not be accurate.

The relation between the projectile energy and the peak position can also be researched for other projectile- and target particles. The projectile is now taken to be He and the target is kept the same, namely H_2. The recoil energy of the peak intensity is again plotted as a function of the projectile energy. This is done for 2 different charge states of the He projectile. The plot is shown in figure 21

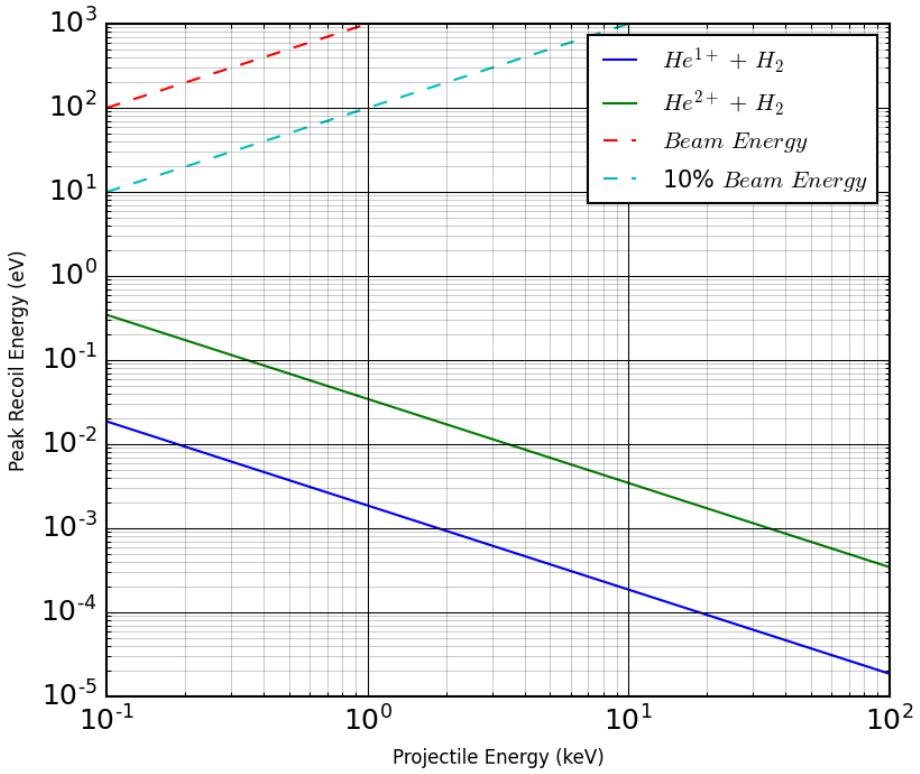

Figure 21: log-log plot of the peak intensity recoil energy in eV as a function of the projectile energy in keV in the case of one electron capture. The projectile ion is He for 2 different charge states. The target particle is H_2.

It can be seen that the recoil energy transferred to the H_2 molecule again decreases exponentially with the projectile energy. The overall peak recoil energy decreases when the positive charge of the He projectile is lower. The overall recoil energy transferred to the target is orders of magnitude lower in the case of a He projectile compared to a Sn projectile of the same kinetic energy. The Sn projectiles are much heavier than the He ions and thus their velocity is as well. This lower velocity implies a much longer interaction time to transfer momenta.

4.2 Two electron capture

4.2.1 Recoil momentum distributions

Now lets look at a charge exchange collision in which two electrons are captured. The projectiles and targets studied remain the same. Sn or He ions as the projectiles and H_2 molecules as the targets. The Sn projectiles in question are of the isotope ^{120}Sn. The results for He ions will be added in the appendix. For the two electron capture calculations, the transverse momentum transferred to the H_2 molecule is calculated as a function of the impact parameter b with equation 8. The transverse momentum transfer is again calculated for 3 different energies of $^{120}Sn^{5+}$ projectile ions. The projectile energies studied are 0.1 keV, 1 keV and 10 keV. Figure 22 shows the graphs for the transverse momentum as a function of the impact parameter b for two electron capture. Only the plots for the $^{120}Sn^{5+}$ projectile energies of 1 keV and 10 keV are shown. The graph for 0.1 keV $^{120}Sn^{5+}$ and the graphs for the case of He projectiles are found in the appendix.

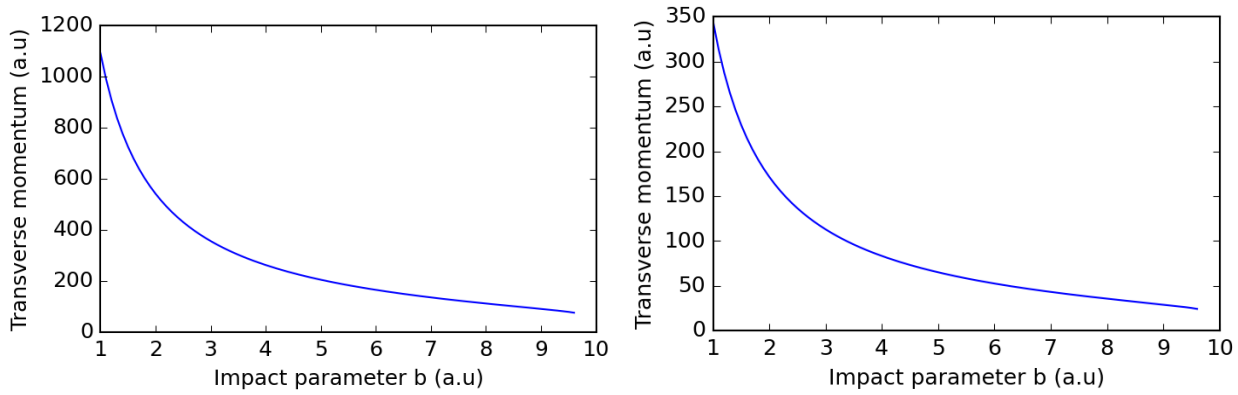

(a) $^{120}Sn^{5+} + H_2$ 1keV **(b)** $^{120}Sn^{5+} + H_2$ 10keV

Figure 22: Transverse momentum as a function of the impact parameter b for two electron capture.

It can be seen that the transverse momentum transferred to the H_2 molecule target decreases exponentially as the impact parameter b increases. This is the same as is seen for one electron capture. In the case of a higher energy projectile of 10 keV, it can again be seen that the overall transverse momentum transfer is lower than that for the lower energy projectile of 1 keV. The overall transverse momentum transferred to the H_2 molecule is higher by about a factor of 2 in the case of two electron capture compared to the one electron capture case.

To get an insight in which of the transverse momenta transferred to the target in the case of two electron capture is most likely, a transverse momentum distribution is determined. The transverse momentum distribution is obtained by plotting the transverse momenta determined with equation 8 and plotting it against its corresponding intensity. This intensity is determined by the probability of a particular transverse momentum to occur and is calculated with equation 10 as discussed in section 3.1.4. The intensity is normalized to give the maximum intensity a value of 1. The transverse momentum distributions for two electron capture with 1 keV and 10 keV $^{120}Sn^{5+}$ projectiles undergoing a charge exchange collision with a H_2 molecule targets are given in figure 23. The graph for 0.1 keV $^{120}Sn^{5+}$ and the graphs for the case of a He projectiles are found in the appendix.

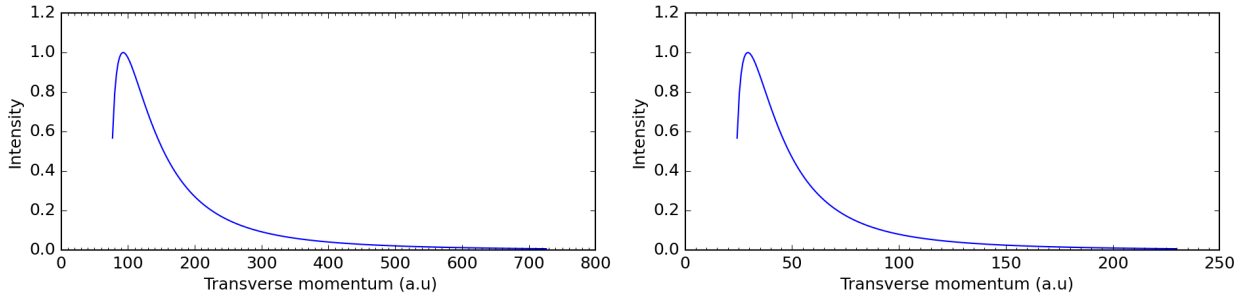

(a) $^{120}Sn^{5+}$ on H_2 1keV

(b) $^{120}Sn^{5+}$ on H_2 10keV

Figure 23: Transverse momentum distribution for two electron capture.

It can again be seen that there is a clear peak in intensity for a particular momentum, just like there is for one electron capture. This peak corresponds to the most likely transverse momentum transferred to the target after a charge exchange collision. In the case of a 1 keV $^{120}Sn^{5+}$ projectiles, this peak lies at about 90 a.u of momentum, which is about a factor two higher compared to the peak transverse momentum for one electron capture with this projectile energy. In the higher energy case of a 10 keV $^{120}Sn^{5+}$ projectiles, it can be seen that this peak lies at a lower value of about 28 a.u of momentum compared to the case of a 1 keV $^{120}Sn^{5+}$ projectiles. Compared to the one electron capture at this projectile energy, the peak transverse momentum is again about a factor two higher.

4.2.2 Angular distribution

In the case of two electron capture it also holds that due the the Coulomb force acting on both the projectile and the target during the charge exchange collision, the flight path of the projectile ion will be altered. The angle between the original straight-line trajectory and the new flight path can be calculated as discussed in section 3.1.4. In figure 24 the angular distribution is shown in the case of two electron capture for 1 keV- and 10 keV $^{120}Sn^{5+}$ projectiles colliding on H_2 molecules.

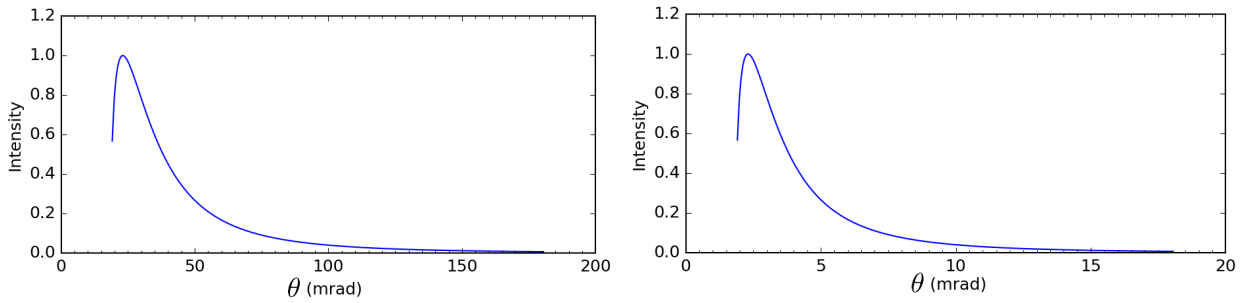

(a) $^{120}Sn^{5+}$ on H_2 1keV

(b) $^{120}Sn^{5+}$ on H_2 10keV

Figure 24: Angular distribution of the projectile ions for two electron capture in mrad.

.

It can be seen that there is again a clear peak in intensity for a particular angle, similarly as in the case of one electron capture. This peak corresponds to the most likely angle between the projectiles angle between the original flight path and the new flight path after a charge exchange collision. In the case of a 1 keV $^{120}Sn^{5+}$ projectile, this peak lies at about 45 milliradian. This is several times more than in the case of one electron capture with this projectile energy. In the higher energy case of a 10 keV $^{120}Sn^{5+}$ projectile, it can be seen that this peak lies at a value of about 4.5 milliradian. This is again several times more than in the case of one electron capture for this projectile energy. However it is about 10 times less compared to the case of 1 keV $^{120}Sn^{5+}$ projectile with two electron capture.

4.2.3 Recoil energy distributions

The transverse momentum that is transferred to the target is again expressed in terms of kinetic energy as discussed in section 3.1.4, but this time in the case of two electron capture. To get an insight in how much recoil energy is transferred to the target, the recoil energy transferred to the H_2 molecule is calculated with equation 12. Figure 25 shows the graphs for the recoil energy as a function of the impact parameter b for two electron capture. Only the plots for the projectile energies of 1 keV- and 10 keV $^{120}Sn^{5+}$ projectiles are shown. The graph for 0.1 keV $^{120}Sn^{5+}$ and the graphs for the case of a He projectiles are found in the appendix.

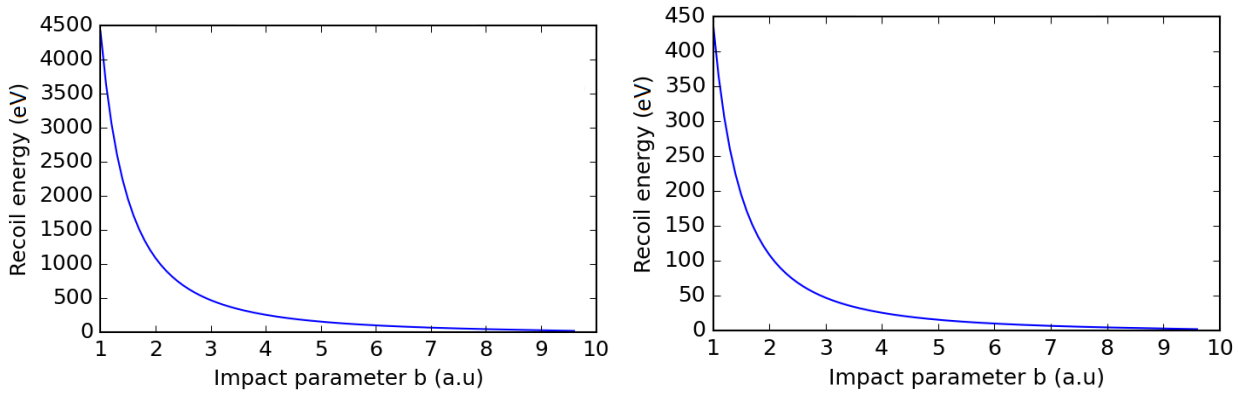

(a) $^{120}Sn^{5+} + H_2$ 1keV **(b)** $^{120}Sn^{5+} + H_2$ 10keV

Figure 25: Recoil energy as a function of the impact parameter b for two electron capture.

It can be seen that the recoil energy transferred to the H_2 molecule decreases exponentially as the impact parameter b increases, similar as for one electron capture. In the case of the higher energy projectile of 10 keV, the recoil energy is once again lower overall than that for the lower energy projectile of 1 keV. Compared to one electron capture, the overall recoil energy is higher.

The recoil energy distributions for two electron capture by 1 keV Sn^{5+} are shown in figure 26.

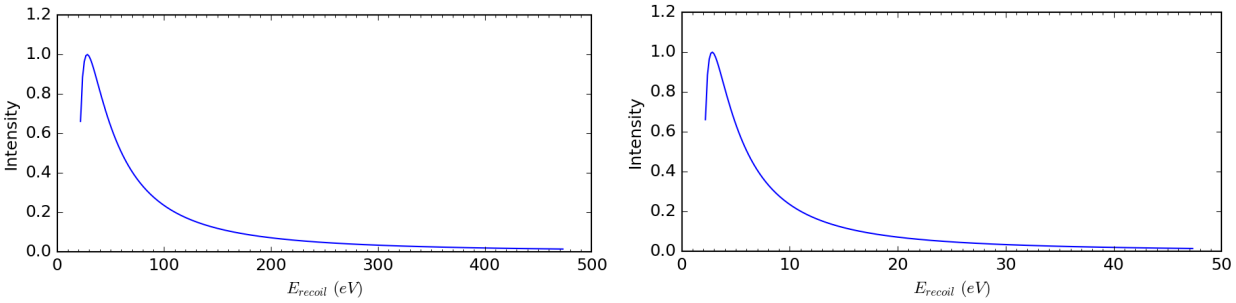

(a) $^{120}Sn^{5+}$ on H_2 1keV

(b) $^{120}Sn^{5+}$ on H_2 10keV

Figure 26: Recoil energy distribution for two electron capture.

It can be seen that, in the case of two electron capture, there is a clear peak in intensity for a recoil energy. This is the same as seen in the case of one electron capture. This peak corresponds to the most likely recoil energy the target obtains after a charge exchange collision. In the case of a 1 keV $^{120}Sn^{5+}$ projectile this peak lies at about 30 eV. In the higher energy case of a 10 keV $^{120}Sn^{5+}$ projectile, it can be seen that this peak lies at a lower value of about 3 eV. The peak intensities for two electron capture are orders of magnitudes higher compared to the case of one electron capture.

4.2.4 Recoil as a function of projectile energy

Figure 27 shows the most likely amount of recoil energy obtained by the H_2 molecule in the case of two electron capture by Sn ions in charge states of 3+ to 7+.

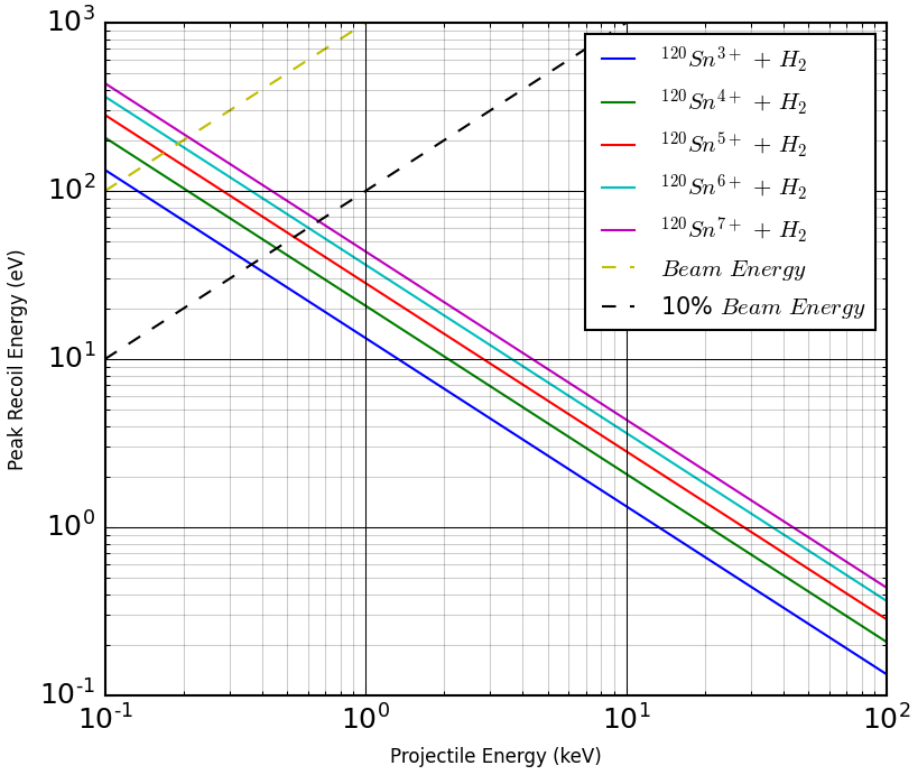

Figure 27: log-log plot of the peak intensity recoil energy in eV as a function of the projectile energy in keV for two electron capture. The projectile ion is ^{120}Sn for several different charge states. The target particle is H_2.

The trend is similar compared to the results of one electron capture. It can be seen that the peak intensity recoil energy transferred to the H_2 molecule decreases exponentially with the projectile energy. The overall peak intensity recoil energy decreases when the positive charge of the Sn projectile is lower. The overall peak intensity recoil energy transferred to the H_2 molecule target particle is approximately an order of magnitude higher than in the case of one electron capture.

Figure 27 shows the most likely amount of recoil energy obtained by the H_2 molecule in the case of two electron capture by He ions in charge state of 2+.

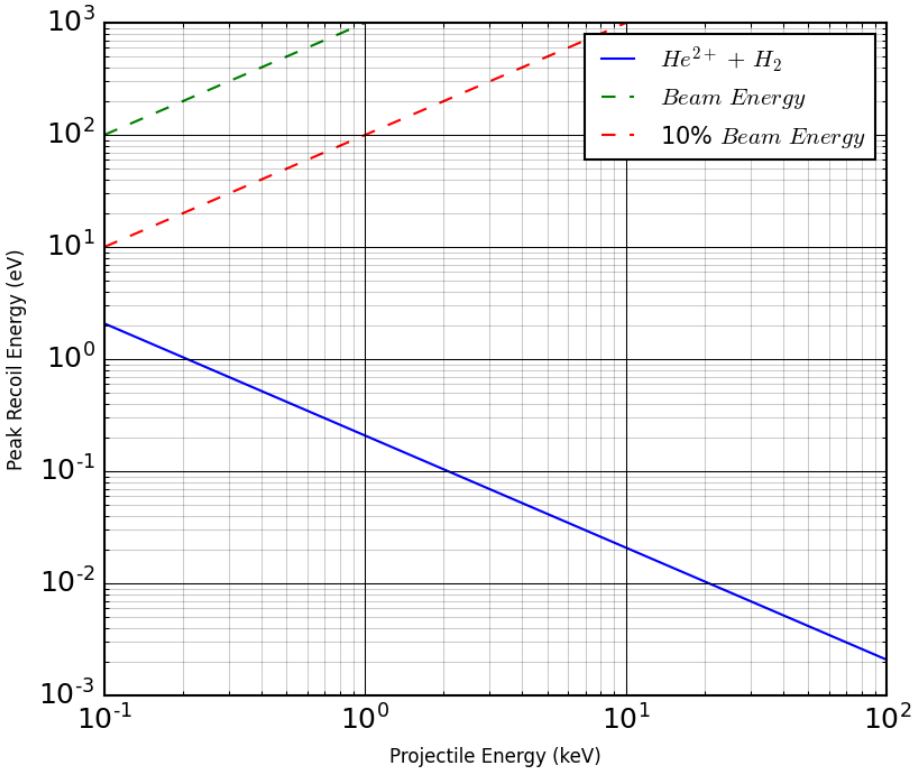

Figure 28: log-log plot of the peak intensity recoil energy in eV as a function of the projectile energy in keV in the case of one electron capture. The projectile ion is He for 1 specific charge states. The target particle is H_2.

The trend is similar compared to the results of one electron capture. It can be seen that the recoil energy transferred to the H_2 molecule decreases exponentially with the projectile energy. The overall recoil energy transferred to the target is an order of magnitude lower in the case of a He projectile compared to a Sn projectile. The overall recoil energy transferred to the target is orders of magnitudes higher in the case of two electron capture compared to the case of one electron capture.

4.3 SIMION simulations with energetic protons

4.3.1 Time-of-flight (ToF) histograms

In the simulation software SIMION a 3D model has been made of the full time of flight system as described in section 3.4.2. This model consists of the extraction region and the actual time of flight spectrometer. SIMION time of flight simulations are done by creating H^+ ions in the middle of the extraction field. Each H^+ ion is given a kinetic energy of about 9.7 eV that corresponds to the energy released by the fragmentation of fully ionized H_2. The kinetic energy gives the H^+ ions an initial velocity v_0 in a random direction. The total number of H^+ ions simulated per simulation run is 10000. Namely, 5000 forward- and 5000 backward emitted H^+ ions. To learn more about how these H^+ ions move through the system, the time of flight of the H^+ ions that reach the MCP at the end of the drift tube is tracked. Only the ions that are transmitted through the diaphragm in the model will reach the MCP. A time of flight spectrum is created by making a histogram in which all the H^+ ions that reach the MCP are counted at their corresponding arrival time. The bin size of each channel in every histogram is 1 ns. A histogram is made for several types of sources from which the ions are emitted in the extraction region of the model.

Figure 29 shows 4 histograms corresponding to 4 different source types. Figure 29c corresponds to a cylindrical source with a radius of 0.75 mm and a length of 5 mm. Figure 29d corresponds to a cylindrical source with a radius of 0.75 mm and a length of 10 mm. Figure 29b corresponds to a spherical source with a radius of 0.75 mm and Figure 29a corresponds to a point source. The radius of 0.75 mm for the sources is taken to be equal to the typical radius of the ion beam used in the actual experiment to resemble.

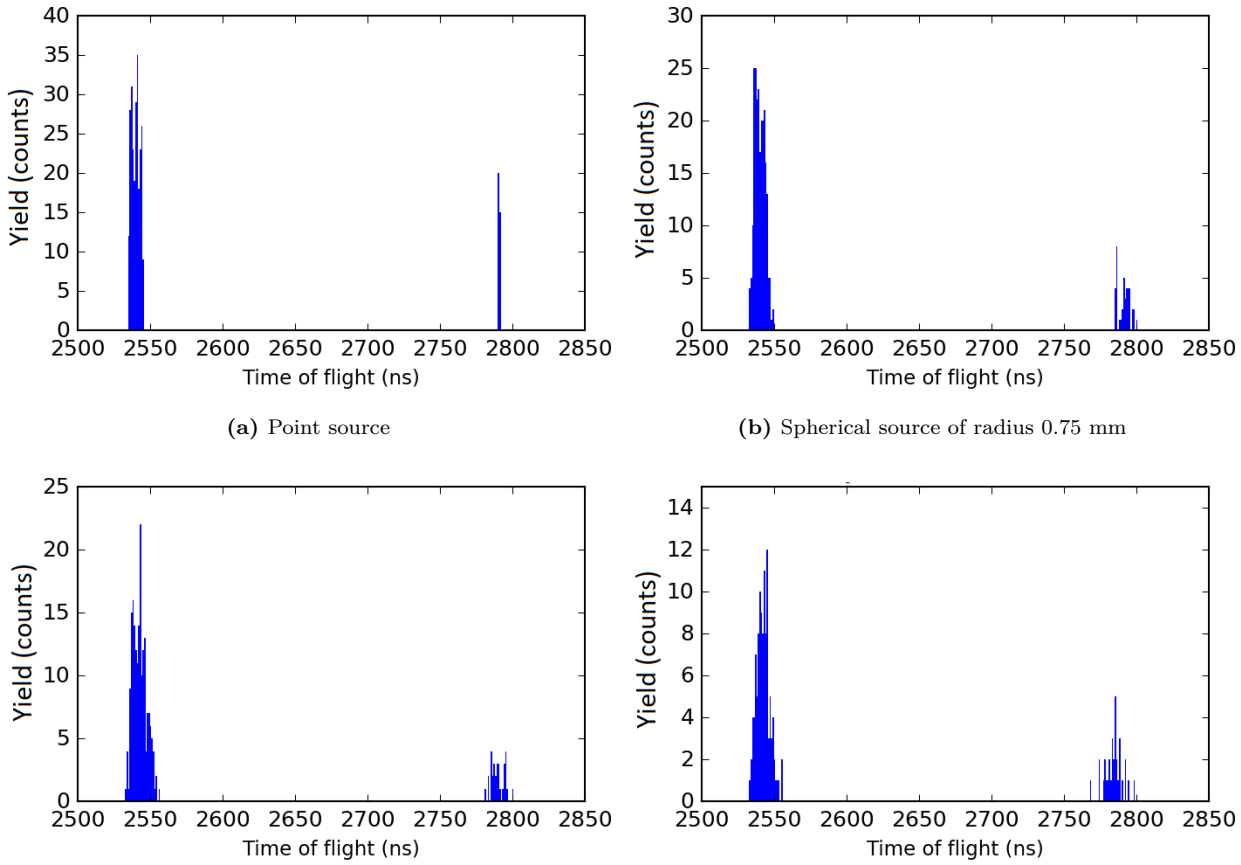

(a) Point source

(b) Spherical source of radius 0.75 mm

(c) Cylindrical source of length 5 mm and radius 0.75 mm

(d) Cylindrical source of length 10 mm and radius 0.75 mm

Figure 29: Time of flight histograms created by simulating H^+ ions with various source types. Each ion is given a kinetic energy of 9.7 eV, giving them an initial velocity v_0 in a random direction.

Looking at the figures, two distinct peaks can be seen. The forward emitted ions arrive earlier at the MCP than the backward emitted ions, hence the peak corresponding to the forward emitted ions is seen on the left in the histograms and the peak corresponding to the backward emitted ions is seen on the right in the histograms. The peak of the forward emitted ions is higher and has a larger area compared to the peak the backward emitted ions. This indicates that more forward emitted ions reach the MCP compared to backward emitted ions. It can be seen that the peak width for both peaks is smallest for the histogram of the point source. In the histograms of the cylindrical sources and the spherical source the peak widths are wider. This difference in peak width is most clearly seen in the peak of the backward emitted ions on the left in the histograms.

4.3.2 Time difference Δt

There is a time difference Δt in travel time between a forward emitted ion and a backward emitted ion (section 3.3.3). This time difference is also clearly seen in the time of flight histograms shown in figure 29 by the two distinct peaks corresponding to H^+ ions that arrive at different times. The difference in travel time between the forward and the backward emitted ions can be calculated with equation 13 in the case of a point source. The result of this calculation gives a time difference Δt of about 241 ns. Several simulations are done with the SIMION model to get an insight in if the analytically determined value for Δt resembles the Δt seen in the simulations. The four different H^+ ion source types mentioned above are used for the simulations as well as an ion pair perfectly emitted in line with the diaphragm. The H^+ ions start out with an energy of 9.7 eV. The ions are extracted towards the MCP by electric fields as described in section 3.4.2. For each ion the time of flight to reach the space directly behind the diaphragm and the time of flight to reach the MCP is listed. This is done for forward- and backward emitted ions separately. The total number of H^+ ions simulated per simulation is 10000. Namely, 5000 forward- and 5000 backward emitted H^+ ions. The left extraction electrode is set to +20 V, the right extraction electrode is set to -20 V. The average time of flight of the forward- and backward emitted ions is determined for every source type. The difference is taken between the average time of flight of the forward emitted ions and the average time of flight of the backward emitted ions. This difference gives a value for Δt.

In table 1 the time differences Δt and the average time of flight for the ions to reach the space directly behind the diaphragm are given for the different source types as well as an for an ion pair perfectly emitted in line with the diaphragm. In table 2 the same is done, but now for the average time of flight to reach the MCP.

Source type	Average forward ToF (ns)	Average backward tof (ns)	Δt
Point	146.3	396.4	250.1
Spherical	146.6	396.8	250.2
Cylindrical (L = 5)	147.7	394.7	247.0
Cylindrical (L = 10)	152.6	387.9	235.3
Perfect pair	143.2	397.6	254.4

Table 1: Time of flight for forward- and backward emitted H^+ ions counted directly behind the diaphragm, as well as the the time difference Δt. The table shows data for various different source types and an ion pair perfectly emitted in line with the diaphragm.

Source type	Average forward tof (ns)	Average backward ToF (ns)	Δt
Point	2540.4	2791.1	250.7
Spherical	2540.5	2791.6	251.1
Cylindrical (L = 5)	2543.0	2790.0	247.0
Cylindrical (L = 10)	2542.8	2784.3	241.5
Perfect pair	2536.2	2790.5	254.4

Table 2: Time of flight for forward- and backward emitted H^+ ions counted at the MCP, as well as the the time difference Δt. The table shows data for various different source types and an ion pair perfectly emitted in line with the diaphragm.

From table 1 and 2 it can be seen that the time difference Δt is very similar for both of the measurement positions. It can also be seen that for the different source types, the average time of flight for the forward emitted ions is the shortest in the case of a point source. When the sources start to deviate from the point source more, the average time of flight will increase. In the case of a spherical source the time of flight for the forward emitted H^+ ions is higher compared to the case of the point source and in the case of a cylindrical source the time of flight for the forward emitted H^+ ions is higher compared to the case of the spherical source as well as the point source. The opposite holds for the backward emitted ions. In that case, when the sources start to deviate from the point source more, the average time of flight of the H^+ ions will decrease. This leads to a decrease in the time difference Δt when the source type has less resemblance to a point source. For the ion pair perfectly emitted in line with the diaphragm, the time difference Δt is the largest compared to the others sources. It is the same for both the measurement behind the diaphragm and the measurement at the MCP. This is what is expected as stated in section 3.3.3. The analytically determined value for Δt of 241 ns is lower than the Δt found for the ion pair perfectly emitted in line with the diaphragm.

4.3.3 Transmission ratio

The transmission ratio that describes the number of ions that are transmitted through the diaphragm compared to the total number of ions that are created can be determined analytically for both forward- and backward emitted ions as explained in section 3.3.4. This is done with equation 22 for H^+ ions created in a point source in the middle of the extraction field. The ions are given an initial energy of 9.7 eV. The transmission ratio can also be expressed as a transmission percentage. The analytically found values for the transmissions are compared to values for the transmissions found with SIMION simulations. This to get an insight in if the transmissions found with SIMION simulations resemble the theory. The total number of H^+ ions simulated per simulation is 10000. Namely, 5000 forward- and 5000 backward emitted H^+ ions. The transmission ratios are determined from SIMION simulations by dividing the number of either the forward- or backward emitted ions that arrive at the MCP by the total number of forward- or backward emitted ions emitted from the source.

In table 3, the analytic and simulated values for the transmissions are given. The ratio between the forward- and backward transmission is also given for analytic-, simulated- and experimental transmission ratios. The transmission ratio for the experimental results is determined by dividing the area of the peak corresponding to the backward emitted ions by the area of the peak corresponding to the forward emitted ions in the time of flight spectrum of a general time of flight measurement. The analytical value found for the transmission can best be compared to the transmission value found with the SIMION simulation done with a point source. This because this will resemble the situation used for the analytical determination most accurately. The experimental transmission ratio can best be compared to the SIMION simulation done with a cylindrical source of length 10 mm. This because this resembles the region where H^+ ions are created in the case of an actual ion beam passing through the extraction region.

	Analytic			Simulated			Experimental
Source type	f(%)	b(%)	b/f	f(%)	b(%)	b/f	b/f
Point	8.52	1.19	0.140	4.65	0.72	0.16	-
Spherical	-	-	-	4.70	0.77	0.16	-
Cylindrical (L=5)	-	-	-	4.64	0.69	0.15	-
Cylindrical (L=10)	-	-	-	4.26	0.76	0.18	0.44

Table 3: transmissions for forward- (f%) and backward emitted H^+ ions (b%) in the CHEOPS setup. The transmission describes the number of ions that are transmitted through the diaphragm compared to the total number of ions that are created. The transmissions are given for various source types determined analytically or by the aid of simulations. In addition the ratio between the backward- and forward transmission (b/f) is given.

From table 3 it can be seen that the analytical transmissions and the simulated transmissions for a point source differ almost by a factor of 2. The ratio between the backward- and forward transmissions are however fairly similar. For the different source types simulated in the SIMION model, the transmissions for the forward- and backward emitted ions and their ratios are fairly similar. The experimental transmission ratio is more than 2 times higher compared to both the analytical method and the SIMION simulations. This indicates that in the experiment relatively more backward emitted ions are transmitted.

The electric extraction field as in the SIMION model shows is not completely uniform due to for instance the diaphragm itself. A uniform electric field is assumed in the analytical determination of the transmission. To rule out that the factor 2 difference of the transmissions between the two is due to this difference in electric field, a second perfect capacitor SIMION model is build that does have a uniform electric field. A new analytical value for the transmissions is determined for this new SIMION model since the dimensions differ because the diaphragm is removed. The electric field in the new model is made such that the electric field strength is the same as original SIMION model. In table 4, the analytic and simulated values for the transmissions and their corresponding ratios are given for forward- and backward emitted ions in the perfect capacitor SIMION model.

	Analytic			Simulated		
Source type	f(%)	b(%)	b/f	f(%)	b(%)	b/f
Point	18.3	1.57	0.0857	12.1	0.97	0.08
Spherical	-	-	-	12.2	1.20	0.098
Cylindrical (L=5)	-	-	-	11.5	1.02	0.089
Cylindrical (L=10)	-	-	-	10.1	1.13	0.11

Table 4: transmissions for forward- (f%) and backward emitted H^+ ions (b%) in the perfect capacitor model. The transmission describes the number of ions that are transmitted through the diaphragm compared to the total number of ions that are created. The transmissions are given for various source types determined analytically or by the aid of simulations. In addition the ratio between the backward- and forward transmission (b/f) is given.

From the simulations with the perfect capacitor SIMION model the transmissions found are higher overall compared to the transmissions of the true extraction setup. This is also seen in the analytically determined transmissions. This is due to the fact that the thickness of the extraction plate with the diaphragm is not taken into account. In the case of a point source the transmissions found are 12.1% for forward-, and 0.97% for backward emitted H^+ ions. The analytical values for the transmissions in the case of a point source calculated for this model are 18.3% for forward-, and 1.57% for backward emitted H^+ ions. There is still a discrepancy between the two methods for determining the transmissions, but the difference between them is smaller than the factor 2 found for the imperfect field. The ratio between the backward- and forward transmissions are again fairly similar for both the analytically determined values and the values following from the SIMION simulation. However, they are almost half of the ratios seen in the experimental system. The same is seen for the other source types in the SIMION simulations. The transmission ratios seen in the perfect capacitor model are all lower compared to the transmission ratios seen in the CHEOPS time of flight

setup. This indicates that relatively more backward emitted ions are transmitted in the CHEOPS time of flight spectrometer compared to the perfect capacitor model.

4.3.4 Shift x position

If the projectile ion beam does not pass through the centre between the extraction plates as seen in figure 7 but has an offset in the x direction, then the H^+ ions created by the charge exchange collisions between a projectile ion in the ion beam and a target particle in the H_2 gas will be created with an offset as well. Therefor SIMION simulations are done with a point source that shifts position in the x direction. This to get an insight in the effect of an offset in the x direction of the projectile ion beam on the transmission ratios through the diaphragm. The offset is measured from the centre of the extraction region. The x axis is the axis that lies parallel to the time of flight spectrometer axis. The y and z position are 0 for these simulations. The x, y and z position are taken relative to the centre of the extraction region. The point source is simulated at different positions ranging from -4.5 mm to 4.5 mm in the x direction in steps of 1.5 mm, bringing it closer to the diaphragm with each step. As before, the total number of H^+ ions simulated per position is 10000, 5000 forward- and 5000 backward emitted H^+ ions. The extraction plates are charged to +20 and -20 V just like before. From the simulations done it was concluded that if the y and z coordinates are kept at 0, all the ions that are transmitted through the diaphragm will also reach the MCP. Hence, the transmissions measured directly behind the diaphragm are the same as the transmissions measured at the MCP in these simulations.

Figure 30 shows transmissions of forward- and backward emitted H^+ ions that are transmitted through the diaphragm as a function of the x position of the point source in mm in the time of flight extraction field.

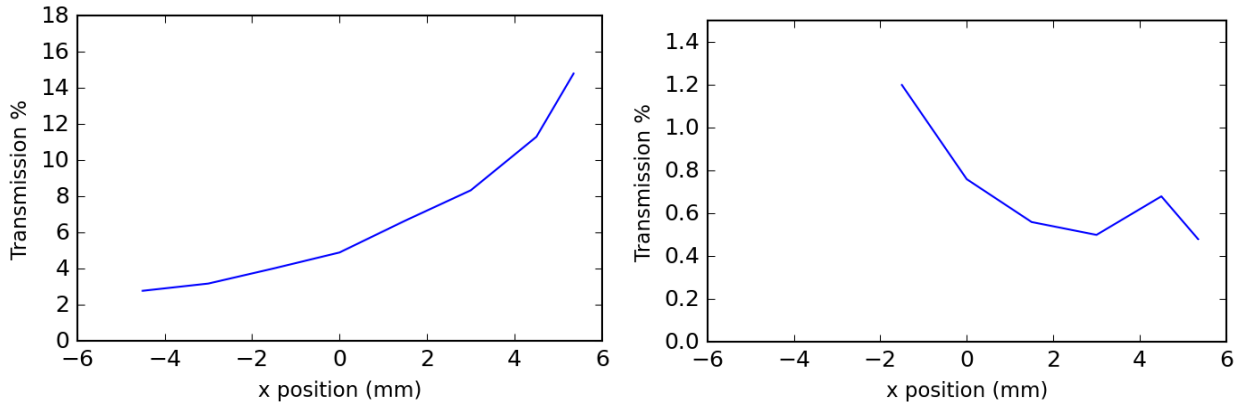

(a) Forward emitted H^+ ions transmission

(b) Backward emitted H^+ ions transmission

Figure 30: transmission of forward- (30a) and backward (30b) emitted H^+ ions as a function of the x position for H^+ ions simulated in the extraction region of the CHEOPS setup SIMION model. The H^+ ions are measured directly behind the diaphragm. The y and z position are 0 for these simulations. The x, y and z position are taken relative to the centre of the extraction region. The point source simulated is moved from -4.5 mm to 4.5 mm in steps of 1.5 mm, bringing it closer to the diaphragm with each step. The energy given to the H^+ ions is 9.7 eV.

In figure 30a it can be seen that the transmission increases when the source of H^+ ions is put closer to the diaphragm in the case of forward emitted ions. The opposite seems to happen for the backward emitted ions. The transmission ratio for these ions will decrease as the source of H^+ ions is put closer to the diaphragm. Only when the source is put very close to the diaphragm a small increase is seen again. The overall transmission is higher for the forward emitted ions as compared to the backward emitted ions. Note that the first two data points are 0 for figure 30b. This is due to the fact that the H^+ ions hit the back plate of the reaction chamber since the backward moving ions are emitted too close to that plate in the first two simulations.

In figure 31 the two graphs are divided by each other to give the backward/forward transmission ratio as a function of the x position.

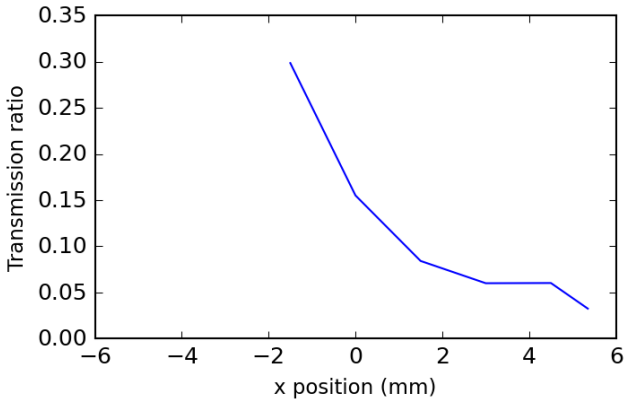

Figure 31: backward/forward transmission ratio as a function of the x position for H^+ ions simulated in the extraction region of the CHEOPS setup SIMION model. The H^+ ions are measured directly behind the diaphragm. Note that this graph shows the data from figure 30a and figure 30b divided by each other. The y and z position are 0 for this simulation. The x, y and z position are taken relative to the centre of the extraction region. The point source simulated is moved from -4.5 mm to 4.5 mm in steps of 1.5 mm, bringing it closer to the diaphragm with each step. The energy given to the H^+ ions is 9.7 eV.

It can be seen that the backward/forward transmission ratio decreases with an increase of the x coordinate, meaning that the ratio lowers as the position shifts more closer to the diaphragm.

One might expect that the transmissions of both the forward- and the backward emitted ions will increase when the source is moved closer to the diaphragm. When looking at figure 30b, this is not seen for the backward emitted ions. To see if these counter intuitive results are due to the fact that the field in the extraction region is not perfectly uniform, the same simulation is done in the SIMION model of a perfect capacitor in which a perfectly uniform electric field is generated of the same strength. The results of this simulation are shown in figure 32.

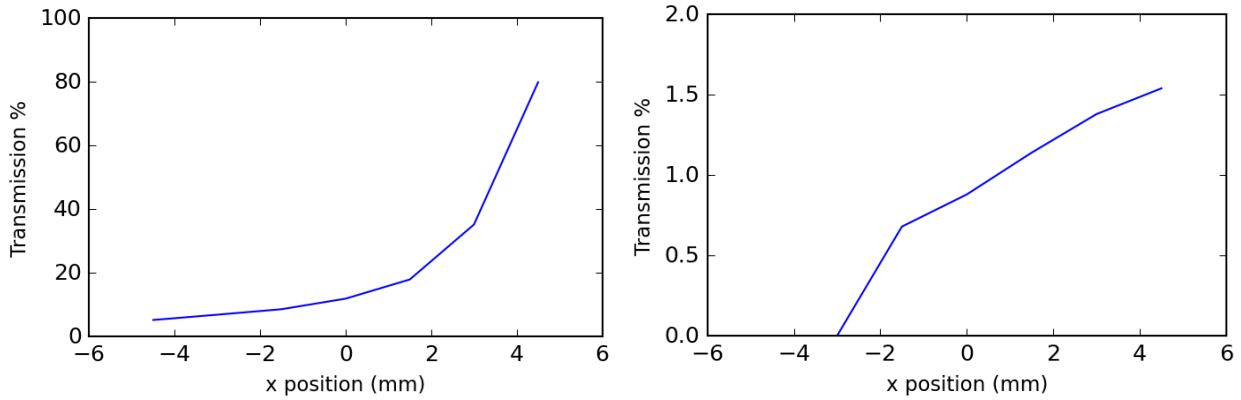

(a) Forward emitted H^+ ions transmission

(b) Backward emitted H^+ ions transmission

Figure 32: transmission of forward- (32a) and backward (32b) emitted H^+ ions as a function of the x position for H^+ ions simulated in a perfect capacitor. The y and z position are 0 for these simulations. The x, y and z position are taken relative to the centre of the extraction region. The point source simulated is moved from -4.5 mm to 4.5 mm in steps of 1.5 mm, bringing it closer to the diaphragm with each step. The energy given to the H^+ ions is 9.7 eV.

It can be seen that for the simulations with the perfect capacitor model, the transmission of the forward emitted ions increases when the source of H^+ ions is put closer to the diaphragm. This is shown in figure 32a. This is the same relation as is seen in the SIMION simulations done with the true configuration. The transmission of the backward emitted H^+ ions in the perfect capacitor model increases more in a linear fashion when the source of H^+ ions is put closer to the diaphragm. This is shown in figure 32b. This is different compared to the simulations done with the true configuration from which the results are shown in figure 30. There the transmission of the backward emitted ions decreases when the ion source is moved closer to the diaphragm. Only when the source is put really close to the diaphragm we see a very small increase in transmission again. The overall transmission is higher for the forward emitted ions compared to the backward emitted ions. Note that the first two data points are 0 for figure 32b. This is due to the fact that the H^+ ions hit the back plate of the reaction chamber since the backward moving ions were emitted too close to that plate in the first two simulations. In figure 33 the two graphs are divided by each other to give the backward/forward transmission ratio as a function of the x position.

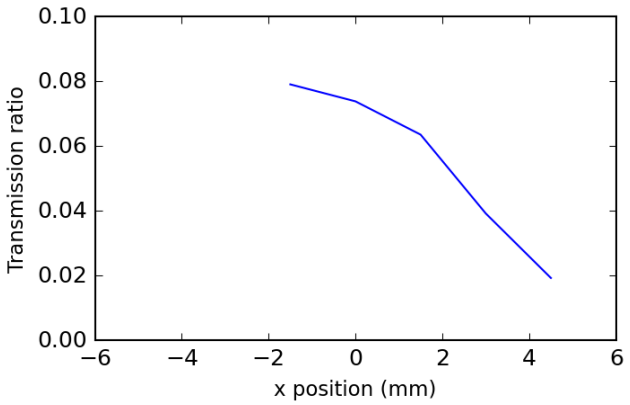

Figure 33: backward/forward transmission ratio as a function of the x position for H^+ ions simulated in a perfect capacitor. Note that this graph shows the data from figure 32a and figure 32b divided by each other. The y and z position are 0 for this simulation. The x, y and z position are taken relative to the centre of the extraction region. The point source simulated is moved from -4.5 mm to 4.5 mm in steps of 1.5 mm, bringing it closer to the diaphragm with each step. The energy given to the H^+ ions is 9.7 eV.

It can be seen that the backward/forward transmission ratio decreases with an increase of the x coordinate. This is the same as is seen for the simulations done with the true configuration. Though the overall backward/forward transmission ratio is lower compared to the simulations done with the true configuration. This indicates that with the perfect capacitor SIMION model relatively more forward emitted ions are transmitted than backward emitted ions compared to simulations done with inclusion of the diaphragm.

4.3.5 Shift y position

In the same manner as for a shift in the x direction, simulations for a shift in the y direction are done. A point source is moved in the y direction while the x and z position are kept 0. The y axis is the axis lies perpendicular to the time of flight spectrometer axis. Note that in the case of an offset in the y direction, some of the H^+ ions that are transmitted through the diaphragm may hit the wall of the time of flight spectrometer. Hence, the transmissions measured directly behind the diaphragm are not the same as the transmissions measured at the MCP in these simulations. Figure 34 shows transmissions of forward- and backward emitted H^+ ions that are transmitted through the diaphragm as a function of the y position of the point source. The transmitted ions are measured directly behind the diaphragm.

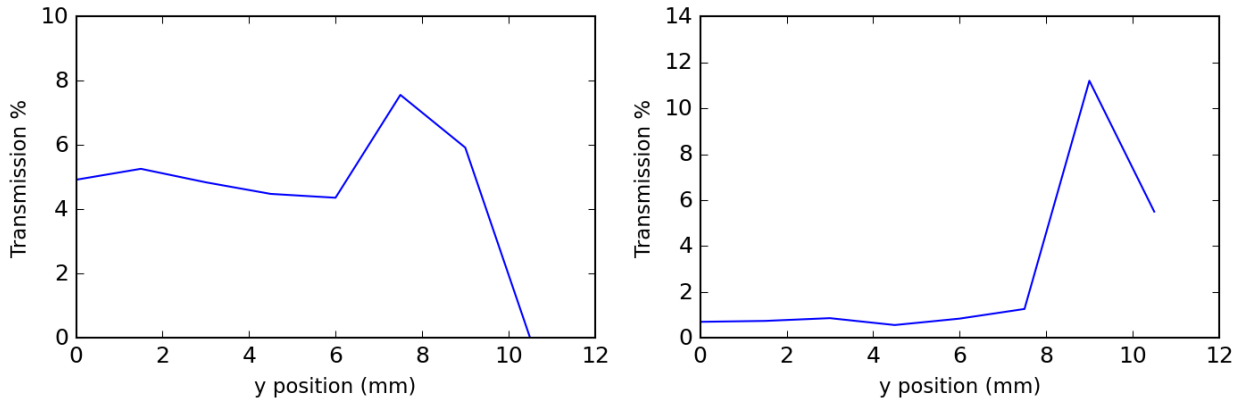

(a) Forward emitted H^+ ions transmission

(b) Backward emitted H^+ ions transmission

Figure 34: transmission of forward- (34a) and backward (34b) emitted H^+ ions as a function of the y position for H^+ ions simulated in the extraction region of the CHEOPS setup SIMION model. The H^+ ions are measured directly behind the diaphragm. The x and z position are 0 for these simulations. The x, y and z position are taken relative to the centre of the extraction region. The point source simulated is moved from 0 mm to 10.5 mm in steps of 1.5 mm. The energy given to the H^+ ions is 9.7 eV.

It can be seen that the transmission for both the forward- and the backward emitted H^+ ions is relatively constant for a y shift less than 6 mm from the centre of the extraction region. In this range of y positions the transmission of the forward emitted ions is about 5%, which is about 5 times higher than that of the backward emitted ions that have a transmission ratio of about 0.8%. When the shift in y surpasses 6 mm we see a big increase in transmission through the diaphragm for both the forward- and backward emitted ions. At this range of y positions the transmission of the backward emitted ions is higher than that of the forward transmitted ions. In figure 35 the two graphs are divided over each other to give the backward/forward transmission ratio as a function of the y position measured directly behind the diaphragm.

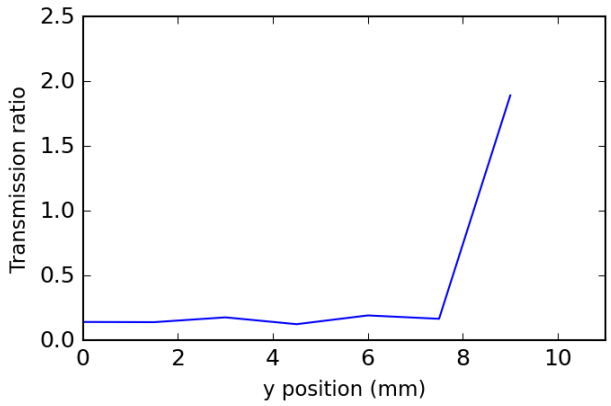

Figure 35: backward/forward transmission ratio as a function of the y position for H^+ ions simulated in the extraction region of the CHEOPS setup SIMION model. The H^+ ions are measured directly behind the diaphragm. Note that this graph shows the data from figure 34a and figure 34b divided over each other. The x and z position are 0 for this simulation. The x, y and z position are taken relative to the centre of the extraction region. The point source simulated is moved from 0 mm to 10.5 mm in steps of 1.5 mm. The energy given to the H^+ ions is 9.7 eV.

It can be seen that the backward/forward transmission ratio is is relatively constant for a y shift less than 7 mm from the centre of the extraction region. When the shift in y surpasses 7 mm we see a big increase in the transmission ratio.

To get a better insight in the region of y shift where the transmissions increase, lets zoom in on this particular region. A new set of simulations is done with a point source that shifts position in the y direction, but now it is moved from 8 mm to 10.4 mm in steps of 0.4 mm. This is shown in figure 36, which is a zoomed in version of figure 34.

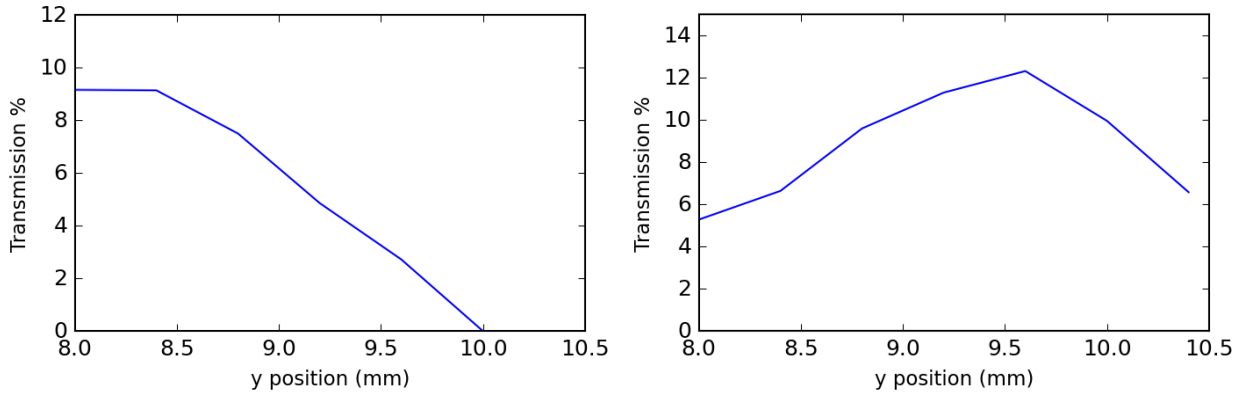

(a) Forward emitted H^+ ions transmission

(b) Backward emitted H^+ ions transmission

Figure 36: Zoomed in version of the transmission of forward- (36a) and backward (36b) emitted H^+ ions as a function of the y position for H^+ ions simulated in the extraction region of the CHEOPS setup SIMION model. The x and z position are 0 for these simulations. The x, y and z position are taken relative to the centre of the extraction region. The point source simulated is moved from 8 mm to 10.4 mm in steps of 0.4 mm. The energy given to the H^+ ions is 9.7 eV.

It can be seen that for the forward emitted ions the peak in transmission lies at a y position of about 8 mm. The transmission at the peak is around 9%. For the backward transmitted ions the peak in transmission lies at a y position of about 9.5 mm an has a value of about 12%.

In figure 37 the two graphs are divided over each other to give the backward/forward transmission ratio as a function of the y position. This is a zoomed in version of figure 35.

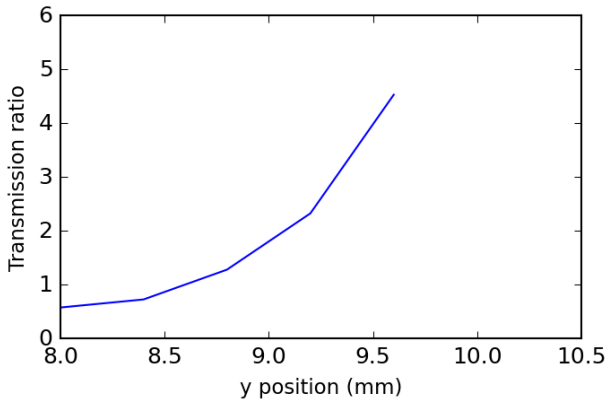

Figure 37: Zoomed in version of the backward/forward transmission ratio as a function of the y position for H^+ ions simulated in the extraction region of the CHEOPS setup SIMION model. The H^+ ions are measured directly behind the diaphragm. Note that this graph shows the data from figure 36a and figure 36b divided by each other. The x and z position are 0 for this simulation. The x, y and z position are taken relative to the centre of the extraction region. The point source simulated is moved from 8 mm to 10.4 mm in steps of 0.4 mm. The energy given to the H^+ ions is 9.7 eV.

In the region where the shift in y position is greater than 8 mm we see a strong growth in the transmission ratio when the positions y increases.

Since some of the H^+ ions that are transmitted through the diaphragm will hit the wall of the time of flight spectrometer, the simulations done with measuring the ions directly behind the diaphragm do not resemble data one would see in the experiment. In the lab setup ions will only be counted if they reach the MCP. To obtain simulation data that more accurately resembles the data obtained with the setup in the lab, the transmissions for forward- and backward emitted ions are also determined when the H^+ ions are measured at the MCP instead of directly behind the diaphragm. The point source simulated for the forward emitted H^+ ions is moved from 0 mm to 3 mm in steps of 0.375 mm. This gives the corresponding transmissions shown in figure 38a. The point source simulated for the backward emitted H^+ ions is moved from 0 mm to 7 mm in steps of 1 mm. This gives the corresponding transmissions shown in figure 38b. The rest of the simulation parameters is kept the same as for the simulations done where the ions are measured directly behind the diaphragm.

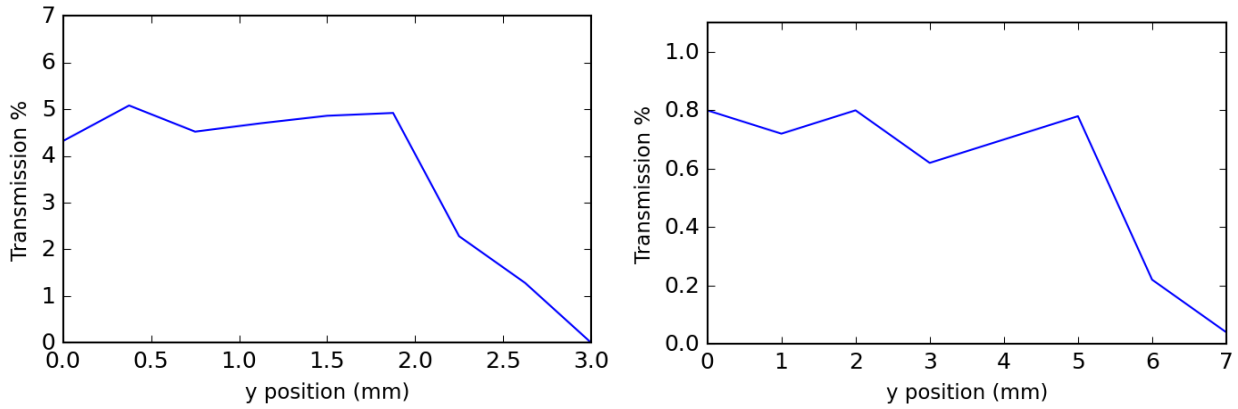

(a) Forward emitted H^+ ions transmission

(b) Backward emitted H^+ ions transmission

Figure 38: transmission of forward- (38a) and backward (38b) emitted H^+ ions as a function of the y position for H^+ ions simulated in the extraction region of the CHEOPS setup SIMION model. The H^+ ions are measured at the MCP. The x and z position are 0 for these simulations. The x, y and z position are taken relative to the centre of the extraction region. The point source simulated for the forward emitted H^+ ions (38a) is moved from 0 mm to 3 mm in steps of 0.375 mm. The point source simulated for the backward emitted H^+ ions (38b) is moved from 0 mm to 7 mm in steps of 1 mm. The energy given to the H^+ ions is 9.7 eV.

It can be seen that the transmission up to the MCP for the forward emitted H^+ ions is relatively constant for a y shift less than 2 mm from the centre of the extraction region. The transmission in this region hovers around the value of 5%. If the y shift surpasses 2 mm, the transmission of ions that will reach the MCP declines fast and it will be 0% after a shift of only 3 mm. A similar trend is seen for the backward emitted ions. For the backward emitted H^+ ions the transmission up to the MCP is relatively constant for a y shift less than 5 mm from the centre of the extraction region. The transmission in this region hovers around the value of 0.8%. This constant region is larger than the constant region of the forward emitted ions. When the y shift surpasses the value of 7 mm the transmission for the backward emitted ions will be 0%. The overall transmission up to the MCP is larger for the forward emitted ions compared to the backward emitted ions. Figure 38 and figure 35 are plotted together into one plot seen in figure 39.

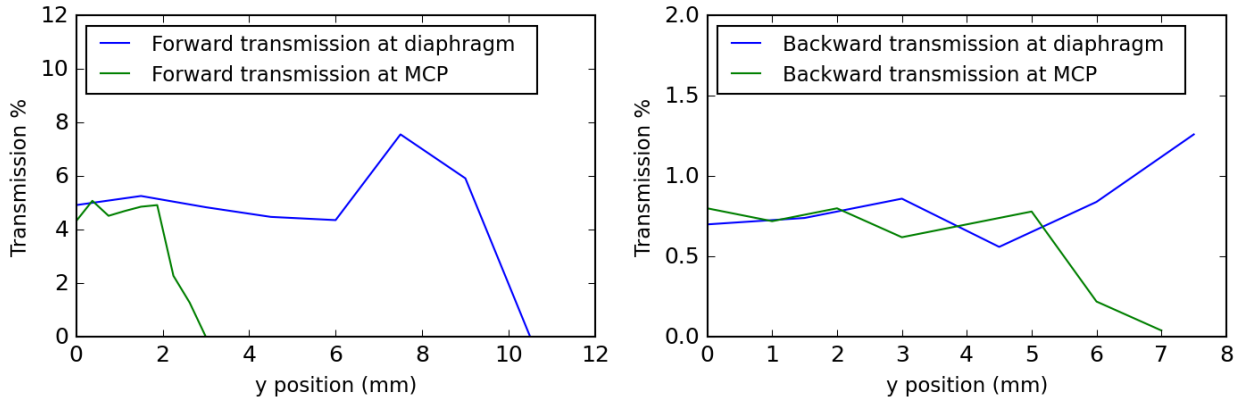

(a) Forward emitted H^+ ions transmission

(b) Backward emitted H^+ ions transmission

Figure 39: transmission of forward- and backward emitted H^+ ions measured directly behind the diaphragm compared to the transmission of the forward- and backward emitted H^+ ions measured at the MCP. Both as a function of the y position in the CHEOPS setup SIMION model. The x and z position are 0 for these simulations. The x, y and z position are taken relative to the centre of the extraction region. The energy given to the H^+ ions is 9.7 eV.

When comparing the simulations where the ions are measured directly behind the diaphragm with the simulations where the ions are measured at the MCP, it can be seen that the transmission for both the forward- and backward emitted ions drops of much earlier. This means that the H^+ ions that are still transmitted through the diaphragm when the shift is larger than 3 mm in the case of forward emitted ions and 7 mm in the case of backward emitted ions will not reach the MCP at the end of the time of flight spectrometer, but will hit the side wall of the time of flight spectrometer instead.

4.3.6 Ion pair transmission

As discussed before (section 3.3.1), the double ionized H_2 molecule fragment in two H^+ ions each having 9.7 eV. These two H^+ ions are referred to as an ion pair. When both the forward- and backward emitted ion of an ion pair are transmitted through the diaphragm and reach the MCP it is counted as an ion pair transmission. A point source is simulated in the extraction region of the CHEOPS setup SIMION model multiple times at different positions for each simulations. It is moved from 0 mm to 2.3333 mm in steps of 0.3333 mm, with an additional step at 2.5 mm. The y axis is the axis that lies perpendicular to the time of flight spectrometer in the model. The ion pair transmissions are determined from the SIMION simulations by dividing the number of transmitted ion pairs that reach the MCP by the total number of emitted ion pairs from the source (5000) for each simulation.

When an ion pair is emitted in the centre of the extraction region (x=y=z=0), it is expected that all the backward emitted ions that are transmitted through the diaphragm, also have their corresponding forward emitted ion transmitted. Hence an ion pair transmission is seen for every backward emitted ion that is transmitted. When the ion pair point source is shifted in the y or z direction, this is in theory no longer necessarily the case. This is why the ion pair transmissions are compared to the transmission of the backward emitted H^+ ions. When the ion pair point source shifts more than the radius of the diaphragm, it is expected that no ion pairs will be transmitted at all. The ions that are transmitted at that point are either a forward- or backward emitted ions that emerged from different ion pair creations. The radius of the diaphragm is 2.5 mm, hence it does not make sense to simulate for a y shift that is larger than 2.5 mm. Figure 40a shows transmissions of H^+ ion pairs and backward emitted H^+ ions as a function of the y position of the point source. Figure 40b shows the ratio between the transmissions of H^+ ion pairs and backward emitted H^+ ions as a function of the y position.

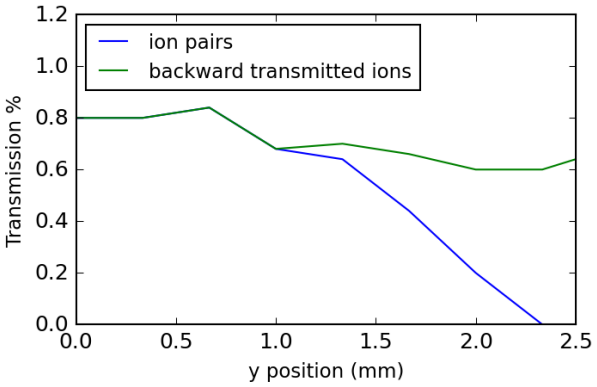

(a) H^+ ion pairs & backward emitted H^+ ions transmission.

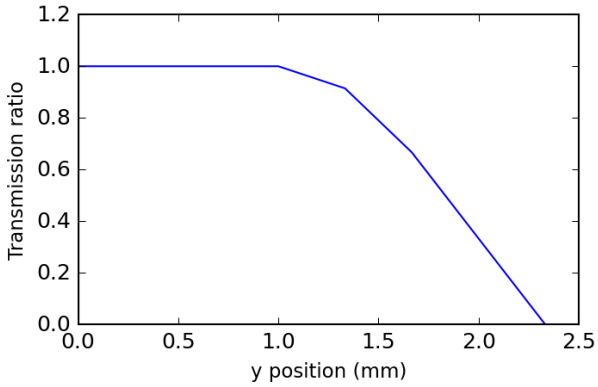

(b) H^+ ion pairs transmission/ backward emitted H^+ ions transmission ratio.

Figure 40: transmission of H^+ ion pairs compared to the transmission of the backward emitted H^+ ions, both measured at the MCP as a function of the y position in the time of flight extraction setup (40a).Figure 40b shows the H^+ ion pairs transmission divided by the backward emitted H^+ ions transmission as a function of the y position. The x, y and z position are taken relative to the centre of the extraction region. The point source simulated for the forward emitted H^+ ions is moved from 0 mm to 2.3333 mm in steps of 0.3333 mm, with an additional step at 2.5 mm. The energy given to each H^+ ion is 9.7 eV.

It can be seen that the transmission of the ion pairs and the transmission of the backward emitted ions remain equal to each other for a y shift less than 1 mm from the centre of the extraction region. The transmission will hover around 0.8% in this region. If the y shift of the point source surpasses 1 mm, the transmission of ion pairs will start to decline while the transmission of the backward emitted ions will remain relatively constant. At a y shift of more than 2.333 mm the transmission of ion pairs is 0%. Dividing the transmission of the ion pair by the transmission of the backward emitted ions gives the transmission ratio plotted in figure 40b. If the y shift is less than 1 mm from the centre of the extraction region, the transmission ratio is equal to 1. If the y shift is larger than 1 mm from the centre of the extraction region, the transmission ratio declines sharply. This indicates that the number of transmitted ion pairs declines fast compared to the number of backward emitted ions that are transmitted.

4.4 Molecular ions

4.4.1 Full histogram

In the experiment the following reaction products are seen: H^+ ions with an energy of about 9.7 eV, stationary H^+ ions with an energy of about 0 eV and most frequently stable stationary H_2^+ ions with an energy of about 0 eV. Thus far the focus has been on the simulations of 9.7 eV H^+ ions. Here the focus shifts to the H_2^+ molecular ions and the full time of flight spectrum.

To get an insight into how the time of flight for each of these ion types compares, SIMION simulations are done with a cylindrical source that has a radius of 0.75 mm and a length of 10 mm. all other settings of the model are kept the same as in previous sections. From this source the 3 types of ions mentioned above is emitted in all directions. In figure 41 the time of flight spectrum for this simulation is shown. The bin size of each channel in the histogram is 1 ns. The peak height corresponds to the ion counts in that particular time bin. The number of ions simulated for each of the 3 groups of ions mentioned above is chosen such that the corresponding peaks will be easily plotted into one histogram. The height of the peak corresponding to the H_2^+ particles is made to be higher than the other peaks because this is typically seen in a time of flight measurement done with the CHEOPS setup in the lab. There are 10000 H^+ ions with an energy of about 9.7 eV eitted from the source. Of those 5000 are forward emitted and 5000 are backward emitted. There are 500 stationary H^+ ions emitted with an energy of about 0 eV and 2500 H_2^+ ions are emitted, also with an energy of about 0 eV. The real ratio of emission between the different groups of ions is unknown. The histogram is used to compare the peak widths and time of flight with the data from lab experiments.

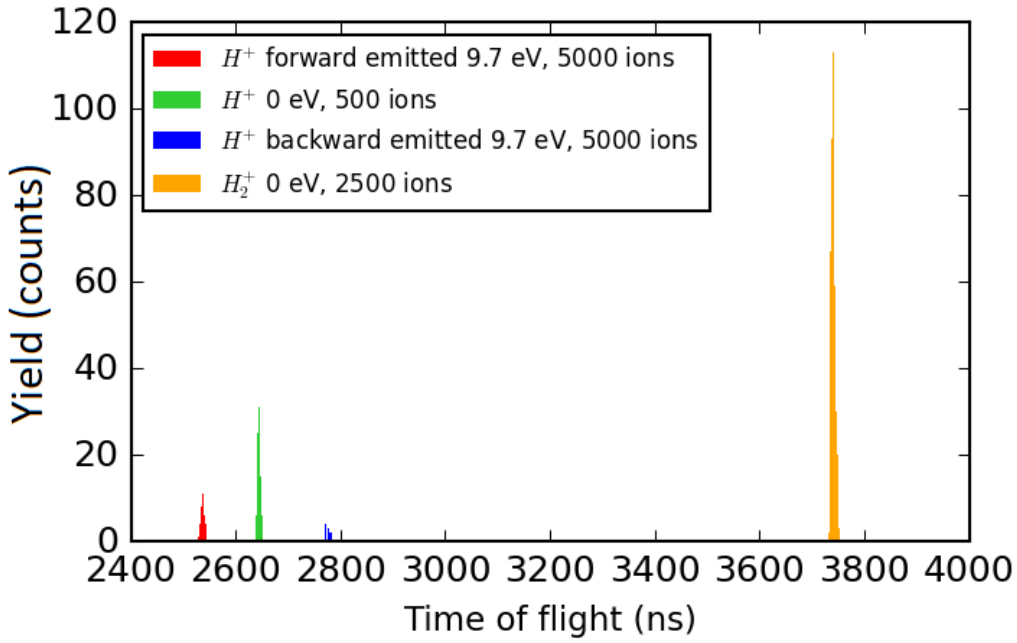

Figure 41: Time of flight histogram of 5000 forward- and 5000 backward emitted H^+ ions with an energy of 9.7 eV, 500 stationary H^+ ions with an energy of 0 eV and 2500 stationary H_2^+ ions with an energy of 0 eV in the CHEOPS setup SIMION model.

The histogram shows 4 distinct peaks corresponding to the forward- and backward emitted H^+ ions with an energy of 9.7 eV, and of H^+ and H_2^+ ions with an energy of 0 eV.

In figure 42 a time of flight spectrum is shown for an actual measurement. This to get an insight into what extend the SIMION model simulations can predict an experiment. The reported experiment was done with 60 keV Sn^{5+} ion. On an individual level these Sn ions undergo a charge exchange collision with the H_2 molecules. Note that the time values that follow from a lab experiment are counted as the time difference between the moment the projectile beam is chopped and the moment the ionized H_2 particle is counted at the MCP as described in 3.3.5. This is different in the SIMION simulation where the time of flight values are counted as the time difference between the moment the H^+ ion is emitted from the source and the moment the H^+ ion is counted at the MCP. The time of flight values from the lab experiment are corrected by subtracting t_0 (the time between beam chopping and the projectile-target collision) from the total time of flight times to be able to compare the time of flight spectra from SIMION simulations with the measured time of flight spectra.

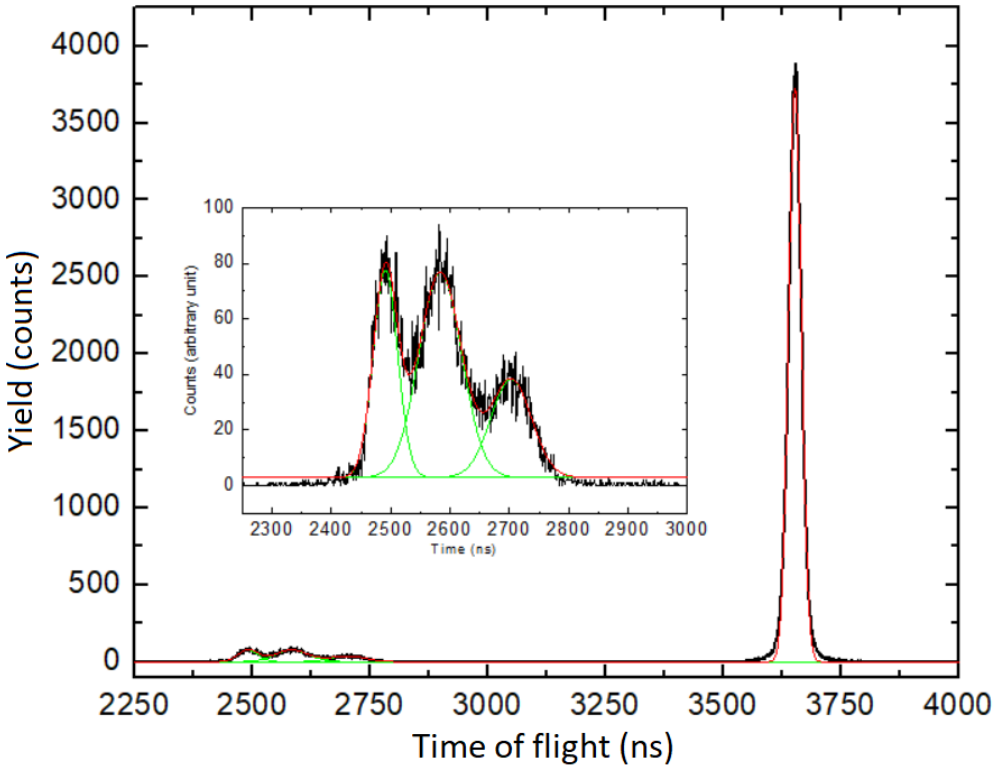

Figure 42: Time of flight spectrum of a variety of reaction products produced during a charge exchange collision reaction of Sn^{5+} ions with H_2 particles. The energy of the projectile beam Sn ions is 60 keV.

The histogram again shows the 4 distinct peaks corresponding to each on the ion types. However, it can be seen that the peak widths of the time of flight spectrum of the SIMION model are much narrower compared to the peak widths in the time of flight spectrum of the measurement. The location of the peak centres of the peaks seem to be roughly at the same time position, although they do differ slightly. This is due to the fact that in the simulations the position of the MCP is slightly closer to the diaphragm compared to in the lab experiment.

4.4.2 Recoil energy effect on time of flight spectrum of H_2^+ ions

The recoil energy values in the case of 10 keV Sn^{5+} ions undergoing a charge exchange collision with H_2 molecules are calculated using the theory in section 3.1.4. This recoil energy is calculated to be 0.48 eV. To get an insight in the effect of this recoil energy on the time of flight spectrum of the H_2^+ ions, SIMION simulations are done to see whether effects of a small recoil energy can be picked up from the peak shape. The recoil energy of 0.48 eV is given to H_2^+ ions that are simulated in the SIMION model of the CHEOPS setup. In figure 43 the time of flight spectrum of H_2^+ ions is shown in the case of a point source. In figure 44 the time of flight spectrum of H_2^+ ions is shown in the case of a spherical source.

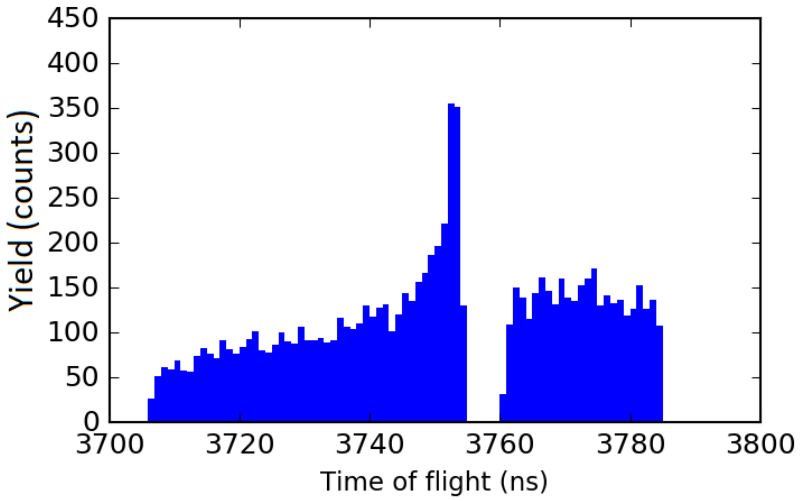

Figure 43: H_2^+ ion point source simulated with SIMION in the time of flight setup. TheH_2^+ ions are given an energy of 0.48 eV.

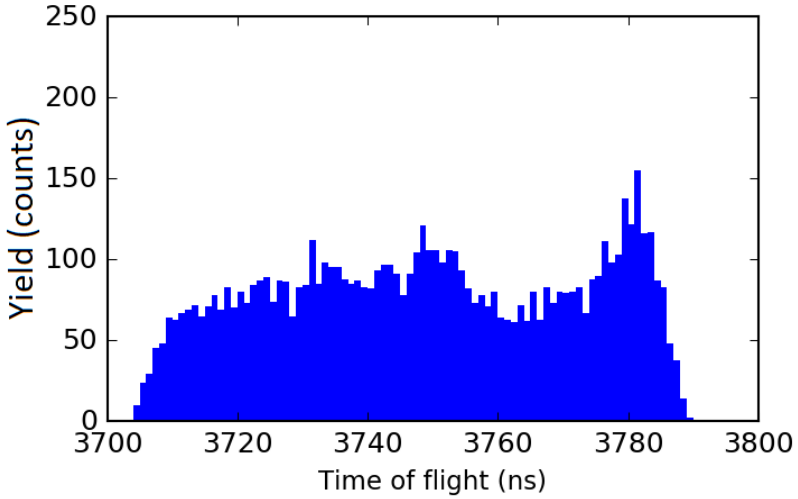

Figure 44: H_2^+ ion spherical source simulated with SIMION in the time of flight setup. The H_2^+ ions are given an energy of 0.48 eV.

It can be seen that in the case of a point source, 2 distinct peaks are seen. These peaks correspond to the forward- and backward emitted ions. Here the forward emitted ions are the ions that due to the recoil energy they obtained, got a velocity with a component in the direction towards the diaphragm. The backward emitted ions are the ions that due to the recoil energy they obtained, got a velocity with a component in the direction away from the diaphragm. The peaks lie closely together since the kinetic energy given to these H_2^+ ions is only 0.48 eV. The peak on the left side of the histogram, corresponding to the forward emitted ions, has a longer tail than the peak on the right side of the histogram corresponding to the backward emitted ions. In the case of a spherical source the 2 distinct peaks are no longer seen. The peaks overlap and form one wide peak. The broadened peak is found to be about about 90 ns wide.

In figure 45 measured time of flight spectra of H_2^+ ions are shown. This to get an insight into what extend the SIMION model simulations can predict an experiment done with the actual lab setup. All time of flight spectra have been adjusted for t_0 as described in section 3.3.5. The Full Width at Half Maximum of the peaks referred to as FWHM, gives an insight in the spread of the peaks. Figure 45a shows the time of flight spectrum of H_2^+ ions that are created by a charge exchange collision with an incoming Sn^{3+} target ion that possesses 18 keV of kinetic energy. The recoil energy of the peak intensity for one electron capture is calculated as is described in section 3.1.4 to be about 0.13 eV. This can also be seen in figure 20. The FWHM of the peak is found to be 35.2 ns. Figure 45b shows the time of flight spectrum of H_2^+ ions that are created by a charge exchange collision with an incoming Sn^{5+} target ion that possesses 60 keV of kinetic energy. The recoil energy of the peak intensity for one electron capture is calculated to be about 0.08 eV and the FWHM of the peak is found to be 50.5 ns. Figure 45c shows the time of flight spectrum of H_2^+ ions that are created by a charge exchange collision with an incoming Sn^{5+} target ion that possesses 120 keV of kinetic energy. The recoil energy of the peak intensity for one electron capture is calculated to be about 0.04 eV and the FWHM of the peak is found to be 32.2 ns.

It is best to compare the lab results with the SIMION simulations done with the spherical source. This source type resembles the circumstances in the lab better than a point source. A cylindrical source would resemble the lab experiments even better, however this simulation has not been done. The results of a spherical source and a cylindrical source are very similar and hence the simulations done with the spherical source will suffice. It can be seen that the H_2^+ ions seen in the lab experiments have a slightly shorter overall time of flight compared to the H_2^+ ions seen in the SIMION simulation in the case of a spherical source, see figure 44 and figure 45. This is probably due to the fact that The MCP in the CHEOPS setup in the lab is slightly closer to the reaction chamber than is modeled in the SIMION model. The lab results are fitted with a Gaussian. It can be seen that the Gaussian does not completely fit the data in the histograms. The actual peak is wider than the fit at the bottom of the peak. A similar peak shape is seen in the data from the SIMION simulation in the case of a spherical source seen in figure 44. This is what is expected to be seen from a recoil energy induced peak broadening, since that basically produces two Gaussian's that overlap with one another. Hence this results in a peak that is slightly wider at the bottom than would be the case for a single Gaussian peak. In the SIMION simulation the broadening of the peak is due to the recoil energy given to the H_2^+ ions. If this recoil energy gets smaller in the case of higher projectile ion energies, this widening effect is expected to disappear. However, a relation between the calculated values of the recoil energy and the width of the peaks seen in the data obtained with lab experiments can not be seen. The broadening near the bottom of the peaks in the lab data does not seem to decrease when the projectile ions in the beam get a higher energy. Furthermore, the FWHM of the peaks does not seem to depend on the magnitude of the recoil energy.

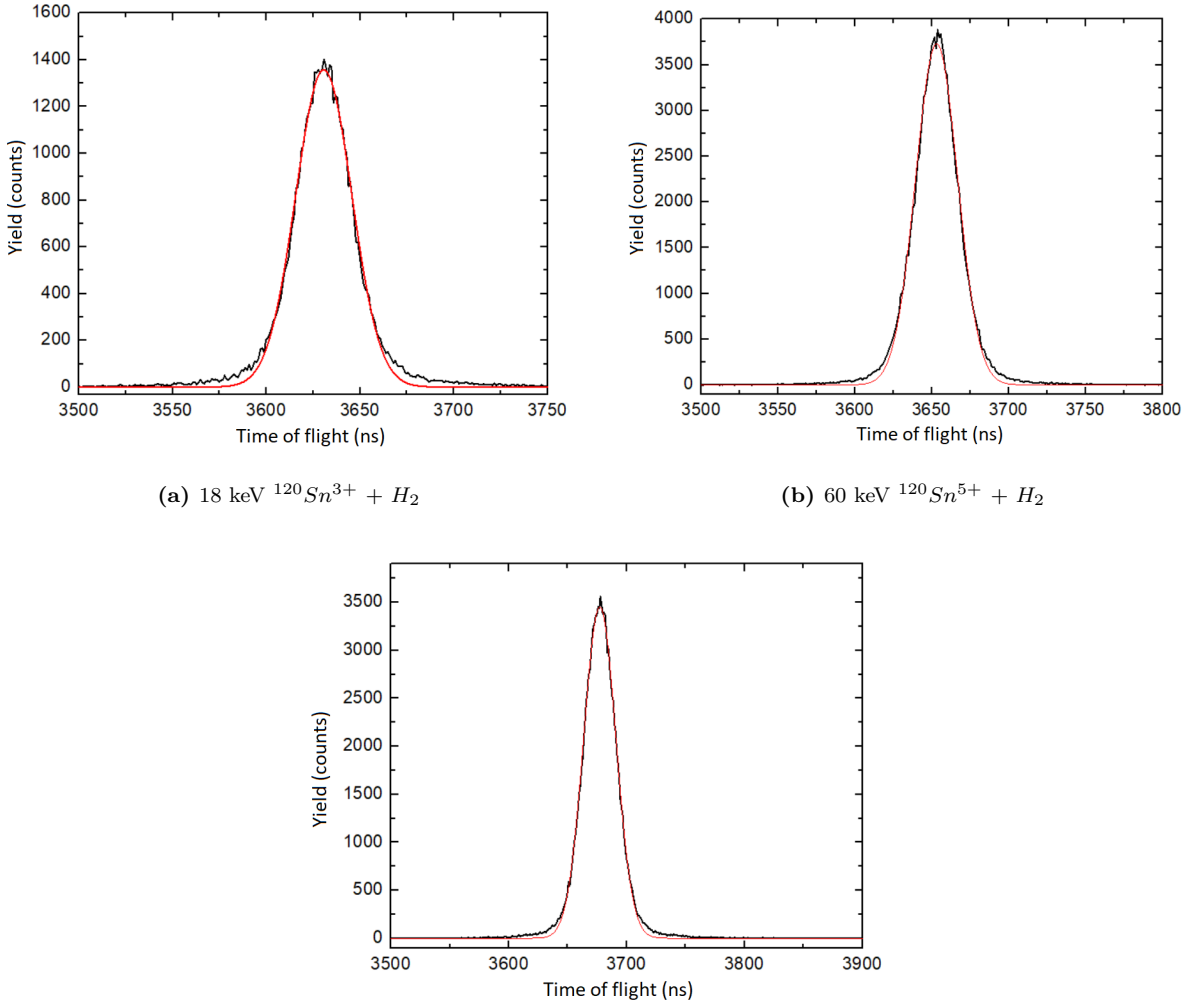

(a) 18 keV $^{120}Sn^{3+}$ + H_2

(b) 60 keV $^{120}Sn^{5+}$ + H_2

(c) 120 keV $^{120}Sn^{5+}$ + H_2

Figure 45: Time of flight spectrum of H_2^+ ions traveling through the CHEOPS setup. The projectile beam consists of ^{120}Sn ions of various charges and energies. The target gas particles are H_2 molecules.

5 Discussion

5.1 Momentum and energy recoil

To build on the theory behind ion-gas particle interactions, the charge exchange collision described by the classical over barrier model of energetic Sn and He ions colliding with H_2 molecules is analytically researched. This analytical research gives the results shown in section 4.1 and 4.2. The main goal of the analytical research is to determine to what extend kinetic energy referred to as recoil energy is transferred from an incoming energetic positively charged projectile ion to a H_2 molecule with which this projectile ion undergoes a charge exchange collision. Furthermore, data is obtained regarding the momentum transfer to the H_2 molecules as well as the angle between the original flight path and the new flight path of the projectile ion. The research is done for both one electron- and two electron capture. The results for one- and two electron capture is discussed separately below.

5.1.1 One electron capture

A charge exchange collision between an energetic Sn ion colliding with a H_2 molecule is considered in the case of one electron capture. The transverse momentum and the recoil energy transferred to the H_2 molecule target is analytically analyzed with the Classical Overbarrier Model described in section 3.1. It is found that both the transverse momentum and the recoil energy transfer to the H_2 molecule target decreases exponentially as the impact parameter b increases. This can be explained by the fact that the electric field around a charged point particle decreases exponentially in strength as a function of the distance from this point particle. The overall transverse momentum and recoil energy transfer is lower when the projectile Sn ions have a higher energy. This can be explained by the fact that, the higher the energy of the Sn ion, the higher the velocity is it possesses. A higher velocity means that the projectile Sn ion passes the H_2 molecule more quickly and the interaction time between the projectile Sn ion and the H_2 molecule is smaller. This shorter interaction time leads to less transverse momentum and recoil energy transfer to the H_2 molecule.

The transverse momentum and recoil energy distribution is determined which gives information about which of the transverse momenta and recoil energies transferred to the target H_2 molecule is most likely to be seen. In the transverse momentum and recoil energy distributions a clear peak in intensity for a particular transverse momentum and recoil energy is seen. This peak corresponds to the most likely transverse momentum transferred to the target after a charge exchange collision. It is found that at the peak intensity, the transverse momentum and recoil energy transfer decreases when the energy of the projectile Sn ion increases. The recoil energy of the peak intensity from the H_2 molecule recoil energy distributions are plotted as a function of the projectile Sn ion energy to determine the relation of this decrease. This is done for several different charge states of Sn and He undergoing a charge exchange collision with a H_2 molecules. It is found that the peak intensity recoil energy transferred to the H_2 molecule decreases exponentially with the projectile energy. This is the case for both the Sn and He projectile ions. However, the overall recoil energy transferred to the target is orders of magnitudes lower in the case of a He projectiles compared to a Sn projectiles. This could be due to the fact that a Sn ion is much heavier and thus possesses much more energy for the same keV/amu. The fact that the peak intensity recoil energy transferred to the H_2 molecule decreases exponentially can be explained again by the interaction time between the projectile ions and the H_2 molecules. The overall peak intensity recoil energy decreases when the positive charge of the projectile ions is lower. If the positive charge of the ions is is lower, the Coulomb force felt between the target and the projectile particles is lower as well. A lower coulomb force leads to less transverse momentum and recoil energy transferred to the H_2 molecule target particle. This explains that overall peak intensity recoil energy decreases when the positive charge of the projectile ions is lower.

The angle between the original flight path and the new flight path of the projectile Sn ion is determined and is plotted against it intensity to give an angular distribution. A clear peak in intensity for a particular angle is seen. This peak corresponds to the most likely angle between the projectiles original flight path and their new flight path after a charge exchange collision. It is found that at the peak intensity, the angle between the original flight path and the new flight path of the projectile Sn ion decreases when the energy of the projectile Sn ion increases. This can again be explained by the differences in interaction times as discussed above.

5.1.2 Two electron capture

Similarly, the transverse momentum and the recoil energy transferred to the H_2 molecule target is analytically analyzed with the Classical Overbarrier Model described in section 3.1, but now in the case of two electron capture. It is found that both the transverse momentum and the recoil energy transfer to the H_2 molecule target decreases exponentially as the impact parameter b increases. The overall transverse momentum and recoil energy transfer is lower when the projectile Sn ions have a higher energy. This is the same as what is found for the one electron capture case and can again be explained by the exponential decrease of the electric field strength as a function of distance and the interaction times between the projectile and the target. The overall transverse momentum and recoil energy transfer to the H_2 molecule is higher in the case of two electron capture compared that with one electron capture. This can be explained by the fact that with two electron capture there is one less electron screening the potential of the positively charged H_2 molecule core for a certain amount of time. When this is the case, the repulsive Coulomb force between the projectile and the H_2 molecule target is larger. This leads to more transverse momentum and recoil energy transfer to the H_2 molecule.

The transverse momentum and recoil energy distribution is determined for two electron capture as well. In the transverse momentum and recoil energy distributions in the case of two electron capture there is also a clear peak in intensity seen for a particular transverse momentum and recoil energy. It is found that at the peak intensity, the transverse momentum and recoil energy transferred decreases when the energy of the projectile Sn ion increases. The recoil energy of the peak intensity from the H_2 molecule recoil energy distributions are again plotted as a function of the projectile energy. This is again done for several different charge states of Sn and He undergoing a charge exchange collision with a H_2 molecules. It is found that the peak intensity recoil energy transferred to the H_2 molecule decreases exponentially with the projectile energy. This is the case for both the Sn and He projectile ions. This is also seen in the case of one electron capture and can again be explained by the interaction time between the projectile ions and the H_2 molecules. The overall recoil energy transferred to the target is again orders of magnitudes lower in the case of a He projectiles compared to a Sn projectiles. This can again be due to the fact that a Sn ion is much heavier and thus possesses much more energy for the same keV/amu value. Similarly as in the case of one electron capture, the overall peak intensity recoil energy decreases when the positive charge of the projectile ions is lower. This can be explained by the fact that if the positive charge of the projectile ions is is lower, the Coulomb force felt between the target and the projectile particles is lower as well. This leads to less transverse momentum and recoil energy transfer to the H_2 molecule target particle. Compared to the case of one electron capture, the transverse momentum and recoil energy transfer to the H_2 molecule at peak intensity is higher in the case of two electron capture. This can again be explained by the fact that with two electron capture there is one less electron screening the potential of the positively charged H_2 molecule core for a certain amount of time as is described above.

The angle between the original flight path and the new flight path of the projectile Sn ion is determined and is plotted against it intensity to give an angular distribution in the case of two electron capture. A clear peak in intensity for a particular angle is again seen. It is found that at the peak intensity, the angle between the original flight path and the new flight path of the projectile Sn ion decreases when the energy of the projectile Sn ion increases. This is again due to the differences in interaction times. The angle between the original flight path and the new flight path of the projectile Sn ion is found to be several times larger in the case of two electron capture compared to the case of one electron capture. This can again be explained by the fact that with two electron capture there is one less electron screening the potential of the positively charged H_2 molecule core as is described before.

5.2 SIMION simulations

5.2.1 Time of flight spectra SIMION model

With the SIMION model of the CHEOPS setup time of flight simulations are done by creating H^+ ions in the middle of the extraction region of the CHEOPS SIMION model. This is done for 4 different types of ion sources, namely a cylindrical source with a radius of 0.75 mm and a length of 5 mm, a cylindrical source with a radius of 0.75 mm and a length of 10 mm, a spherical source with a radius of 0.75 mm and a point source. Each H^+ ion is given a kinetic energy of 9.7 eV. For all the different sources the time of flight spectra show two distinct peaks. The forward emitted ions arrive earlier at the MCP than the backward emitted ions. The peaks left in the time of flight spectra correspond to the forward emitted ions and the peaks right in the time of flight spectra correspond to the backward emitted ions. The peaks of the forward emitted ions is higher and has a larger area compared to the peaks the backward emitted ions. This indicates that more forward emitted ions reach the MCP compared to backward emitted ions. This is due to the fact that more forward emitted ions are transmitted through the diaphragm compared to backward emitted ions. The reason behind this is explained in section 3.3.4. Comparing the time of flight spectra of the simulations with the different sources, the peak widths are smallest for simulations done with the point source. In the histograms of the cylindrical sources and the spherical source the peak widths are broader. This difference in peak width is most clearly seen in the peak of the backward emitted ions on the left in the histograms. This is due to the fact that the ions emitted in all the sources that are not a point source are emitted in broader region. Not all H^+ ions are created exactly in the centre of the extraction region giving them different distances to travel to the MCP and hence different time of flights. This leads to peak broadening as explained in section 3.5.

5.2.2 Time difference Δt

There is a time difference Δt in travel time between a forward emitted ion and a backward emitted ion moving through the CHEOPS setup. The difference in travel time between the forward and the backward emitted ions is calculated with equation 13. This is done for H^+ ions created in a point source in the middle of the extraction region of the CHEOPS setup. Each H^+ ion is created with 9.7 eV of kinetic energy. The result of this calculation gives a time difference Δt of about 241 ns. With the CHEOPS setup SIMION model the time difference Δt is also determined for four different H^+ ion source types, as well as an ion pair perfectly emitted in line with the diaphragm. The different source types are, a cylindrical source with a radius of 0.75 mm and a length of 5 mm, a cylindrical source with a radius of 0.75 mm and a length of 10 mm, a spherical source with a radius of 0.75 mm and a point source. The time difference Δt of the backward- and forward emitted H^+ ions is determined directly behind the diaphragm and at the MCP.

The average time of flight for the forward emitted ions is the shortest in the case of a point source. When the sources are broader than a single point in the case of the spherical source and the cylindrical source, the average time of flight of the forward emitted ions increases. The opposite is true for the backward emitted ions. In that case the average time of flight of the backward emitted H^+ ions decreases. This leads to a decrease in the time difference Δt when the source type is broader than a single point.

This can be explained by the fact that in a cylindrical and a spherical source, ions are transmitted in an area around the centre of the extraction region. An ion emitted farther away from the centre of the extraction region can be transmitted through the diaphragm with trajectory and velocity pointing more in the y or z direction as seen in figure 7. These ions are still emitted with the same energy of 9.7 eV. This means that x component of the velocity as seen in figure 7 is lower. In the case of forward emitted ions, the x component of their velocity is positive. This means that, when the x component of the velocity is lower, the velocity towards the MCP is lower and the ion will reach the MCP at a later time. This will increase the average time of flight for forward emitted ions. In the case of backward emitted ions, the x component of the velocity is negative. This means that when the x component of the velocity is lower, the velocity away from the MCP is lower. Hence, the ion can be turned around in the electric field present in the reaction region in less time and the ion will reach the MCP at an earlier time . This will decrease the average time of flight for backward emitted ions. Hence, the time difference Δt is smaller when the source type is broader than a single point. In the case of an ion pair perfectly emitted in line with the diaphragm, the time difference Δt is the largest compared to the others sources for both the measurement behind the diaphragm and the

measurement at the MCP. This is because in that case the x component of the velocity is maximized and the y and z component of the velocity are 0. This leads to the shortest time of flight for the forward emitted ion and the longest time of flight for the backward emitted ion. Hence, the time difference Δt is largest in this case. The analytically determined value for the time difference Δt of 241 ns is lower than the Δt found for the ion pair perfectly emitted in line with the diaphragm. The reason for this is unknown. It could have something to do with the fact that the perfectly emitted ion pair is not in a uniform electric field in the SIMION simulation due to model geometry. The analytically calculated value for Δt is calculated for a uniform electric field.

5.2.3 Transmission

The transmissions of H^+ ions created in the extraction region of the CHEOPS setup are determined by dividing the number of forward- and backward emitted ions that are counted at the MCP by the total number of forward- and backward emitted ions emitted in the source respectively. This is done analytically and with the aid of the SIMION simulations. There are two SIMION models used for simulating the transmission. The CHEOPS setup SIMION model and a perfect capacitor SIMION model. The analytic- and simulated values for the transmission for forward- and backward emitted ions as well as the ratios between the forward- and backward transmission for the analytic-, simulated- and experimental transmission ratios are compared in section 3.3.4. Four different source types are used to determine the transmission values with SIMION simulations. Namely, a cylindrical source with a radius of 0.75 mm and a length of 5 mm, a cylindrical source with a radius of 0.75mm and a length of 10 mm, a spherical source with a radius of 0.75 mm and a point source. The analytical transmission values are calculated for point source in a perfectly uniform electric field in the extraction region. This uniform electric field is not present in the of CHEOPS setup SIMION model. The perfect capacitor SIMION model does posses a perfectly uniform electric field in the extraction region. This means that analytically calculated values of the transmission can best be compared to the SIMION simulation done with a point source in the perfect capacitor SIMION model. The experimental transmission ratio can best be compared to the SIMION simulation done with a cylindrical source of length 10 mm in the CHEOPS setup SIOMION model. This because this resembles the region where H^+ ions are created in the case of an actual ion beam passing through the extraction region most accurately.

When comparing the simulations done with the different source types in the CHEOPS setup SIMION model, the transmissions for the forward- and backward emitted ions and their ratios are all fairly similar. This means that the source type has a minimal influence on the transmission values. The same is seen when comparing simulations done with the different source types in the perfect capacitor SIMION model.

In the case of the CHEOPS setup SIMION model it is seen that analytical values of the transmission and the simulated values of the transmission for a point source differ almost by a factor of 2. This discrepancy between the analytical and simulated values of the transmission was first thought to be due to the fact that in the SIMION simulations the electric field in the extraction region is not completely uniform. However after comparing the analytical values for the transmission with the point source simulations in the case of the perfect capacitor model, it is seen that there is still a discrepancy between the two methods for determining the transmissions. This time the difference between the two methods is smaller than a factor 2. The reason for this discrepancy is not found. There is likely a mistake somewhere in one of the two ways of determining the transmission that has been overlooked.

The b/f transmission ratios for the different sources in the CHEOPS setup SIMION model are similar to eachother. However, they are almost double that of the b/f ratio's seen in the perfect capacitor SIMION model. This indicates that more backward emitted ions are transmitted compared to the forward emitted ions in the case of the CHEOPS setup SIMION model compared to the perfect capacitor SIMION model. This is most likely due to a lens effect in the electric field in the extraction region of the CHEOPS setup SIMION model. This lens effect focuses the ions towards the middle of the extraction region making them more likely to be transmitted through the diaphragm. The lens effect occurs due to the diaphragm and the hole on the left side of the reaction region. A backward emitted ion spends much more time in the electric field and thus feels this effect more strongly than a forward emitted ion. This leads to relatively more backward emitted ions to be transmitted compared to forward emitted ion when this lens effect is present. Hence, the b/f transmission ratios for the different sources in the CHEOPS setup SIMION model

are larger than that of the ratio's seen in the perfect capacitor SIMION model.

The b/f transmission ratio seen for a general experiment with the CHEOPS setup in the lab is more than 2 time higher compared to both the analytical method and the SIMION simulations in the case of the CHEOPS setup SIMION model. This indicates that in a lab experiment relatively more backward emitted ions are transmitted. This can be due to even e larger lensing effect taking place in a lab experiment or due to an offset of the projectile ion beam in the extraction region. The exact reason for this is not known.

5.2.4 Shift x position

With the SIMION model of the CHEOPS setup, the effect of a shift of a point source in the x direction relative to the centre of the extraction region on the transmission is simulated. This is also done in the perfect capacitor SIMION model. Each H^+ ion simulated possess a kinetic energy of 9.7 eV. The main goal of these SIMION simulations is to determine the effect of an offset in the x direction of the energetic ion beam coming into the extraction region of CHEOPS setup.

From the simulations with the CHEOPS setup SIMION model it can be seen that for the forward emitted ions that are transmitted, the transmission increases exponentially when the source of H^+ ions is put closer to the diaphragm. The opposite seems to happen for the backward emitted ions. The transmission ratio for these ions will decrease as the source of H^+ ions is put closer to the diaphragm. Only when the source is put very close to the diaphragm a small increase is seen again. From the simulations with the perfect capacitor model it can be seen that the transmission of the forward emitted ions increases exponentially when the source of H^+ ions is put closer to the diaphragm. This is the same relation as is seen in the SIMION simulations with the CHEOPS setup SIMION model. The transmission of the backward emitted ions now increases relatively linearly. This is different compared to the simulations done with the CHEOPS setup SIMION model, since there the transmission ratio decreases as the source of H^+ ions is put closer to the diaphragm. This is most likely due to the lens effect discussed earlier in section 5.2.3. This lens effect is present in the CHEOPS setup SIMION model, but not in the perfect capacitor setup SIMION model.

It is also seen that in both of the SIMION models the overall transmission is higher for the forward emitted ions compared to the backward emitted ions. This can be most easily understood by describing all the possible positions of an emitted ion as the boundary of a sphere that grows over time and is accelerated towards the diaphragm. This is explained in more detail in section 3.3.4. A forward emitted ion is defined as an ion that is emitted with a velocity component towards the side of the extraction region where the diaphragm is located (towards the x direction). Hence a forward emitted ion lies on the front half of this sphere that reaches the diaphragm first. A backward emitted ion lies on the back half of this sphere and reach the diaphragm at a later time. This is visualized in figure 12. Since the sphere is continuously growing with time as explained in section 3.3.4, a larger fraction of the front part of the sphere will be transmitted through the diaphragm compared to the fraction of the back part of the sphere. This results in the fact that the overall transmission is higher for the forward emitted ions compared to the backward emitted ions.

The ratio between the number of backward transmitted ions an the number of forward transmitted ions is determined as a function of the x position as well. In the case of the CHEOPS setup SIMION model it can be seen that the backward/forward transmission ratio decreases with an increase of the x coordinate, meaning that the ratio lowers as the position shifts more closer to the diaphragm. This indicates that relatively more backward emitted ions are transmitted compared to forward emitted ions when the source is farther away from the diaphragm. The same is seen in the case of the perfect capacitor setup SIMION model. This means that the closer the source is to the diaphragm, the more forward emitted ions are transmitted compared to backward emitted ions. This is also what is expected if one calculates the transmission with the theory desribed in section 3.3.4. The overall backward/forward transmission ratio in the case of the perfect capacitor SIMION model is lower compared to the simulations done with the CHEOPS setup SIMION model. This indicates that with the perfect capacitor SIMION model relatively more forward emitted ions are transmitted than backward emitted ions compared to simulations done with the CHEOPS setup SIMION model. This can again be explained by the lens effect discussed above in section 5.2.3.

5.2.5 Shift y position

Similarly as for a shift in the x direction, simulations for a shift in the y direction are done. This time only with the CHEOPS setup SIMION model. The main goal of these SIMION simulations is to determine the effect of an offset in the y direction of the energetic ion beam coming into the extraction region of CHEOPS setup.

Two different simulations are done. One simulation where the transmitted ions are counted directly behind the diaphragm and one where they are counted at the MCP ion counter. From the simulation where the transmitted ions are counted directly behind the diaphragm, it can be seen that the transmission for both the forward- and the backward emitted H^+ ions is relatively constant for a y shift less than 6 mm from the centre of the extraction region. At this range of y positions the transmission of the forward emitted ions is higher than that of the backward transmitted ions. When the shift in y surpasses 6 mm a big increase in transmission through the diaphragm for both the forward- and backward emitted ions is seen. At the range of y positions, the transmission of the backward emitted ions is higher than that of the forward emitted ions. It can be seen that for the forward emitted ions the peak in transmission lies at a y position of about 8mm. For the backward transmitted ions the peak in transmission lies at a y position of about 9.5 mm. It can also be seen that the backward/forward transmission ratio is relatively constant for a y shift less than 7 mm from the centre of the extraction region. When the shift in y surpasses 7 mm we see a big increase in the transmission ratio.

From the simulation where the transmitted ions are counted at the MCP, it can be seen that the transmission up to the MCP for the forward emitted ions is relatively constant for a y shift less than 2 mm from the centre of the extraction region. The transmission in this region hovers around the value of 5%. If the y shift surpasses 2 mm, the transmission of ions that will reach the MCP declines fast and it will be 0% after a shift of only 3 mm. This is due to the fact that at a shift in y position that is larger than 3 mm the ions that are transmitted through the diaphragm are transmitted at such an angle that they will hit the wall of the time of flight spectrometer later in their trajectory. They will not reach the MCP. A similar trend is seen for the backward emitted ions, where the transmission up to the MCP ion counter is relatively constant for a y shift less than 5 mm from the centre of the extraction region. The transmission in this region hovers around the value of 0.8%. When the y shift surpasses the value of 7 mm the transmission for the backward emitted ions will be 0%.

5.2.6 Ion pair transmission

Another goal to achieve by the use of SIMION simulations is to determine the ion pair transmission ratio through the diaphragm in the extraction region of the CHEOPS setup. From the ion pair transmission simulations, it can be seen that the transmission of the ion pairs and the transmission of the backward emitted ions remain equal to each other for a y shift less than 1 mm from the centre of the extraction region. The transmission will hover around 0.8% in this region. If the y shift of the point source surpasses 1 mm, the transmission of ion pairs will start to decline while the transmission of the backward emitted ions will remain relatively constant. At a y shift of more than 2.333 mm the transmission of ion pairs is 0%. By dividing the transmissions of the ion pairs by the transmissions of the backward emitted ions, it can be seen what fraction of the transmitted backward emitted ions have their corresponding forward emitted ion transmitted as well (ion pair transmission). If the y shift is less than 1 mm from the centre of the extraction region, the transmission fraction is equal to 1. If the y shift is larger than 1 mm from the centre of the extraction region, the transmission fraction declines sharply. This indicates that the number of transmitted ion pairs declines fast compared to the number of backward emitted ions that are transmitted.

5.2.7 Recoil energy effect on time of flight spectrum Molecular Hydrogen

Lastly SIMION simulations are done to determine the effect of the recoil energies calculated earlier on the time of flight spectrum of H_2^+ ions created by a charge exchange collision moving through the CHEOPS setup. These simulations are done for a point source and a spherical source. In the case of a point source, 2 distinct peaks are seen. These peaks correspond to the forward- and backward emitted ions. Here the forward emitted ions are the ions that, due to the recoil energy (0.48 eV) they obtained, got a velocity with a component in the direction towards the diaphragm. The backward emitted ions are the ions that, due to

the recoil energy they obtained, got a velocity with a component in the direction away from the diaphragm. The peaks lie closely together since the kinetic energy given to these H_2^+ ions is only 0.48 eV. The peak on the left side of the histogram, corresponding to the forward emitted ions, has a longer tail than the peak on the right side of the histogram corresponding to the backward emitted ions. In the case of a spherical source the 2 distinct peaks are no longer seen. This is due to the fact that due to peak broadening effect of the spherical source itself, the two peaks overlap and form one wide peak. The broadened peak in the case of a spherical source is found to be about about 90 ns wide.

The simulation results are compared to 3 different measurements done with the lab setup. One measurement where the H_2^+ ions are created by a charge exchange collision with an incoming Sn^{3+} target ion of 18 keV, giving an expected recoil energy of about 0.13 eV. The FWHM of the peak is found to be 35.2 ns. One measurement where the H_2^+ ions are created by a charge exchange collision with an incoming Sn^{5+} target ion that possesses 60 keV of kinetic energy, giving an expected recoil energy of about 0.08 eV. The FWHM of the peak is found to be 50.5 ns. And one measurement where the H_2^+ ions are created by a charge exchange collision with an incoming Sn^{5+} target ion that possesses 60 keV of kinetic energy, giving an expected recoil energy of about 0.04 eV. The FWHM of the peak is found to be 32.2 ns. The peak base is in all cases larger than the 90 ns seen in the simulation done for the spherical source. If this recoil energy gets smaller, its broadening effect on the peak is also expected to become smaller. This is however not seen in the lab measurements. The FWHM is not seen to decrease when the recoil energy decreases. The peak broadening effect of the recoil energy is most likely small compared to other peak broadening processes. Hence it can not be seen in the lab data.

It can also be seen that all the lab measurements the H_2^+ ions have a slightly shorter overall time of flight compared to the H_2^+ ions in the SIMION simulations. This is probably due to the fact that The MCP in the CHEOPS setup in the lab is slightly closer to the reaction chamber than is modeled in the SIMION model.

6 Conclusion

The following conclusions can be concluded from the results of the analytical research, the SIMION simulations and the lab experiments that have been carried out for this Thesis. The main goal of the analytical research is to determine to what extend kinetic energy referred to as recoil energy was transferred from an incoming energetic positively charged projectile ion to a H_2 molecule target particle with which this projectile ion undergoes a charge exchange collision. It turns out that for a set projectile energy, the recoil energy transferred to the target particle lies on a distribution of possible recoil energies that can be transferred, depending on the impact parameter b. The most likely recoil energy transferred is researched as a function of the projectile energy. The recoil energy decreases exponentially when the projectile energy is increased. It is also found that the higher the charge of the projectile ion, the more recoil energy is transferred to the target particle. Comparing the cases of one electron capture and two electron capture, it is seen that the recoil energy transferred to the H_2 molecule target particle is orders of magnitude higher in the case of two electron capture.

The main goal of the SIMION simulations is to determine the effect of an offset of the energetic ion beam coming into the extraction region of CHEOPS setup. It turns out that an offset in either x or y direction has a big influence on the transmission through the diaphragm as well as on the ratio between the transmission of the backward emitted ions and the transmission of the forward emitted ions. In the case of the simulations done for an offset of the ion source in the x direction with the CHEOPS setup SIMION model, the transmission of the forward emitted ions is seen to increase exponentially when the ion source is brought closer to the diaphragm. However, the transmission of the backward emitted ions is seen to decrease when the source is moved closer to the diaphragm. This leads to a transmission b/f ratio that decreases rapidly when the source is brought closer to the diagram. In the case of the simulations done for an offset of the ion source in the y direction with the CHEOPS setup SIMION model, the transmission up to the MCP is relatively constant in a region where the y shift is not that large. This creates a stable region in which the transmission does not change significantly. Only when the shift of the source surpasses this region, the transmission starts to drop off. This is true for both the backward- and forward emitted ions, although the stable region for the backward emitted ions is smaller than that for the forward emitted ions. Shifting the source beyond the stable region leads the transmission up to the MCP to quickly drop to 0. An offset of the source in the x direction can cause a slight difference between the results of two separate lab experiments. This is due to the fact that there can be a slight difference of the beam alignment in the extraction region in the CHEOPS setup. Since there is a large enough stable region of transmission in the case of an offset in the y direction, this does in all likelihood not lead to any noticeable difference between the results of two separate lab experiments.

Another goal to achieve with the use of SIMION simulations is to determine the ion pair transmission ratio through the diaphragm in the extraction region of the CHEOPS setup. It is expected that all the backward emitted ions that are transmitted through the diaphragm, also have their corresponding forward emitted ion transmitted when the ion point source is exactly in the middle of the reaction region. Hence an ion pair transmission is seen for every backward emitted ion that is transmitted in this case. This is indeed what is seen in the SIMION simulation with a transmission ratio of about 0.8%. It is also expected that no ion pairs will be transmitted at all when the point source shifts in the y or z direction by a larger amount than the radius of the diaphragm. This is also seen in the simulations. For a shift less than 1 mm in the y or z direction there is no effect seen on the ion pair transmission. After a shift of 1.5 mm in the y or z direction, the ion pair transmission declines increasingly fast. Zero ions are transmitted when the shift of the point source in the y or z direction is larger than 2.333 mm. This is lower than the radius of the diaphragm of 2.5 mm.

The recoil energy that is analytically calculated for a particular charge exchange collision is used in SIMION simulations. This energy is given to a H_2^+ ion. The main goal of these SIMION simulations is to determine the effect of the recoil energies on the time of flight spectrum of ions created by a charge exchange collision moving through the CHEOPS setup. In the results of the SIMION simulations there are 2 peaks seen in the time of flight spectrum in the case of a point source and 2 overlapping peaks in the case of a spherical source. The recoil energy seems to broaden the peak as was expected. When looking at results

from lab experiments, a similar broadened peak shape is seen that could be partially due to the recoil energy obtained by the H_2^+ ions. If this recoil energy gets smaller, this broadening effect is expected to disappear. However, there does not seem to be a relation between the calculated values of the recoil energy and the width of the peaks seen in the data obtained with lab experiments. The broadening near the bottom of the peaks in the lab data does not decrease when the projectile ions in the beam get a higher energy. Furthermore, the FWHM of the peaks does not seem to depend on the magnitude of the recoil energy. The effect of the recoil energy seems to be to small to have a significant impact on the time of flight spectra obtained with lab experiments.

7 Outlook

This report is only a small step along the way of understanding charge exchange collisions and how the decay products of such a collision behave in the experimental setup that is used to measure them. To contribute more to the knowledge gained in this report, further research needs to be done. Some suggestions for such research is suggested here.

To build on the analytic research done on the classical over barrier model, there are several research possibilities that can be pursued. One of those is to do further simulations on the transverse momentum transfer and the recoil energy transfer to the target particles based on the classical over barrier model, by using other target- and projectile particle types. This can be done easily with the python script that is already written for this Thesis. To make the simulations more accurate for lower energy projectile ions, it can also be considered to no longer assume the trajectory of the projectile ions to be a straight line trajectory, but to determine the actual trajectory of the particle. Another thing that can be considered is to use a different model than the classical over barrier model to describe the charge exchange collision. This model can then be compared to the classical over barrier model. Something that requires significantly more effort but can be useful in the quest to understand the recoil energy transfer to the target particle in a charge exchange collision, is to design a lab experiment in which the recoil energy can be measured accurately. The results of this experiment can then be compared to the analytically determined values and used to determine the accuracy and limits of the classical over barrier model. This however requires a very specific experimental setup in which one needs to look at individual charge exchange collision events. The impact parameter and the kinetic energy of the projectile and target particles will need to be very accurately controlled.

Regarding the experimental setup that is used in the lab of the QISD group, several things can be researched further to obtain an even better understanding of this setup. The SIMION model of the CHEOPS setup that is build for this Thesis can be used for much more simulation experiments. Specific scenarios can be simulated to improve the knowledge about the setup and to find the measurement limits of the setup. For example the change in extraction voltage or the distance between the extraction plates can be changed. It is also possible to build SIMION models of other sections of the experimental setup in the lab. For example an attempt can be made to model the chopper sweeper system or one of the electrostatic lens systems. Finally these separate modules can be combined into one big SIMION model to model the entire lab setup. There are also some discrepancies found when comparing the analytically results, the results found with the aid of SIMION simulation and the experimental results. A discrepancy is found comparing the analytical values-with the values found with the aid of SIMION simulations of the transmission through the diaphragm in the CHEOPS setup. Some further research can be done to determine the cause of this discrepancy. The same holds true for the time difference Δt between the forward- and backward emitted ion. There is also further research needed to determine the cause of this discrepancy. Lastly, there is a discrepancy found with the ratios between the backward- and the forward emitted ions that are transmitted through the diaphragm (b/f ratio). When comparing the b/f ratio determined with a lab experiment and the b/f ratio determined with a SIMION simulation done with the CHEOPS setup SIMION model, there is a significant difference. The exact reason for this is yet unknown. This is something further research can clear up.

References

[1] Moore, G. E. Cramming more components onto integrated circuits, reprinted from electronics, volume 38, number 8, april 19, 1965, pp.114 ff. *IEEE Solid-State Circuits Society Newsletter* **11**, 33–35 (2006).

[2] Moore, G. Progress in digital integrated electronics [technical literaiture, copyright 1975 ieee. reprinted, with permission. technical digest. international electron devices meeting, ieee, 1975, pp. 11-13.]. *IEEE Solid-State Circuits Society Newsletter* **20**, 36–37 (2006).

[3] Pirati, A. *et al.* The future of EUV lithography: enabling Moore's Law in the next decade. In *Society of Photo-Optical Instrumentation Engineers (SPIE) Conference Series*, vol. 10143 of *Society of Photo-Optical Instrumentation Engineers (SPIE) Conference Series*, 101430G (2017).

[4] Versolato, O. O. Physics of laser-driven tin plasma sources of EUV radiation for nanolithography. *Plasma Sources Science and Technology* **28**, 083001 (2019).

[5] Moore, G. E. Lithography and the future of Moore's law. In Warlaumont, J. M. (ed.) *Electron-Beam, X-Ray, EUV, and Ion-Beam Submicrometer Lithographies for Manufacturing V*, vol. 2437, 2 – 17. International Society for Optics and Photonics (SPIE, 1995).

[6] van Setten, E. *et al.* High NA EUV lithography: Next step in EUV imaging . In Goldberg, K. A. (ed.) *Extreme Ultraviolet (EUV) Lithography X*, vol. 10957, 9 – 18. International Society for Optics and Photonics (SPIE, 2019).

[7] Hasan, R. & Luo, X. Promising lithography techniques for next generation logic devices: a review. *Nanomanufacturing and Metrology* (2018).

[8] Kozhevnikov, I., Yakshin, A. & Bijkerk, F. Wideband multilayer mirrors with minimal layer thicknesses variation. *Opt. Express* **23**, 9276–9283 (2015).

[9] Kuang, S.-q., Wang, J.-b., Yang, H.-g., Huo, T.-l. & Zhou, H.-j. Design and fabrication of robust broadband extreme ultraviolet multilayers. *AIP Advances* **9**, 045027 (2019).

[10] Tao, Y. & Tillack, M. S. Mitigation of fast ions from laser-produced sn plasma for an extreme ultraviolet lithography source. *Applied Physics Letters* **89**, 111502 (2006).

[11] Knoop, S. *Electron Dynamics in Ion-Atom Interactions.* Ph.D. thesis (2006).

[12] Niehaus, A. A classical model for multiple-electron capture in slow collisions of highly charged ions with atoms. *Journal of Physics B: Atomic and Molecular Physics* **19**, 2925–2937 (1986).

[13] Winters, D. F. A. *Polarization transfer in ion-surface scattering.* Ph.D. thesis (2004).

[14] Juhász, Z. *Charge exchange processes that make comets radiate.* Ph.D. thesis (2004).

[15] Alvarado Chacon, F. *Ion induced radiation damage on the molecular level.* Ph.D. thesis (2007).

[16] Brinkhuis, E. *Energetic ions traversing hydrogen gas: charge exchange reactions and pulse length considerations.* Bachelor's thesis (2020).

[17] Kamp, R. *Shooting tin bullets at hydrogen gas.* Master's thesis (2020).

[18] Folkerts, H. O. *Molecular dissociation induced by electron transfer to multicharged ions.* Ph.D. thesis (1996).

[19] Ladislas Wiza, J. Microchannel plate detectors. *Nuclear Instruments and Methods* **162**, 587–601 (1979).

[20] G. Choppin, J. R., J.O. Liljenzin & Ekberg, C. *Chapter 9 - Detection and Measurement Techniques.* (2013), fourth edn.

[21] Martínez, S., Bernardi, G., Focke, P., González, A. & Suárez, S. H2 dissociation by h+ and he2+ projectiles at intermediate energies. *Journal of Physics B: Atomic, Molecular and Optical Physics* **36**, 4813 (2003).

Appendix

7.1 One electron capture

7.1.1 Transverse momentum

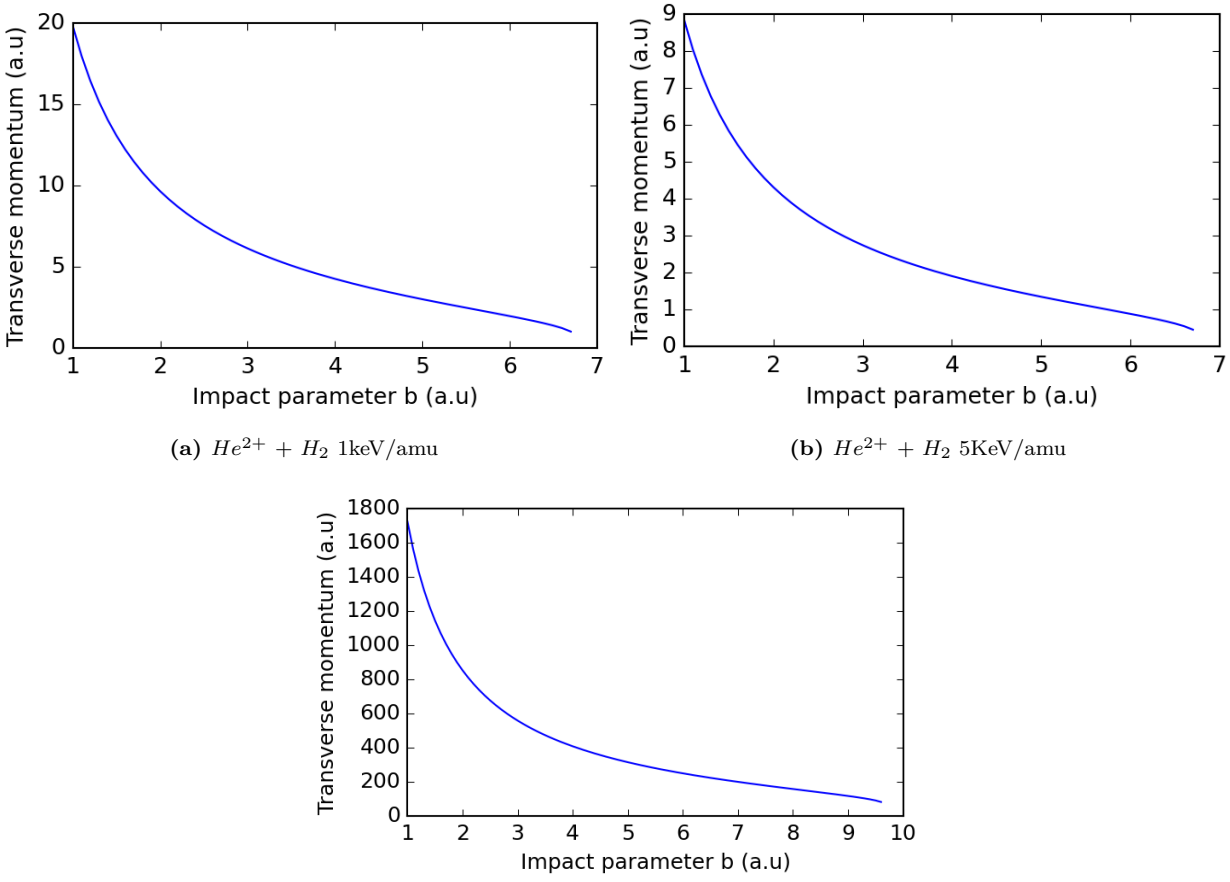

(a) He^{2+} + H_2 1keV/amu

(b) He^{2+} + H_2 5KeV/amu

(c) $^{120}Sn^{5+}$ + H_2 0.1keV

Figure 46: Transverse momentum as a function of the impact parameter b for one electron capture.

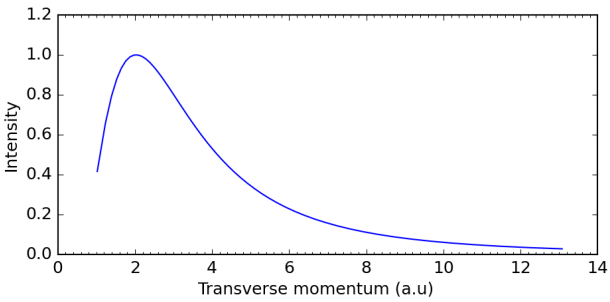

(a) He^{2+} on H_2 1keV/amu

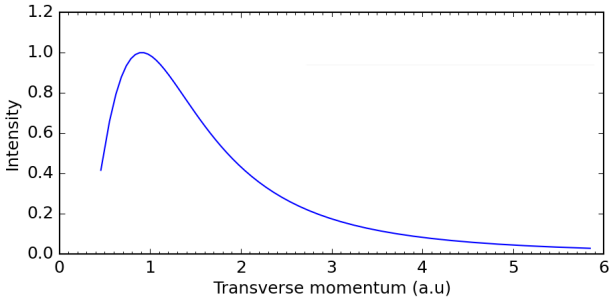

(b) He^{2+} on H_2 5keV/amu

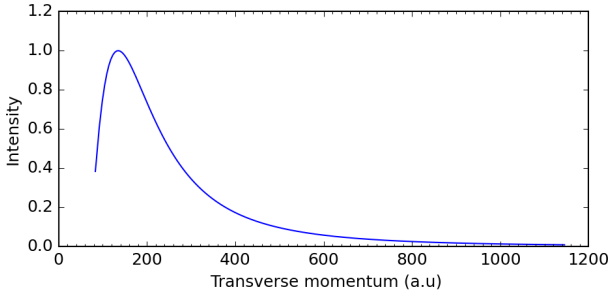

(c) $^{120}Sn^{5+}$ on H_2 0.1keV

Figure 47: Transverse momentum distribution for one electron capture.

7.1.2 Angular distribution

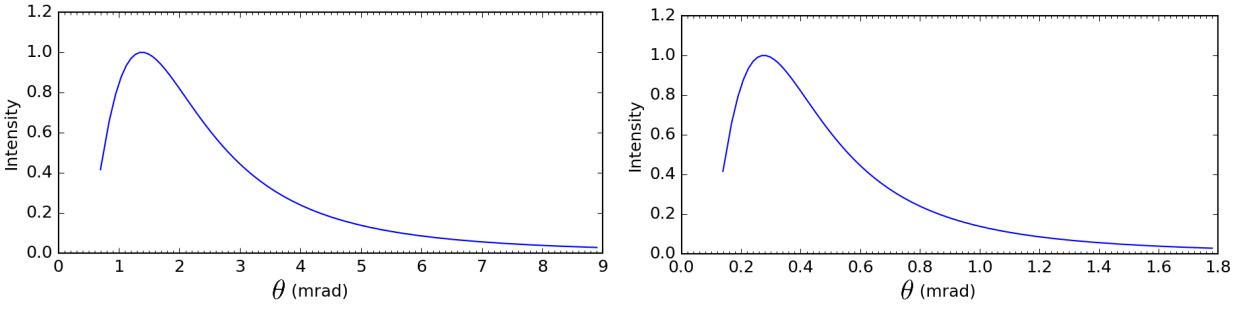

(a) He^{2+} on H_2 1keV/amu

(b) He^{2+} on H_2 5keV/amu

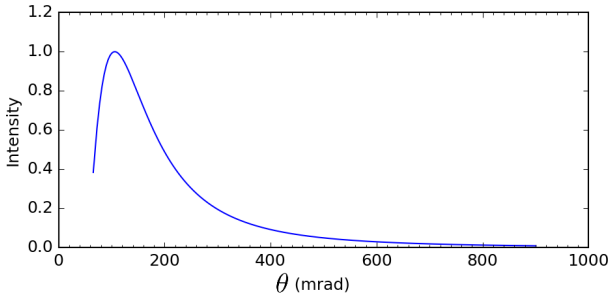

(c) $^{120}Sn^{5+}$ on H_2 0.1keV

Figure 48: Angular distribution of the projectile ions for two electron capture.

7.1.3 Recoil energy

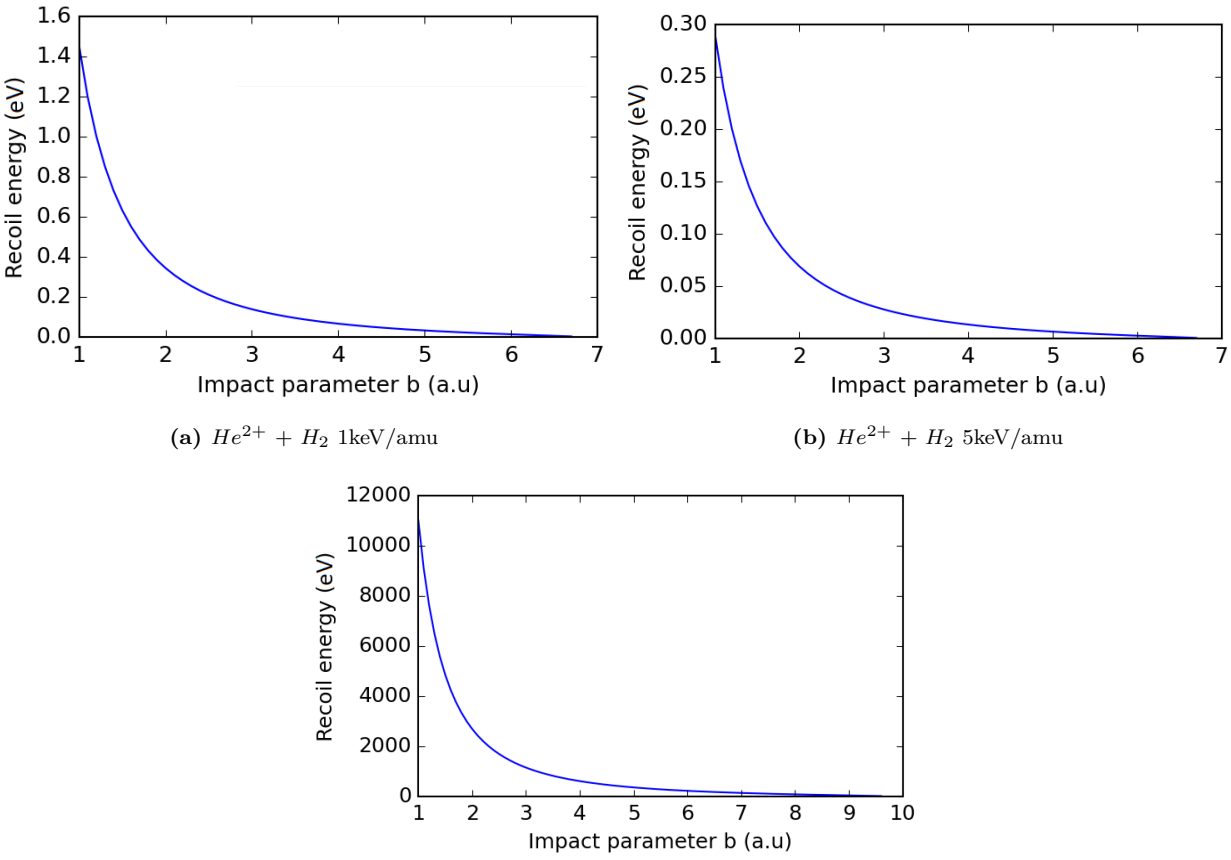

(a) He^{2+} + H_2 1keV/amu

(b) He^{2+} + H_2 5keV/amu

(c) $^{120}Sn^{5+}$ + H_2 0.1keV

Figure 49: Recoil energy as a function of the impact parameter b for one electron capture.

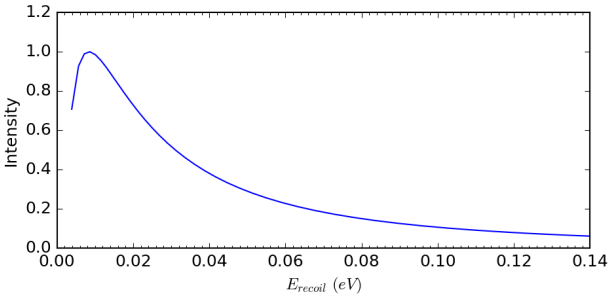

(a) He^{2+} on H_2 1keV/amu

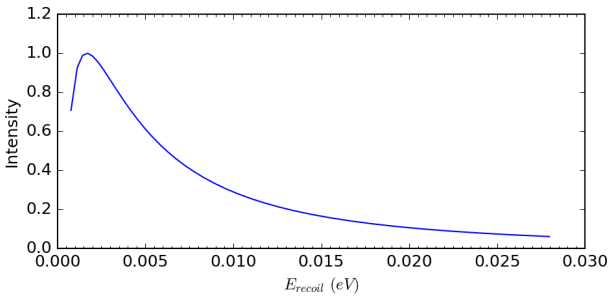

(b) He^{2+} on H_2 5keV/amu

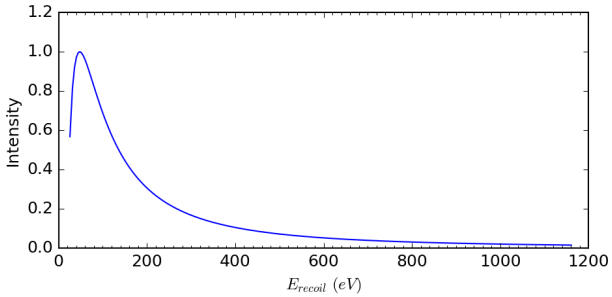

(c) $^{120}Sn^{5+}$ on H_2 0.1keV

Figure 50: Recoil energy distribution for one electron capture.

7.2 Two electron capture

7.2.1 Transverse momentum

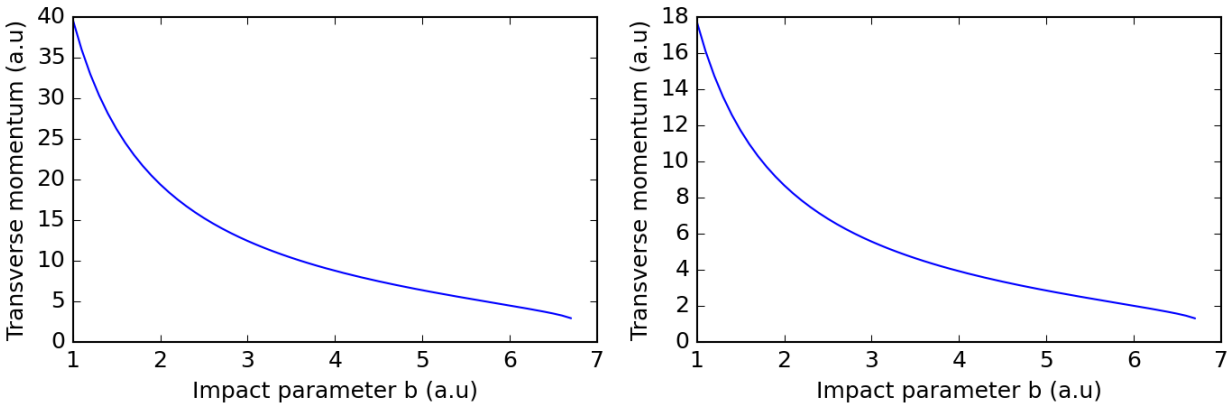

(a) He^{2+} + H_2 1keV/amu

(b) He^{2+} + H_2 5keV/amu

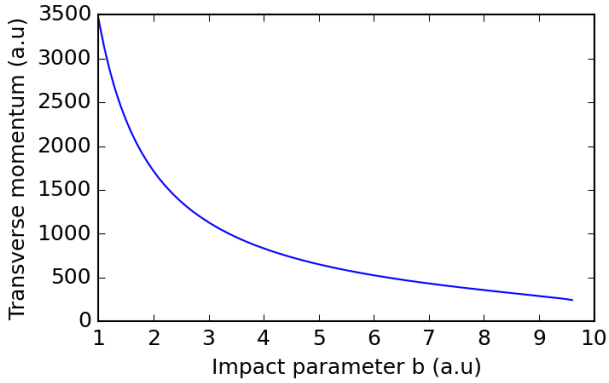

(c) $^{120}Sn^{5+}$ + H_2 0.1keV

Figure 51: Transverse momentum as a function of the impact parameter b for two electron capture.

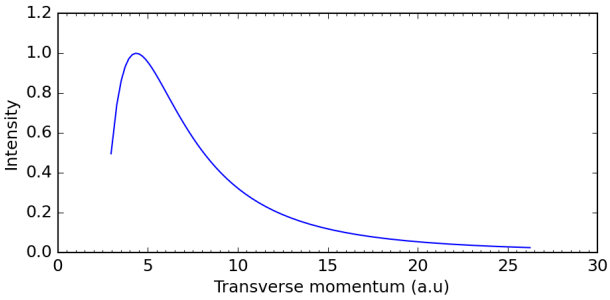

(a) He^{2+} on H_2 1keV/amu

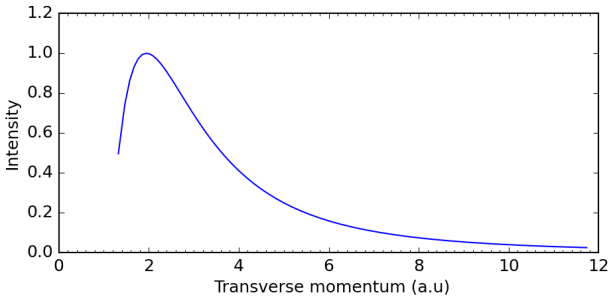

(b) He^{2+} on H_2 5keV/amu

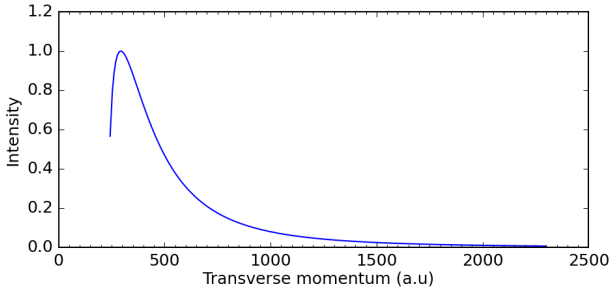

(c) $^{120}Sn^{5+}$ on H_2 0.1keV

Figure 52: Transverse momentum distribution for two electron capture.

7.2.2 Angular distribution

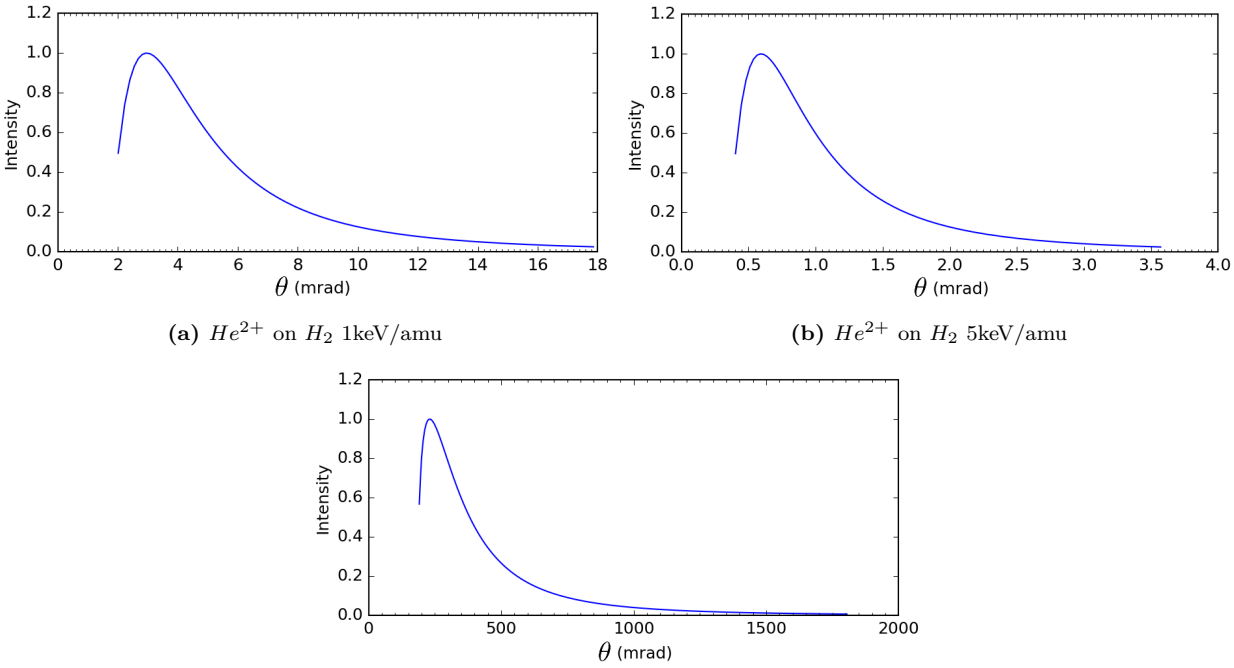

(a) He^{2+} on H_2 1keV/amu

(b) He^{2+} on H_2 5keV/amu

(c) $^{120}Sn^{5+}$ on H_2 0.1keV

Figure 53: Angular distribution of the projectile ions for two electron capture.

7.2.3 Recoil energy

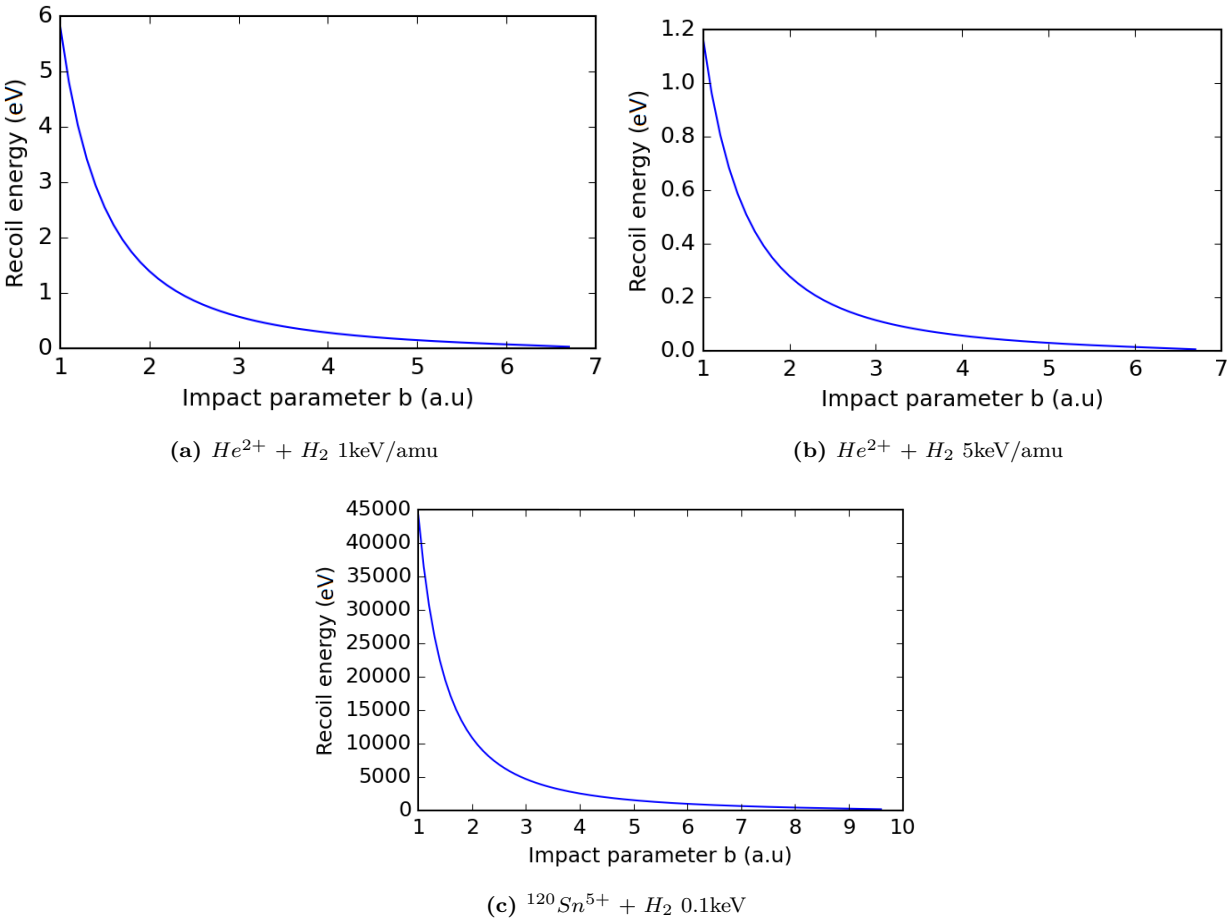

(a) He^{2+} + H_2 1keV/amu

(b) He^{2+} + H_2 5keV/amu

(c) $^{120}Sn^{5+}$ + H_2 0.1keV

Figure 54: Recoil energy as a function of the impact parameter b for two electron capture.

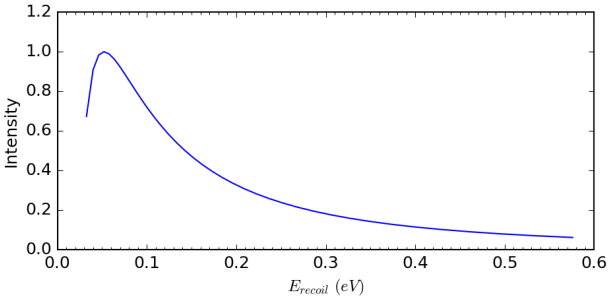

(a) He^{2+} on H_2 1keV/amu

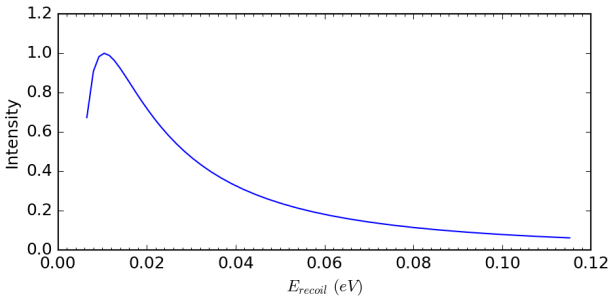

(b) He^{2+} on H_2 5keV/amu

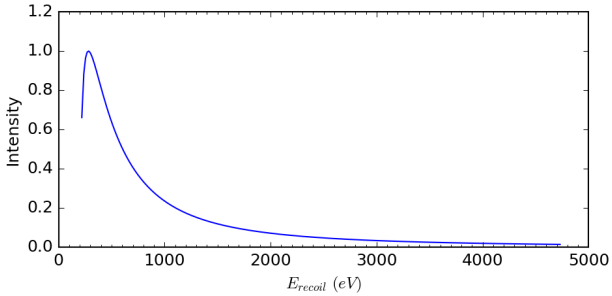

(c) $^{120}Sn^{5+}$ on H_2 0.1keV

Figure 55: Recoil energy distribution for two electron capture.